Hydraulics Research
Wallingford

AFFLUX AT BRITISH BRIDGES
Interim Report

P M Brown

Report No SR 60
October 1985

Registered Office: Hydraulics Research Limited,
Wallingford, Oxfordshire OX10 8BA.
Telephone: 0491 35381. Telex: 848552

ABSTRACT

It was evident from Water Authorities in Britain that there is a large number of bridges which, because of their structural design, cause substantial obstructions to flow, thereby raising upstream river levels. Often these bridges are of medieval arch design protected by preservation rulings. Present day formulae on bridge hydraulics are intended to represent modern day bridge design practice and are inappropriate to ancient arch structures. This interim report details laboratory model tests on various semi-circular arch bridges with square edged piers. Interpretation of results showed a comprehensive relation between non-dimensional sets of hydraulic parameters which has been represented graphically. An engineer may use the graph by an iterative procedure to obtain afflux values for the type of bridges tested from known downstream river conditions. The report also indicates future tests designed to extend the application of the empirical formula.

CONTENTS

TABLES

FIGURES

PLATES

SYMBOLS

B Width of channel

d_1 normal depth of flow upstream

d_3 normal depth of flow downstream

C_D coefficient of drag

mass density of water

V_1 mean velocity of flow at Section 1

V_3 mean velocity of flow at Section 3

g acceleration due to gravity

F Froude number = $V/\ gd$

Q discharge

J Blockage area/area of flow in absence of bridge

h afflux, $(d_1 - d_3)$

h' afflux, defined to contain no friction loss term

1 INTRODUCTION

The flows on most rivers are affected by man made structures which have often unusual or non standard designs. This is particularly the case in the UK where some medieval bridges still exist. Such structures impede the flow but are often scheduled historic monuments and cannot be removed. Standard empirical formulae have not been validated for such structures since the formulae are intended to represent modern design practice and not ancient custom. The engineer is faced with the problem of adequately representing the effects of such idiosyncratic structures when examining river improvement works. Hydraulics Research Limited have developed a suite of programs called FLUCOMP which are designed to simulate and predict flow conditions within river channels and on flood plains. FLUCOMP uses a design method derived by USPBR (Ref 1) to predict afflux, the increase in water level caused by a structure which impedes or blocks flow.

Old multiple arched bridges can block up to 50% of the flow area of the river channel. This degree of blockage is far beyond the scope of data used to construct the USPBR design method, which is considered to provide the best design guide for bridge afflux calculations at present. Prototype and experimental data for analysing such cases are sparse.

The purpose of this study was, by means of laboratory model tests, to relate this increase in water level or afflux caused by various designs of arch bridges to determinable hydraulic parameters. Such relations would be validated with prototype data and presented in the form of an engineering design guide which would enable an engineer to obtain afflux values from known bridge geometry and predetermined flow conditions in the absence of a bridge. The relationships would be included as a refinement to the FLUCOMP mathematical model.

As an initial approach to the study, physical model tests were carried out on semi-circular arch bridges. An enquiry was also set up to identify prototype bridges with high afflux and to gather relevant hydraulic information with which to test the empirical formulae.

2 PROTOTYPE DATA

Letters were sent to 55 regional Water Authorities in England, Wales and Scotland to explain the proposed research programme and enquire whether they could make available details of bridges within their area which created large afflux. The response was very enthusiastic and showed a genuine interest in the study and willingness to participate in the investigation.

Table 1, which lists the large number of bridges identified by the Water Authorities as creating large afflux which often led to flooding problems, clearly confirms the need to understand better the flow behaviour at these structures.

Following our approach, some Authorities have installed flood level gauges at selected bridge sites to monitor water levels either side of the structure during periods of high flow. Table 1 shows the large number of bridge sites for which all the data required for comparative analysis to the physical model tests has been made available, ie water levels upstream and downstream of the bridge, discharge and bridge geometry and configuration.

Much of the data recorded by the Water Authorities in previous years has yet to be collected and assessed and the very dry summer of 1984 produced low river flows which were not sufficient to trigger the flood level recorders. There is, therefore, insufficient field data to make an analysis at this time but an initial appraisal will be made in the near future when all available data is processed.

3 MODEL TESTS

Model tests were carried out in a 2.4 m wide by 15 m long flume. Flow was fed into the flume from a 0.17 m^3/s pump and discharged over a B.S half 90° V-notch at low to medium flows and over a B.S rectangular notch at high flows. Downstream water levels were controlled with a horizontal hinged tailgate. The layout of the flume is shown in Fig 1 and Plate 1.

The model bridges were designed with a semi-circular arch and constructed from wood. They were contained between the side of the flume and an adjustable right bank vertical wall of sufficient length to ensure uniform approach flow.

A set of dimensionless parameters, relating the bridge dimensions of length, width and height to pier width were obtained from analysis of prototype data. These parameters were reproduced on the model to give practical working limits for testing. Further limits imposed were that flow was not allowed to overtop or bypass the bridge.

The model river bed was constructed of painted wood to be smooth and horizontal. Varying roughness and slope factors could be introduced at a later stage if it became apparent that they influenced results. The channel banks, also of wood, were designed to be vertical and smooth and positioned at a half pier width either side of the bridge to define a rectangular channel.

The results from the tests will apply to any size bridge by considering changes in scale. All analyses would consider dimensionless parameters.

Static head water levels were measured from side tappings on the left wall of the flume at several locations either side of the bridge. Water levels were read directly with micrometer screw point gauges reading to an accuracy of 0.00003 m. Fig 1 shows the positions of the tapping points along the flume. Water levels along the centre line of the channel were measured directly using an electronic water sensitive point gauge. Velocities were measured with a miniature propeller current meter at 0.6 depth on sections either side of the bridge, away from its immediate influence (Plate 2).

The testing procedure was to measure, at constant low discharge and tailwater level, the side and centre channel water surface profiles along the flume and also velocities at sections upstream and downstream of the bridge. Whilst maintaining the discharge, the tailwater level was increased and the series of measurements repeated until the upstream water level was close to the top of the bridge. The discharge was then increased and the procedure repeated. Various conditions were photographed.

The initial model tested in this way was a basic semi-circular arched bridge shown in Fig 2 (Plate 3). Tests 2a to 5b cover the range of flow conditions observed with this structure. Resultant water surface profiles are reproduced in Figs 3 to 6 and velocities profiles shown in Figs 31 and 32.

The second series of tests were with bridge length in the direction of flow increased by 200%, (Fig 2, Plate 4). Results of these tests, 6a to 9b, are plotted on Figs 7 to 10, and Figs 33 to 34.

Blockage ratio is defined in this report as the total area of structure beneath the water surface which impedes or obstructs flow divided by the total available flow area in the absence of a structure.

The effective blockage capacity or area of the bridge which impeded flow was subsequently increased in two stages in Tests 10a to 20a by a symmetrical increase in pier widths, (Fig 2, Plate 5). This extension was carried to the full height of the bridge and increased the blockage to flow by 12% and 35% respectively.

Water surface profiles from the tests with the bridge widened to 0.38 m are given in Figs 11 to 14 and velocity profiles in Figs 35 and 36. Similar profiles for the bridge widened to 0.46 m are shown on Figs 15 to 21 and Figs 36 to 39.

The set of tests, 21a to 29b was with three basic bridge units combined widthways across the flume to form a multiple arch structure with two central piers of full width, (Fig 2, Plate 6). Longitudinal water surface profiles were taken along the centre of the channel through the centre arch and are shown in Figs 22 to 30. Velocity traverses were taken upstream and downstream of the bridge across the full channel width and are shown on Figs 39 to 42.

The plots of the water surface profiles taken along centre and side channels show a relatively clear picture of conditions in the flume during each test. Measurement of water level in the downstream channel was often difficult in the tests involving high flow and low tailwater owing to the highly turbulent, and often supercritical flow. In these tests the plotted profiles only reproduce an instantaneous condition of an irregular water surface. It was appreciated that these conditions are rare in the prototype but the tests were designed to give a comprehensive coverage of all flow conditions. Conditions can be fully appreciated from Plates 7 and 8.

The mid depth velocity profiles, Figs 31 to 42, show flow was evenly distributed in the approach channel throughout most of the tests. Downstream of the three arched bridge interfering flow emerging from the arches caused a maximum velocity core to wander down the flume.

Shallow intermitted vortices or surface dimples frequently occurred at high flows immediately upstream of the bridge piers and central arch, (Plate 9). Under surcharged conditions an oscillating surface layer of slack water overlay the main flow which plunged through the bridge arch. Plate 10 shows this overlying layer as a series of surface ripples.

4 DATA EXTRACTION AND ANALYSIS

As previously discussed, the increase in water level upstream of a structure over that level which would have occurred in the absence of a structure is termed the afflux. Afflux is more generally regarded as the difference in water level upstream and downstream of a structure but difficulties arise in defining the positions of water level measurement.

For the purpose of this study afflux was calculated using two methods. Afflux may be defined as being inclusive of a channel friction loss as well as an energy loss due to the presence of the bridge, Method 1, or may be defined without the friction term, Method 2. Both methods are discussed in this report and resultant afflux values used in the analysis. The first method involved calculating the difference between static water levels measured at tapping points 1 and 12, furthest from the bridge, and away from its immediate influence. The second method was based on that used to calculate total energy losses at surcharged manholes, (Ref 2). The hydraulic gradient between tapping points 12 and 9 upstream was projected to intersect the front face of the bridge for each test. Applying the same hydraulic gradient to the water level at the downstream tapping point 1 and projecting back to the bridge enabled total energy loss to be determined as the vertical distance between the two projected gradients at their intersection with the bridge. Defining head loss in this way removed the natural friction loss of the flume from consideration and allowed energy losses caused by the presence of the bridge, in the form of turbulence, to be dominant. It was regarded as unrealistic to apply the same hydraulic gradient to both upstream and downstream of the bridge in the extreme cases of supercritical conditions downstream. In these instances the data have not been considered. Table 2 lists values of afflux calculated by the two methods detailed above.

Direct measurements of velocity taken at each test gave an indication of the flow distribution in the approaches to the bridge and in the downstream channel beyond the immediate influence of the bridge. Mean velocities were calculated for the sections at which afflux was determined, tappings 1 and 12, and these values were used in the calculation of Froude numbers.

Blockage ratio was defined earlier as the area of obstruction to flow divided by flow area. Fig 43 illustrates the calculation of blockage ratio for the semi-circular arched bridge. The maximum value of blockage ratio for the semi-circular arched bridge is $1 - (\pi R^2/2)/Bd$, where B is the channel width, d is depth of flow and R is radius of the arch.

Table 3 lists the hydraulic parameters of discharge, upstream and downstream water levels, blockage ratio and Froude number which were either measured or calculated for each test condition.

5 DETERMINATION OF AFFLUX IN FLUCOMP

The FLUCOMP package is limited to treating subcritical flow through bridges and in the absence of any flow bypassing the structure the afflux caused by the bridge is given by

$$\Delta h = K \ Href$$

where Href is a reference velocity head and K is the backwater coefficient. The value of the coefficient K is built up from the equations in the USPBR manual. The principle effects of the geometry of the bridge site are contained in the coefficient K and these are defined as Kb, which depends on constriction to flow by embankments, Kp dependant on pier blockage and shape, Ke and Ks dependant on eccentricity and skew of the bridge crossing. The USPBR manual defines K by $K = Kb + Kp + Ke + Ks$. Each of the sub-coefficients can be determined from a series of curves derived by USPBR and reproduced in the manual (Ref 1). The reference velocity head Href is defined as the velocity head that would occur if all the flow were to pass in the constricted section between bridge abutments at the undisturbed water level without any piers. Href is modified by an energy coefficient which the USPBR manual implies is applicable over the live stream rather than the complete wetted cross section. Relationships between the energy coefficient at a reference section and a section upstream of the bridge are given in figures in the USPBR manual. The energy coefficient is further modified by the blockage ratio which is defined as the ratio of flow which can pass unimpeded through the bridge to the total flow of the river. This term differs by definition from that used in the present analysis.

The water level at the bridge is obtained in FLUCOMP by computing a steady flow backwater profile between two cross sections either side of the bridge and assuming that the water surface varies linearly between the two. This water level is used to obtain the blockage ratio and flow area of the bridge and the computed reference velocity head is then adjusted by a total backwater coefficient. When considering extreme flood conditions when the arches of a bridge becomes surcharged, FLUCOMP calculates the afflux from an orifice flow equation.

5.1 Comparison between FLUCOMP predictions and physical model results

The ability of the FLUCOMP mathematical model to predict water level upstream of a bridge from pre-determined downstream data was assessed using the results from the model bridge tests.

The mathematical model considered all dimensions and descriptions of the flume and bridges in prototype terms using a scale factor of 1:100. The bridge was assumed to be at cross section 500 with the flume or channel being described by sections at 180, 300, 400, 480, 520, 600, 700, 800, 900 and 1000 m. A flume roughness value of Ks = 0.0001 m was assumed ie 0.01 m prototype for the earlier tests. For most of the later tests a lower roughness value of Ks = 0.005 m was adopted as being more realistic. Resultant water levels, however, were not very sensitive to these changes.

In FLUCOMP the bridge cross section was specified as consisting of a channel and two flood plains. The channel was assumed to start at the left offset, or springing point, of the first arch and end at the right offset of the final arch. Floodplains were flow areas outside these limits.

The model bridges were treated as having the standard description as above and also with the piers/abutments included in the 'channel'. This second description specified two minute arches at either end of the bridge with negligible flow areas. The two descriptions give different blockage ratios.

Each tested bridge was treated as aligned normal to the flow direction and standard coefficients were applied as derived from USPBR method. The manual gives a constant coefficient of discharge of 0.8 when considering surcharged flow, based on the common expression for sluice gate flow. However, a different interpretation of the graph relating depth of water above bridge soffit to coefficient of discharge (Ref 1, p 43) suggests a varying surcharged coefficient is more appropriate. This supposition is borne out by the comparison between model results and FLUCOMP calculated results (Fig 44) where large discrepancies occur at surcharged flow.

The main coefficient for describing the bridge is the pier factor. It is dependant upon blockage ratio as defined by USPBR as well as actual geometry of the pier. A pier factor of 5 was used which applies to square or rectangular piers or to a bridge with no piers and a non-rectangular opening. This was therefore applicable to both descriptions of the bridge mentioned above.

Backwater profiles were calculated for each type of structure from the appropriate discharge and downstream water level (at tapping 1) obtained from each model test. Fig 44 shows the comparison between measured upstream water level (at tapping 12) and that calculated using FLUCOMP. It is clear that FLUCOMP overestimates afflux at high discharges and particularly when the bridge is surcharged. The situation is more severe than shown in the figure since flow was allowed over the top of the bridge in FLUCOMP but not permitted in the model tests. Afflux would have increased had this 'road flow' been prevented. Table 4 lists the measured and calculated upstream water levels for each test.

On average FLUCOMP overestimated afflux by 10% but with the lengthened bridge overestimate was of the order of 20%.

6 INTERPRETATION OF EXPERIMENTAL RESULTS

6.1 General

Figs 46, 47 and 48 are plots of the predetermined conditions of tailwater level and discharge set for each test. Each figure shows any variation of afflux from the single arch bridge caused by either lengthening or widening the bridge or combining into a triple arch structure.

Compared with the single arch bridge under the same flow conditions, tests 2a to 5b, lengthening the bridge by an additional 200% in the direction of flow caused a small reduction in afflux. This comparative reduction increased with discharge and was of the order of 3% at the highest flow. The difference was discernable at upstream levels close to bridge soffit and above.

Fig 47 shows the comparison between upstream levels of the basic unit arch bridge of total width 0.34m and the bridge with both piers widened by 0.06m, to give a total bridge width of 0.46m, under the same flow conditions. Widening the piers reduced the effective area of the arch and increased the blockage ratio. The figure shows afflux values to be larger at the wider bridge. This difference became greater as discharge increased. The 35% increase in pier width raised afflux values by approximately 14% at high flows.

The flow conditions at the three arch structure was compared with the single arch basic unit and results reproduced on Fig 48. The criteria behind the comparison was that the multiple arch structure would reproduce conditions through each of the arches that were similar to those measured on the single arch bridge. However Fig 48 clearly shows this is not the case, as for similar tailwater and discharge parameters the afflux caused by the multiple arch structure was larger than that measured on the single arch structure. The affect was apparent over the whole range of tested levels and varied with discharge. At the maximum surcharged condition afflux values had increased by 25%. Flow conditions at a multiple arch structure cannot be assessed accurately from appraisal of one of the arches.

6.2 Theoretical approach

The purpose of the analysis was to evolve relationships for the elevation of water level caused by constriction to flow through an arched bridge. This afflux upstream of a bridge and the related energy loss are both dependant on the drag characteristics of the bridge. The following analysis follows a similar method suggested by Ranga Raju et al (Ref 3) which assessed the blockage effect in flow past smooth circular cylinders. Their studies were carried out under subcritical flow conditions using cylinders of various blockage ratios but of known drag coefficients.

Fig 45 shows the effect of a channel constriction on the water surface profile. In this figure, B is the width of channel, b is the arch diameter, w is the pier width, d_1 is the increased depth of flow at section 1, d_3 is the normal depth of flow. Δh represents the afflux caused by the presence of the bridge. The figure shows two definitions of afflux considered in this report.

Applying momentum principle between sections 1 and 3

$$\rho g\frac{d_1}{2} \cdot d_1B - \rho g\frac{d_3}{2} \cdot d_3B - C_D\,\rho(J_1 \cdot d_1B)\frac{V_1^2}{2}$$

$$= \rho V_3 d_3 B(V_3 - V_1) \qquad (1)$$

where

J_1 = upstream blockage ratio

$= \dfrac{\text{blockage area of bridge at depth } d_1}{\text{area of flow } d_1B}$

ρ = mass density of water

g = acceleration due to gravity

Here the coefficient of drag $C_D = \frac{F_D}{\frac{1}{2}\rho v_1^2 . (J_1 . Bd_1)}$

where F_D is the drag force on the bridge
$\frac{1}{2}\rho V_1^2$ is the kinetic energy of flow
$J_1 Bd_1$ is the blockage area of the bridge

V_1 and V_3 = mean velocity of flow at sections 1 and 3 respectively

From continuity principle

$$d_1 BV_1 = d_3 BV_3$$

and using (2)

$$V_1 = \frac{d_3 V_3}{d_1}$$

$$\rho\delta\frac{d_1{}^2 B}{2} - \rho\delta\frac{d_3{}^2 B}{2} - \frac{C_D \rho}{2}(d_1 J_1 B)\frac{d_3{}^2 V_3{}^2}{d_1{}^2} =$$

$$\rho V_3 d_3 B\left(V_3 - \frac{d_3 V_3}{d_1}\right) \tag{3}$$

Multiply by d_1 to give

$$\rho g\, d_1{}^3 \frac{B}{2} - \rho g \frac{d_3{}^2}{2} B\, d_1 - C_D \rho J_1 B \frac{d_3{}^2 V_3{}^2}{2} =$$

$$\rho V_3 d_3 B d_1 - \rho V_3{}^2 d_3{}^2 B \tag{4}$$

Divide by $\frac{\rho g B d_3{}^3}{2}$ to give

$$\frac{d_1{}^3}{d_3{}^3} - \frac{d_1}{d_3} - \frac{C_D J_1 V_3{}^2}{g d_3} = \frac{2V_3{}^2 d_1}{d_3{}^2 g} - \frac{2V_3{}^2}{g d_3}$$

$$\frac{d_1{}^3}{d_3{}^3} - \frac{d_1}{d_3} - 2V_3{}^2\frac{d_1}{d_3{}^2} + 2\frac{V_3{}^2}{g d_3} - C_D J_1 \frac{V_3{}^2}{g d_3} = 0 \tag{5}$$

Substituting $\Delta h = d_1 - d_3$ and $F_3 = \frac{V_3}{\sqrt{g d_3}}$ and expanding gives

$$\left(\frac{\Delta h}{d_3}\right)^3 + 3\left(\frac{\Delta h}{d_3}\right)^2 + 2\frac{\Delta h}{d_3} - 2F_3{}^2\frac{\Delta h}{d_3} - C_D J_1 F_3{}^2 = 0 \tag{6}$$

Neglecting the $\left(\frac{\Delta h}{d_3}\right)^3$ term since it is very small the above equation becomes a quadratic

$$\frac{\Delta h}{d_3} = \frac{(F_3^2 - 1) + \left((F_3^2 - 1)^2 + 3\ C_D\ J_1\ F_3^2\right)^{\frac{1}{2}}}{3} \qquad (7)$$

The above theoretical approach was similarly applied using the downstream blockage ratio J_3,

$$\text{where } J_3 = \frac{\text{blockage area of bridge at depth } d_3}{\text{area of flow, } d_3 B}$$

Considering this term transformed equation 6 into

$$\left(\frac{\Delta h}{d_3}\right)^3 + 3\left(\frac{\Delta h}{d_3}\right)^2 + 2\frac{\Delta h}{d_3} - 2F_3^2\frac{\Delta h}{d_3} - C_D\ J_3\ F_3^2\frac{d_3}{d_1} = 0 \qquad (8)$$

and since $d_1 = \Delta h + d_3$, equation 8 becomes

$$\left(\frac{\Delta h}{d_3}\right)^3 + 3\left(\frac{\Delta h}{d_3}\right)^2 + 2\frac{\Delta h}{d_3} - 2F_3^2\frac{\Delta h}{d_3} - C_D\frac{J_3\ F_3^2}{(\Delta h/d_3 + 1)} = 0 \qquad (9)$$

It may be seen from equations 6 and 9 that the ratio $\frac{\Delta h}{d_3}$ depends on F_3, C_D and either J_1 or J_3.

The extreme case of long bridges where flow resembles that through a culvert may be considered using standard culvert formulae (Ref 4).

6.3 Afflux function

6.3.1 Graphical representation

Fig 49 shows the dimensionless ratio $\Delta h/d_3$ plotted against the downstream Froude number F_3 and upstream blockage ratio J_1. Afflux values were calculated, using Method 1 in Section 4, to be the difference between water levels at tapping points 1 and 12. Blockage ratios were calculated from gauged levels at the most upstream section and Froude numbers were determined from gauged depths and mean velocities at tapping point 1, the furthest downstream section. Data from all the tests are plotted on the figure including surcharged conditions and also the extreme supercritical flow cases.

Initially the curves of equal blockage ratio, J_1, were fitted by eye. These fitted reasonably well except in the region of low Froude numbers and afflux ratio. This area of minimal flow and afflux is probably of least importance for an engineer concerned with flood control.

The graph may be used by means of an iterative procedure to obtain values of afflux caused by a semi-circular arched bridge from predetermined downstream conditions. As previously discussed the Flucomp mathematical model considers the problem of bridge afflux by initially computing normal flow conditions in the absence of the bridge and then applying a backwater coefficient. The graphical method requires an estimate to be made of upstream water level, and hence blockage ratio J_1. Computations of normal downstream depth and velocity allow values of afflux Δh and downstream Froude number to be determined. From the curves an initial value of F_3 is found, compared with the calculated value, and the procedure repeated until the difference between calculated and graphically determined F_3 values is tolerable. Alternatively since for small changes in F_3 there may be large changes in Δh it may be more realistic to iterate around the Δh term until differences are until an acceptable error. Appendix 1 gives an example calculation of afflux worked in this way.

6.3.2 Mathematical representation

Although Fig 49 may be used directly and applies to all types of bridges tested to date, mathematical representation would be more applicable to the Flucomp method of analysis. A number of methods using mathematical and computer techniques were tried in order to more accurately represent the data from all the tests.

A visual fitting of the curves in Fig 49, indicated a polynomial of the form $\Delta h/d_3 = aF_3^2 + b F_3 + c$ (10)

This can be expanded to

$$\Delta h/d_3 = (a_1 J_1^2 + a_2 J_1 + a_3) F_3^2 + (b_1 J_1^2 + b_2 J_1 + b_3) F_3 + (c_1 J_1^2 + c_2 J_1 + c_3) \quad (11)$$

with a, b and c dependent on and having a systematic change with blockage ratio J_1. The terms c_1, c_2 and

c_3 can be disregarded since they represent the 'no flow' case and a_3, b_3 and c_3 can be eliminated as they represent a 'no bridge' situation.

Quadratic equations were obtained for each of the curves of blockage ratio 0.2 to 0.7 from a best fit polynomial program. Resultant equations are tabulated in Table 5. In order to obtain a comprehensive equation (10) to fit all the data, the coefficients of the F_3^2 term (a) and the F_3 term (b) were plotted separately against J_1. This method enabled a mathematical expression for a and b to be obtained.

Fig 50 shows the linear regression relation between a and J_1 as

$$a = 1.257\ J_1 + 0.0257 \qquad (12)$$

with an associated correlation coefficient of 0.98. The intercept value of 0.0257 was initially thought representative of the friction loss in the flume. In the absence of a bridge

$$\frac{\Delta h}{d_3} = 0.0257\ \frac{V^2}{gd_3}$$

and for uniform flow

$$\frac{\Delta h}{\Delta x} = \frac{Q^2}{A^2\ 32gd\ \log^2\left(\frac{14.8\ d}{Ks}\right)}$$

Evaluating friction loss at one section where

$d_3 = 0.1$, and $x = 5$m

$$\log^{-1}\left(\frac{14.8\ d_3}{Ks}\right) = \frac{(0.0257 \times 32 \times 0.1)^{\frac{1}{2}}}{5}$$

gives an extremely low roughness coefficient Ks unrepresentative of the flume. It was considered therefore that the intercept value was a result of scatter in the data due to visual curve fitting.

Considering now the b coefficient of the F_3 term in equation 10, Figs 51, 52 and 53 show various regression analyses on the variables b and J_1. Although each plot shows a degree of scatter the best correlation coefficient of 0.98 was attached to the relation

$$b = 1.9\ J_1^{2.5} + 0.024 \qquad (13)$$

The full expansion of equation (10) from the above mathematical interpretation became

$$\frac{\Delta h}{d_3} = (1.257\ J_1 + 0.0257)\ F_3^2 + (1.9\ J_1^{2.5} + 0.024)\ F_3 \tag{14}$$

The present mathematical method of estimating afflux incorporated into the Flucomp model utilises the downstream water level, in a region of re-established uniform flow, to determine the amount of obstruction to flow caused by a bridge. If a relation could be established which included blockage ratio J_3 calculated from a known downstream depth instead of upstream depth then a similar plot of Fig 49 or resultant equation could be used directly from known downstream conditions.

Fig 54 shows a plot of $\Delta h/d_3$ against F_3 with visually fitted contours of downstream blockage ratio J_3 described. There was more scatter of points within blockage ratio ranges than on Fig 49 and it was difficult to achieve a best fit family of curves, even excluding those points for which flow was supercritical. However best fit polynomials were obtained for the curves of blockage ratio from 0.2 to 0.6 and are listed in Table 6. A similar analysis to that described above to obtain the a and b coefficients in the general equation (10)

resulted in

$$a = 9.87\ J_3 - 1.524 \tag{15}$$

Although the correlation coefficient of 0.919 for this linear relation indicated a good fit, the standard deviation in the y direction, σ_y, (coefficient of the F_3^2 term) had a large value of 1.5; σ_x was 0.14.

Applying a power regression analysis to the plot of coefficients of the F_3^2 term against J_3 gave a better relationship of the form

$$a = 2.19\ J_3^{1.538} \tag{16}$$

with correlation coefficient of 0.917 and standard deviation in the y direction much lower at 0.65; σ_x had however, increased to 0.39.

It proved to be an unsolvable task to determine the coefficient b in equation (1), from the hand fitted curves of Fig 54. It was therefore concluded that there was no simple relation between afflux ratio, downstream Froude number and blockage ratio based on downstream depth. The often turbulent conditions in the downstream channel and supercritical flow within the bridge arch may have relatively little influence an upstream levels.

A computer graphics program was used to more accurately present the curves on Fig 49 and produce a representative equation for the surface. This data smoothing technique allowed the generation of a smooth surface through the use of representative polynomials. The program generated polynomial coefficients from the data $\frac{\Delta h}{d_3}$, F_3 and J_1 and used the coefficients to produce a surface grid. The method of least squares was applied to obtain the surface equation.

Fig 55 shows the resultant 'smooth surface contours' generated by this method. The program is obviously extremely sensitive to the neighbourhood density of points, the curve smoothing may be greatly influenced by an isolated point producing infinite gradients which the program could not cope with. Also the plot required all curves to originate at zero. To overcome these difficulties the parameters of $\frac{\Delta h}{d_3}$, F_3 and J_1 were plotted in a different form so that the program could more easily fit curves. Fig 56 shows the parameter $\frac{J_1}{1-J_1}$ as a function of F_3 and $\frac{\Delta h}{d_3}$.

The generated polynomial from this surface plot was

$$\frac{\Delta h}{d_3} = -\,0.02 - 0.065\left(\frac{J_1}{1-J_1}\right) + 0.0127\left(\frac{J_1}{1-J_1}\right)^2 + 0.0819\,F_3 + 0.175\,F_3^{\,2} + 0.626\left(\frac{J_1}{1-J_1}\right)F_3 \qquad (17)$$

6.4 Friction loss

As mentioned in Section 4 a second method of calculating afflux eliminated headloss due to friction of the channel by extrapolating hydraulic gradients to the bridge face. Table 2 lists afflux values calculated in this way, and compares with Method 1.

The table shows that in the cases of the single arch bridge and lengthened bridge, removal of the friction term caused afflux to be lowered by between 10% and 20%. However as the channel was widened and blockage ratio increased causing discharge range to be limited, as in Tests 10-20, there was virtually no friction loss due to the channel.

It was anticipated that reduction in afflux due to friction loss would be of the same degree with the triple arch bridge was with the single arch unit. However relatively steep water surface slopes of the multiple arch bridge showed large friction losses.

Afflux calculation by Method 2 was very sensitive to slope measurement, in fact at low flows with the three arch bridge, afflux measurements were negative. Since at the high flows on the three arch bridge friction losses accounted for 10-20% of the total headloss, as with the single arch unit, it was believed that the error in the high values of friction loss calculated at the lower flows were within the tolerance of experimental slope measurements.

Total headloss measured throughout the tests was reduced by 10-20% by losses due to channel friction. As the channel became wider, and discharges accordingly lower due to blockage increase, friction loss became negligible.

The reduced headloss values Δ/h' are plotted in Fig 57 with afflux ratio as a function of F_3 and J_1. Table 2 shows higher than average friction loss values measured at low flows and these are reflected in the amount of scatter in this area of the plot. Curves in the figure were visually fitted. A similar mathematical technique to that discussed earlier to represent the whole plot as a single comprehensive equation was applied. However there was more scatter involved in Fig 57 and no simple mathematical function could be fitted.

6.5 Drag coefficient

The theoretical approach to an understanding the behaviour of flow through arch bridges was based on that developed by Ranga Raju et al (Ref 3). Their experiments were with cylindrical cylinders placed in open channels for which the drag coefficients C_D had been predetermined.

Equation 7 showed the theoretical relationship between afflux, downstream Froude number, blockage ratio and drag coefficient

$$\frac{\Delta h}{d_3} = \frac{(F_3^2 - 1) + ((F_3^2 - 1)^2 + 3\ C_D\ F_3^2\ J_1)^{\frac{1}{2}}}{3} \qquad (7)$$

The plot of Fig 49 relating the parameters indicated a unique relation for all the types of bridges tested. This led to the proposition that there was a C_D relation which would apply to all the tests, since it would primarily depend on bridge shape and configuration and hence blockage ratio. It was expected that C_D would vary with dramatic changes in bridge shape such as pier or arch geometries.

Equation 7 was rearranged into the form

$$C_D = \frac{[3\frac{\Delta h}{d_3} - F_3{}^2 + 1]^2 - [F_3{}^2 - 1]^2}{3\, F_3{}^2\, J_1} \tag{18}$$

and in order to assess the influence of blockage to flow on the drag coefficient, C_D was plotted against $1/J_1$, Fig 58. The figure clearly shows that coefficient of drag increases steadily to a value of approximately 1.0 as the area available to flow becomes proportionally less tending to J_1 of 0.4. Above this value of 1.0 the coefficient of drag increases rapidly as blockage is increased and the bridge arch acts as a submerged orifice or undershot sluice.

The tests fall on three curves. For a given blockage value below 0.4 an effectively wider pier (Tests 10 to 20) caused a higher drag coefficient. Similarly, an increase in the number of arches caused larger coefficients.

The basic theoretical equation (1)

$$\rho g \frac{d_1}{2} d_1 B - \rho g \frac{d_3}{2} d_3 B - C_D \rho (J_1 d_1 B) \frac{V_1{}^2}{2}$$

$$= \rho V_3 d_3 B (V_3 - V_1) \tag{1}$$

shows that as the constriction through the bridge becomes smaller and contraction losses and expansion losses larger, the large velocities actually at the constriction are not wholly accounted for in the $C_D \rho J_1 d_1 B \frac{V_1{}^2}{2}$ term by the upstream velocity and therefore the C_D value has compensated by dramatic increases.

7 SUMMARY OF RESULTS

1. It was found that lengthening a single semi-circular arch bridge by up to 3 times its original length caused afflux to be reduced as compared with the original basic bridge. This lowering effect increased with discharge and occurred when levels were close to or above bridge soffit.

2. An increase in pier width, or an effective reduction in opening area available to flow, raised afflux as compared with the basic original

width bridge. This effect increase with discharge over full range of water levels.

3. Behaviour of flow through a single arch unit cannot be similarly attributed to a multiple arch bridge made up of combinations of the single arch. For a given unit discharge and tailwater level, afflux was larger with the three arch bridge than the single arch bridge. This increase varied with flow and was apparent over the full tested range of water levels.

4. It was shown theoretically that afflux caused by an obstruction to flow was dependent upon downstream Froude number F_3 and blockage ratio J_1. Data from all the bridges tested fitted well on a plot of $\frac{\Delta h}{d_3}$ against F_3 and upstream blockage ratio J_1 and this set of curves may be used iteratively to determine afflux caused by a semi-circular arch from known downstream normal flow conditions.

5. Mathematical representations of the plot were made using a technique to fit polynomials to visually fitted curves and also a computer program which produced a smooth surface grid to the data points. The first technique was susceptible to errors in fitting the curves visually and this was reflected in the degree of scatter in the mathematical relations.

6. A method of determining afflux from the measured data was used by extrapolating the normal flow hydraulic gradient to either side of the bridge, thereby eliminating the channel friction loss. Channel friction loss accounted for between 10% and 20% of the total headloss.

7. For the same degree of blockage to flow the coefficient of drag was greater for a bridge with wider piers or multiple arches. Considering the tests as a whole, drag coefficient increased uniformly as blockage to flow increased until blockage reached 40%. Beyond this value the coefficient of drag rapidly enlarged due to the effective constriction area becoming so small that flow characteristics were similar to an undershot sluice or submerged orifice.

8. For the same flow conditions, the Flucomp mathematical model technique overestimated bridge afflux by as much as 20% compared to the physical model tests, in the region of flows above bridge

soffit. Below soffit levels computed and measured levels agreed well.

9. Afflux caused by a semi-circular arch bridge may be determined from a set of curves relating on afflux/depth ratio to normal depth Froude number and a blockage ratio. Predetermined parameters of discharge, normal depth of flow and hence Froude number, allow an initial estimate of afflux to be made from which a blockage ratio is calculated. Using the curves a final value of afflux is arrived at iteratively.

8 FUTURE RESEARCH

It is intended to continue experimental and field work to extend the series of tests already carried out to investigate

(i) the effect of pier shape, cutwaters etc

(ii) the effect of different soffit levels for multiple arched bridges

(iii) skewed and eccentric arch bridges

(iv) the effect of different arch shapes

(v) hydraulically long bridges

(vi) compare experimental and field data

(vii) produce an engineering guide and associated software.

9 ACKNOWLEDGEMENTS

This work was sponsored by the Ministry of Agriculture, Fisheries and Food as part of a strategic research programme of Hydraulics Research. The opinions expressed in this report however do not reflect the views or policy of the Ministry. The author carried out the work in Mr E Whitehead's Section of the River Engineering Department headed by Dr W R White. The author acknowledges the efforts of Miss J White who undertook a substantial amount of laboratory tests.

10 REFERENCES

1. Hydraulic of bridge waterways. US Dept. of Transport, Bureau of Public Roads, Washington, 1970.

2. Head losses and air entrainment at surcharged manholes B Archer, F Bettess, P J Colyer. HRS Report No IT 185, November 1978.

3. Rational assessment of blockage effect in channel flow past smooth circular cylinders. K G Ranga Raju, G L Asawa, O P S Rana, A S N Pillai. J. Hyd. Res. V 21, 1983 No 4.

4. Open channel hydraulics. Ven Te Chow, McGraw Hill.

5. Hydraulics of single span arch bridge constrictions. J. Hyd. Res. V 88, No HY2, March 1962, Part 1.

APPENDIX

Calculation of afflux: a worked example using the graphical method

Consider a semi-circular arched bridge of arch radius R of 15m in a rectangular channel 9.2m wide. The piers or abutments 1.6 mare wide and square edged. The overall height of the bridge is 5m. Assuming flood discharge is $47.4m^3/s$ and normal downstream depth is 3.55m, the associated Froude number $F_3 = v_3/\sqrt{gd_3}$ is 0.2464.

Let the first estimate of upstream depth d_1 be 3.8m. The total area of bridge causing blockage to flows above soffit level is

$$BA = 2\left[\frac{BR}{2} - \mathrm{Sin}^{-1}\ \frac{1}{360°}\ \pi R^2\right] + \left[(d_1 - R)\ B\right] \text{ (see Fig 43)}$$

$$= 2\ [4.6 \times 3.0 - 0.25 \times 3.142 \times 9.0] + [0.8 \times 9.2]$$

$$= 20.822m^2$$

$$\text{Blockage ratio } J_1 = \frac{BA}{\text{total area of flow}} = \frac{20.822}{B.d_1}$$

$= 0.5959$

From Figure 49, when $F_3 = 0.2464$ once $J_1 = 0.5959$

$\Delta h/d_3 = 0.155$

$\therefore$ since $\Delta h = d_1 - d_3$
$d_1 = 4.096m$

Using this new value of d_1 and repeating the procedure

$BA = 23.52m^2$

$J_1 = 23.52\ /\ (9.2 \times 4.096)$
$= 0.6241$

From Figure 49, $\frac{\Delta h}{d_3} = 0.18$

$d_1 = 4.184m$

Iterating again, using the new value of d_1 above gives

$BA = 24.32 m^2$

$J_1 = 24.32 / (9.2 \times 4.184)$
$= 0.6318$

From Figure 49, $\frac{\Delta h}{d_3} = 0.19$

$d_1 = 4.22m$

Iterating further, $BA = 24.68m^2$

$J_1 = 24.68 / (9.2 \times 4.22)$
$= 0.6357$

From Figure 49, $\frac{\Delta h}{d_3} = 0.192$

$d_1 = 4.226$

The iteration closes around the value of upstream water level of 4.23m.

TABLES.

TABLE 1

Field Data - response from Water Authorities

Water Authority	No of bridges with high afflux	Details
Wessex Water (Avon & Dorset Division)	16	6 bridges nowhere max. level recorders
Welsh Water (Dee & Clywd Division)	5	Measurements available for 2 sites
Wessex Water (Bridgewater)	18	2 sites to be monitored
Anglian Water (Oundle Division)	6	Incomplete data available
Tay River Purification Board (Perth)	12	2 sites to be monitored
Yorkshire Water (Northern area)	32	Details available for 32 sites
Yorkshire Water (Western District)	6	Details available for 2 sites
Southern Water (Isle of Wight)	6	Incomplete data available
Severn Trent Water (Lower Trent Division)	1	Details available for 1 site
Northumbrian Water (Tees Division)	4	Incomplete data available
Severn Trent Water (Avon Division)	32	Details available for 32 sites
Northumbrian Water (Tyne & Wear Division)	6	Details available for 4 sites
Wessex Water (Bristol Avon Division)	3	Incomplete data available
Anglian Water (Colchester Division)	9	Incomplete data available
Yorkshire Water (Leeds)	Numerous	Intensive coverage of Batley Beck with level recorders. River has many bridges and culverts. 6 bridge sites on River Spen also monitored
Thames Water (Eastern Division)	11	Limited details available for 2 sites

TABLE 1 (Cont'd)

Water Authority	No of bridges with high afflux	Details
Welsh Water (Taff Division)	31	Incomplete data available
Southern Water (Kent Division)	15	Data available for 2 sites
North West Water (Rivers Division)	8	Details available for 4 sites

TABLE 2

Comparison of headlosses calculated by Methods 1 and 2.

Δh = afflux calculated between tappings 1 and 12 (Method 1)
$\Delta h'$ = afflux calculated at bridge from extrapolated hydraulic gradients (Method 2)

TEST NO	Δh (m)	$\Delta h'$ (m)	TEST NO	Δh (m)	$\Delta h'$ (m)
2a	0.0049	0.0049	10a	0.0080	0.0056
b	0.0031	-	b	0.0040	0.0037
c	0.0020	-	c	0.0036	0.0030
d	0.0019	0.0013	d	0.0037	0.0034
e	0.0026	0.0055	e	0.0042	0.0039
f	0.0031	0.0040	f	0.0046	0.0046
3a	0.0344	0.0262	11a	0.0439	0.0392
b	0.0172	0.0113	b	0.0251	0.0213
c	0.0144	0.0103	c	0.0191	0.0162
d	0.0182	0.0065	d	0.0213	0.0192
e	0.0204	0.0209	e	0.0273	0.0249
4a	0.0613	0.0537	12a	0.0895	0.0857
b	0.0353	0.0253	b	0.0461	0.0414
c	0.0345	0.0298	c	0.0440	0.0387
d	0.0406	0.0371	d	0.0497	0.0476
5a	0.1392	0.1339	13a	0.1641	0.1603
b	0.0792	0.0751	14a	0.0121	0.0118
6a	0.0054	0.0030	b	0.0067	0.0069
b	0.0027	0.0018	c	0.0050	0.0053
c	0.0022	0.0013	d	0.0047	-
d	0.0023	0.0023	e	0.0051	0.0057
e	0.0032	0.0029	f	0.0058	0.0067
f	0.0037	0.0022	g	0.0061	0.0067
7a	0.0329	0.0256	15a	0.0570	0.0561
b	0.0118	0.0077	b	0.0406	0.0397
c	0.0115	0.0088	c	0.0321	0.0315
d	0.0153	0.0126	d	0.0303	0.0306
e	0.0216	0.0198	e	0.0342	0.0345
8a	0.0640	0.0537	f	0.0374	0.0377
b	0.0383	0.0307	g	0.0378	0.0378
c	0.0292	0.0233	16a	0.0726	0.0717
d	0.0366	0.0337	b	0.0451	0.0436
9a	0.1400	0.1344	c	0.0394	0.0391
b	0.0618	0.0568	d	0.0378	0.0372
			e	0.0409	0.0403
			f	0.0432	0.0439
			17a	0.1092	0.1162
			b	0.0635	0.0623
			c	0.0615	0.0609
			d	0.0602	0.0599
			e	0.0589	0.0589
			18a	0.1276	0.1261
			c	0.0767	0.0758
			d	0.0725	0.0725
			e	0.0729	0.0708

TABLE 2 (Cont'd)

Comparison of headlosses calculated by Methods 1 and 2 (Cont'd)

TEST NO	Δh (m)	$\Delta h'$ (m)
19a	0.1333	0.1409
b	0.0834	0.0869
c	0.0856	0.0844
20a	0.1458	0.1437
25a	0.0081	0.0022
b	0.0061	0.0011
c	0.0073	0.0029
d	0.0095	0.0048
e	0.0109	0.0065
26a	0.0141	0.0056
b	0.0133	0.0063
c	0.0182	0.0120
d	0.0202	0.0146
27a	0.0270	0.0188
b	0.0272	0.0204
c	0.0338	0.0270
28a	0.0381	0.0302
b	0.0393	0.0322
29a	0.0792	0.0704
b	0.0549	0.0844

TABLE 3

Data from Model Tests

TEST	Q (m^3/s)	d_1 (m)	d_3 (m)	J_1	J_3	F_3	Depth at G9 (m)	MODEL DESCRIPTION
2A	.01	.0747	.0698	.1556	.1506	.5092	.0747	SINGLE ARCH BRIDGE
2B	.01	.0907	.0876	.1748	.1707	.3622	.0890	WIDTH 0.34m
2C	.01	.1227	.1207	.2295	.2254	.2239	.1220	"
2D	.01	.1487	.1468	.3016	.3000	.1669	.1485	"
2E	.01	.1875	.1849	.4456	.4378	.1181	.1885	"
2F	.01	.2136	.2105	.5133	.5062	.0972	.2139	"
3A	.025	.1189	.0845	.2217	.1668	.9557	.1161	"
3B	.025	.1354	.1182	.2598	.2203	.5777	.1334	"
3C	.025	.1571	.1427	.3383	.2809	.4355	.1557	"
3D	.025	.1989	.1807	.4774	.4247	.3056	.1949	"
3E	.025	.2379	.2175	.5630	.5221	.2314	.2381	"
4A	.035	.1625	.1012	.3603	.1901	1.0209	.1599	"
4B	.035	.1713	.1360	.3932	.2614	.6553	.1679	"
4C	.035	.2043	.1698	.4912	.3878	.4697	.2027	"
4D	.035	.2363	.1957	.5601	.4688	.3796	.2351	"
5A	.044	.2311	.0919	.5502	.1765	1.4831	.2293	"
5B	.044	.2348	.1556	.5573	.3319	.6732	.2334	"
6A	.0098	.0767	.0713	.1578	.1521	.4834	.0759	SINGLE ARCH BRIDGE
6B	.0098	.1134	.1107	.2110	.2060	.2498	.1131	LENGTH 0.06m
6C	.0098	.1446	.1424	.2869	.2799	.1712	.1443	"
6D	.0102	.1679	.1656	.3809	.3723	.1421	.1679	"
6E	.0102	.1993	.1961	.4784	.4699	.1103	.1992	"
6F	.0102	.2365	.2328	.5605	.5535	.0853	.2360	"
7A	.0248	.1196	.0867	.2231	.1696	.9122	.1171	"
7B	.0245	.1429	.1311	.2815	.2488	.4847	.1415	"
7C	.0245	.1728	.1613	.3984	.3555	.3551	.1719	"
7D	.0248	.2037	.1884	.4897	.4482	.2847	.2028	"
7E	.025	.2417	.2201	.5699	.5277	.2273	.2411	"
8A	.035	.1643	.1003	.3673	.1887	1.0347	.1608	"
8B	.035	.1683	.1300	.3823	.2462	.7012	.1657	"
8C	.035	.1878	.1586	.4465	.3446	.5203	.1858	"
8D	.035	.2359	.1993	.5593	.4784	.3694	.2349	"
9A	.044	.2288	.0888	.5457	.1723	1.5614	.2269	"
9B	.044	.2352	.1734	.5580	.4005	.5722	.2335	"
10A	.0105	.0795	.0715	.2492	.2415	.4614	.0787	SINGLE ARCH BRIDGE
10B	.0104	.1123	.1083	.2922	.2858	.2452	.1122	WIDTH 0.38m
10C	.0106	.1416	.1380	.3535	.3441	.1737	.1414	"
10D	.0103	.1692	.1655	.4503	.4380	.1285	.1691	"
10E	.01	.1996	.1954	.5340	.5240	.0973	.1995	"
10F	.01	.2318	.2272	.5987	.5906	.0775	.2318	"
11A	.0249	.1282	.0843	.3217	.2542	.8547	.1266	"
11B	.0248	.1375	.1124	.3429	.2924	.5529	.1362	"
11C	.025	.1589	.1398	.4147	.3487	.4018	.1579	"
11D	.0248	.1901	.1688	.5107	.4490	.3004	.1894	"
11E	.0247	.2388	.2115	.6105	.5602	.2134	.2380	"
12A	.035	.1787	.0892	.4795	.2599	1.1038	.1774	"
12B	.035	.1868	.1407	.5021	.3511	.5572	.1852	"
12C	.035	.2165	.1725	.5704	.4608	.4104	.2147	"
12D	.0349	.2481	.1984	.6251	.5312	.3318	.2474	"
13A	.0429	.2376	.0735	.6085	.2434	1.8089	.2363	"

TABLE 3 (Cont'd)

Data from Model Tests

TEST	Q (m^3/s)	d_1 (m)	d_3 (m)	J_1	J_3	F_3	Depth at G9 (m)	MODEL DESCRIPTION
14A	.0110	.0838	.0717	.3835	.3736	.3977	.0837	SINGLE ARCH BRIDGE
14B	.0105	.1039	.0972	.4046	.3969	.2405	.1040	WIDTH 0.46m
14C	.0104	.1304	.1254	.4435	.4349	.1625	.1305	"
14D	.0102	.1576	.1529	.5125	.4975	.1184	.1567	"
14E	.0104	.1847	.1796	.5840	.5722	.0948	.1849	"
14F	.0104	.2192	.2134	.6495	.6399	.0732	.2195	"
14G	.0103	.2447	.2386	.6860	.6780	.0613	.2449	"
15A	.0258	.1402	.0832	.4628	.3830	.7462	.1399	"
15B	.0262	.1439	.1033	.4713	.4039	.5477	.1436	"
15C	.0260	.1621	.1300	.5260	.4428	.3850	.1619	"
15D	.0261	.1889	.1586	.5933	.5155	.2868	.1890	"
15E	.0265	.2115	.1773	.6367	.5666	.2464	.2116	"
15F	.0264	.2362	.1988	.6747	.6135	.2067	.2363	"
15G	.0262	.2483	.2105	.6906	.6350	.1883	.2483	"
16A	.0290	.1529	.0803	.4975	.3805	.8845	.1526	"
16B	.0285	.1537	.1086	.5001	.4104	.5527	.1532	"
16C	.0288	.1713	.1319	.5515	.4463	.4173	.1712	"
16D	.0285	.1936	.1558	.6031	.5068	.3217	.1934	"
16E	.0290	.2203	.1794	.6512	.5717	.2649	.2201	"
16F	.0285	.2482	.2050	.6904	.6252	.2131	.2483	"
17A	.0360	.1936	.0844	.6031	.3841	1.0190	.1960	"
17B	.0355	.1943	.1308	.6046	.4443	.5209	.1939	"
17C	.0352	.2120	.1505	.6376	.4895	.4184	.2118	"
17D	.0350	.2276	.1674	.6624	.5335	.3547	.2275	"
17E	.0347	.2465	.1876	.6883	.5904	.2964	.2465	"
18A	.0385	.2141	.0865	.6411	.3860	1.0504	.2136	"
18C	.0378	.2101	.1334	.6343	.4491	.5385	.2098	"
18D	.0373	.2275	.1550	.6623	.5043	.4242	.2275	"
18E	.0380	.2385	.1656	.6778	.5360	.3914	.2378	"
19A	.0398	.2236	.0903	.6564	.3897	1.0180	.2262	"
19B	.0394	.2229	.1395	.6550	.4613	.5248	.2230	"
19C	.0400	.2467	.1611	.6885	.5231	.4294	.2463	"
20A	.0412	.2392	.0934	.6788	.3928	1.0018	.2385	"
21A	.0038	.0636	.0619	.1448	.1434	.0768	.0622	THREE ARCH BRIDGE
21B	.0029	.1073	.1062	.2001	.1982	.0262	.1060	WIDTH 1.02m
21C	.0028	.1572	.1561	.3387	.3341	.0145	.1558	"
21D	.0029	.2022	.2011	.4859	.4831	.0101	.2009	"
21E	.0029	.2449	.2444	.5755	.5747	.0075	.2421	"
22A	.0099	.0743	.0726	.1552	.1534	.1584	.0722	"
22B	.0099	.1138	.1129	.2117	.2101	.0817	.1126	"
22C	.0100	.1527	.1513	.3192	.3129	.0532	.1515	"
22D	.0102	.1995	.1977	.4789	.4742	.0365	.1976	"
22E	.0100	.2403	.2387	.5674	.5645	.0268	.2388	"
23A	.0254	.0935	.0892	.1787	.1728	.2984	.0915	"
23B	.0256	.1402	.1373	.2733	.2650	.1575	.1388	"
23C	.0253	.1942	.1906	.4647	.4546	.0952	.1929	"
23D	.0257	.2333	.2289	.5544	.5459	.0734	.2313	"
24A	.0347	.1021	.0966	.1915	.1831	.3618	.1005	"
24B	.0343	.1484	.1445	.3004	.2866	.1954	.1468	"

TABLE 3 (Cont'd)

Data from Model Tests

TEST	Q (m^3/s)	d_1 (m)	d_3 (m)	J_1	J_3	F_3	Depth at G9 (m)	MODEL DESCRIPTION
24C	.0350	.1863	.1813	.4420	.4266	.1419	.1848	"
24D	.0340	.2218	.2152	.5313	.5170	.1066	.2199	"
24E	.0358	.2494	.2417	.5832	.5699	.0943	.2866	"
25A	.0445	.1117	.1036	.2079	.1939	.4177	.1097	"
25B	.0442	.1439	.1378	.2847	.2664	.2705	.1422	"
25C	.0443	.1768	.1695	.4120	.3867	.1987	.1753	"
25D	.0441	.2143	.2048	.5149	.4924	.1489	.2127	"
25E	.0441	.2453	.2344	.5762	.5565	.1216	.2438	"
26A	.0611	.1308	.1167	.2481	.2173	.4797	.1279	"
26B	.0612	.1719	.1586	.3953	.3446	.3033	.1695	"
26C	.0617	.2115	.1933	.5085	.4622	.2272	.2094	"
26D	.0608	.2413	.2211	.5692	.5298	.1830	.2394	"
27A	.0800	.1558	.1288	.3328	.2433	.5417	.1530	"
27B	.0795	.1976	.1704	.4739	.3900	.3538	.1953	"
27C	.0792	.2391	.2053	.5652	.4937	.2665	.2368	"
28A	.0930	.1741	.1360	.4029	.2614	.5804	.1714	"
28B	.0900	.2325	.1932	.5529	.4619	.3317	.2301	"
29A	.1100	.2199	.1407	.5273	.2747	.6524	.2169	"
29B	.1100	.2270	.1721	.5421	.3960	.4823	.2248	"

TABLE 4

Comparison between Flucomp and Physical Model Results

TEST NO	DOWNSTREAM WATER LEVEL (m)	UPSTREAM WATER LEVEL PHYSICAL MODEL (m)	UPSTREAM WATER LEVEL FLUCOMP (m)
2a	0.0698	0.0747	.0771
b	.0876	.0907	.0921
c	.1207	.1227	.1236
d	.1468	.1487	.1524
e	.1849	.1875	.1915
f	.2105	.2136	.2170
3a	.0845	.1189	.1183
b	.1182	.1354	.1368
c	.1427	.1571	.1696
d	.1807	.1989	.2216
e	.2175	.2379	.2580
4a	.1012	.1625	.1521
b	.1360	.1713	.1689
c	.1698	.2043	.2501
d	.1957	.2363	.2753
5a	.0919	.2311	.1833
b	.1556	.2348	.2841
6a	.0713	.0767	.0775
b	.1107	.1134	.1136
c	.1424	.1446	.1459
d	.1656	.1679	.1725
e	.1961	.1993	.2029
f	.2328	.2365	.2386
7a	.0867	.1196	.1167
b	.1311	.1429	.1537
c	.1613	.1728	.2008
d	.1884	.2037	.2284
e	.2201	.2417	.2587
8a	.1003	.1643	.1507
b	.1300	.1683	.2136
c	.1586	.1878	.2391
d	.1993	.2359	.2705
9a	.0888	.2288	.2618
b	.1734	.2352	.2818
14a	.0717	.0838	.0848
b	.0972	.1039	.1043
c	.1254	.1304	.1302
d	.1529	.1576	.1597
e	.1796	.1847	.1866
f	.2134	.2192	.2197
g	.2386	.2447	.2433
15a	.0832	.1402	.1346
b	.1033	.1439	.1437
c	.1300	.1621	.1745
d	.1586	.1889	.2028
e	.1773	.2115	.2224
f	.1988	.2362	.2437
g	.2105	.2482	.2518

TABLE 4 (Cont'd)

Comparison between Flucomp and Physical Model Results

TEST NO	DOWNSTREAM WATER LEVEL (m)	UPSTREAM WATER LEVEL PHYSICAL MODEL (m)	UPSTREAM WATER LEVEL FLUCOMP (m)
16a	0.0803	0.1529	0.1461
b	.1086	.1537	.1582
c	.1319	.1713	.1864
d	.1558	.1936	.2086
e	.1794	.2203	.2329
f	.2050	.2482	.2555
17a	.0844	.1936	.1857
b	.1308	.1943	.2137
c	.1505	.2120	.2310
d	.1674	.2276	.2447
e	.1876	.2465	.2590
18a	.0865	.2141	.2022
c	.1334	.2101	.2271
d	.1550	.2275	.2449
e	.1656	.2385	.2547
19a	.0903	.2236	.2105
b	.1395	.2229	.2404
c	.1611	.2467	.2598
20a	.0934	.2392	.2198
21a	.0619	.0636	.0621
b	.1062	.1073	.1062
c	.1561	.1572	.1561
d	.2011	.2022	.2012
e	.2444	.2449	.2444
22a	.0726	.0743	.0734
b	.1129	.1138	.1132
c	.1513	.1527	.1520
d	.1977	.1995	.1985
e	.2387	.2403	.2393
23a	.0892	.2333	.2332
b	.1373	.1402	.1392
c	.1906	.1942	.1952
d	.2289	.0935	.0926
24a	.0966	.1021	.1021
b	.1445	.1484	.1506
c	.1813	.1863	.1902
d	.2152	.2218	.2234
e	.2417	.2494	.2492
25a	.1036	.1117	.1117
b	.1378	.1439	.1435
c	.1695	.1768	.1838
d	.2048	.2143	.2188
e	.2344	.2453	.2466
26a	.1167	.1308	.1297
b	.1586	.1719	.1861
c	.1933	.2115	.2208
d	.2211	.2413	.2469

TABLE 4 (Cont'd)

Comparison between Flucomp and Physical Model Results

TEST NO	DOWNSTREAM WATER LEVEL (m)	UPSTREAM WATER LEVEL PHYSICAL MODEL (m)	UPSTREAM WATER LEVEL FLUCOMP (m)
27a	0.1288	0.1558	0.1507
b	.1704	.1976	.2164
c	.2053	.2391	.2487
28a	.1360	.1741	.1968
b	.1932	.2325	.2506
29a	.1407	.2199	.2308
b	.1721	.2270	.2573

TABLE 5

Quadratic equations for J_1 curves from Fig 49

J_1	Equations
0.2	$\Delta h/d_3 = 0.324\ F_3^2 + 0.100\ F_3 - 0.021$
0.3	$\Delta h/d_3 = 0.410\ F_3^2 + 0.112\ F_3 - 0.014$
0.4	$\Delta h/d_3 = 0.462\ F_3^2 + 0.239\ F_3 - 0.028$
0.5	$\Delta h/d_3 = 0.639\ F_3^2 + 0.252\ F_3 - 0.008$
0.6	$\Delta h/d_3 = 0.750\ F_3^2 + 0.587\ F_3 - 0.026$
0.7	$\Delta h/d_3 = 0.964\ F_3^2 + 0.824\ F_3 - 0.006$

TABLE 6

Quadratic equations for J_3 curves from Fig 54

J_3	Equations
0.2	$\Delta h/d_3 = 0.944\ F_3^2 - 0.432\ F_3 + 0.071$
0.3	$\Delta h/d_3 = 1.134\ F_3^2 - 0.319\ F_3 + 0.058$
0.4	$\Delta h/d_3 = 1.500\ F_3^2 - 0.069\ F_3 + 0.0001$
0.5	$\Delta h/d_3 = 4.193\ F_3^2 - 0.931\ F_3 + 0.082$
0.6	$\Delta h/d_3 = 4.350\ F_3^2 - 0.225\ F_3 + 0.021$

FIGURES.

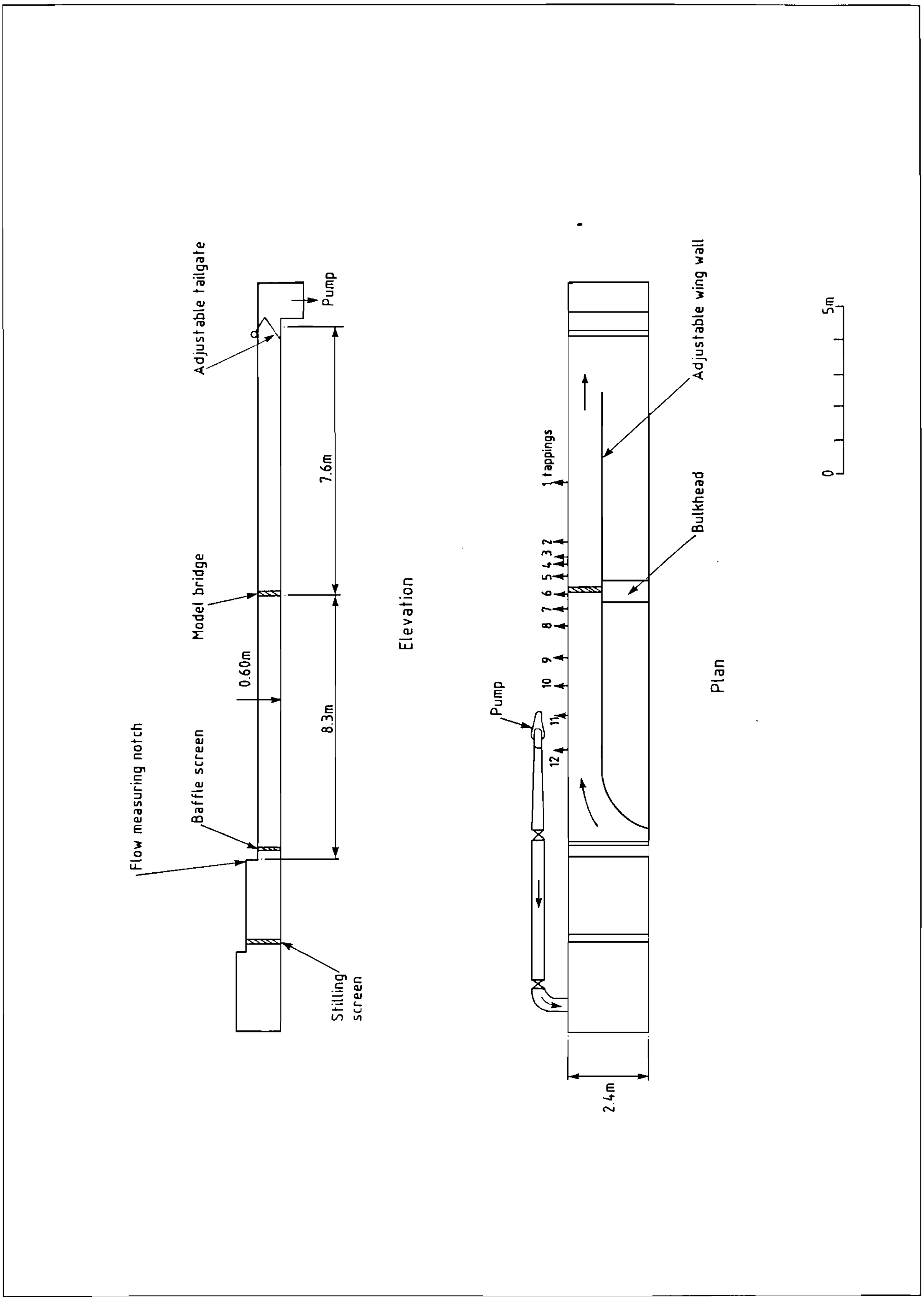

Fig 1 Layout of model

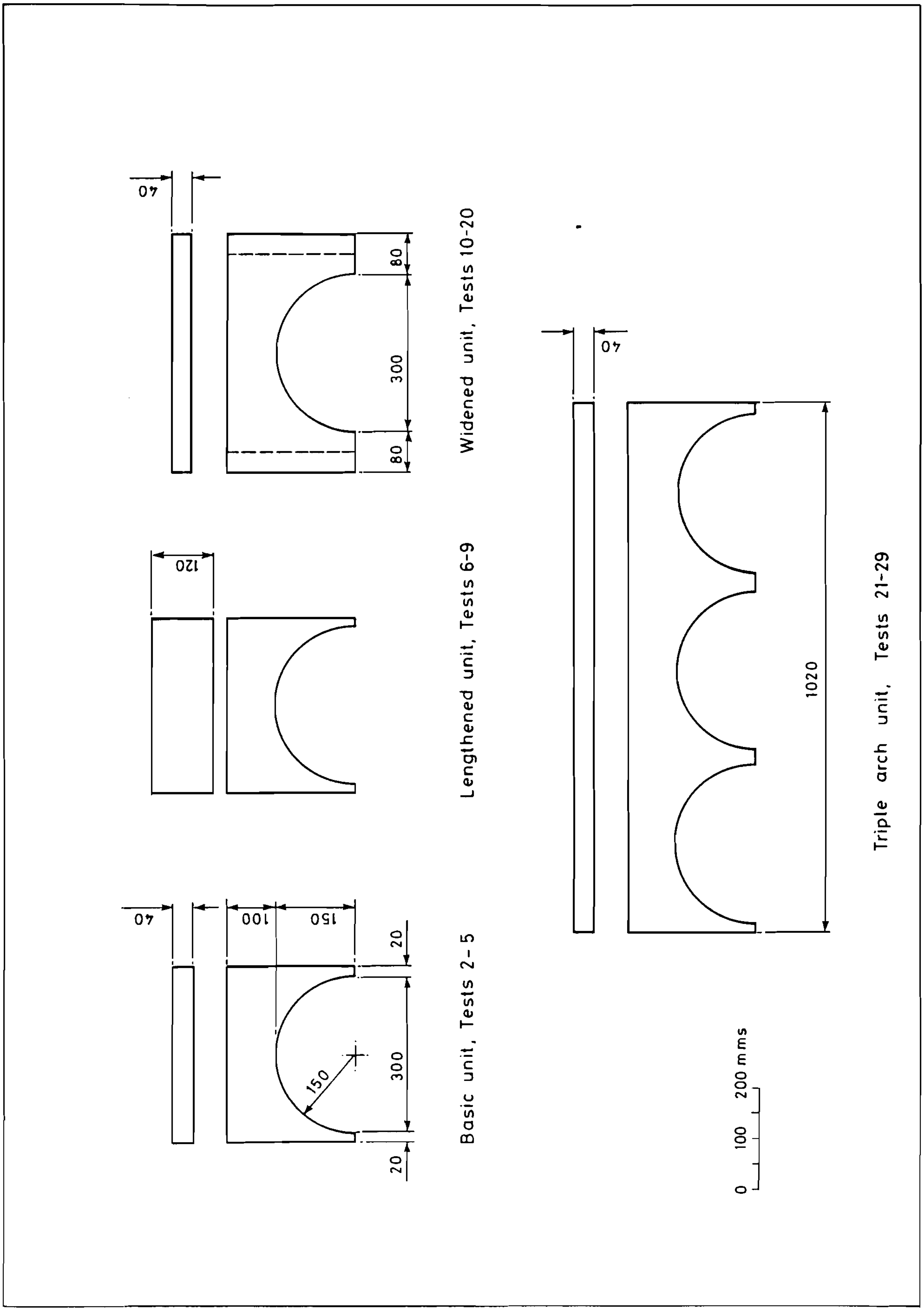

Fig 2 Model bridge designs

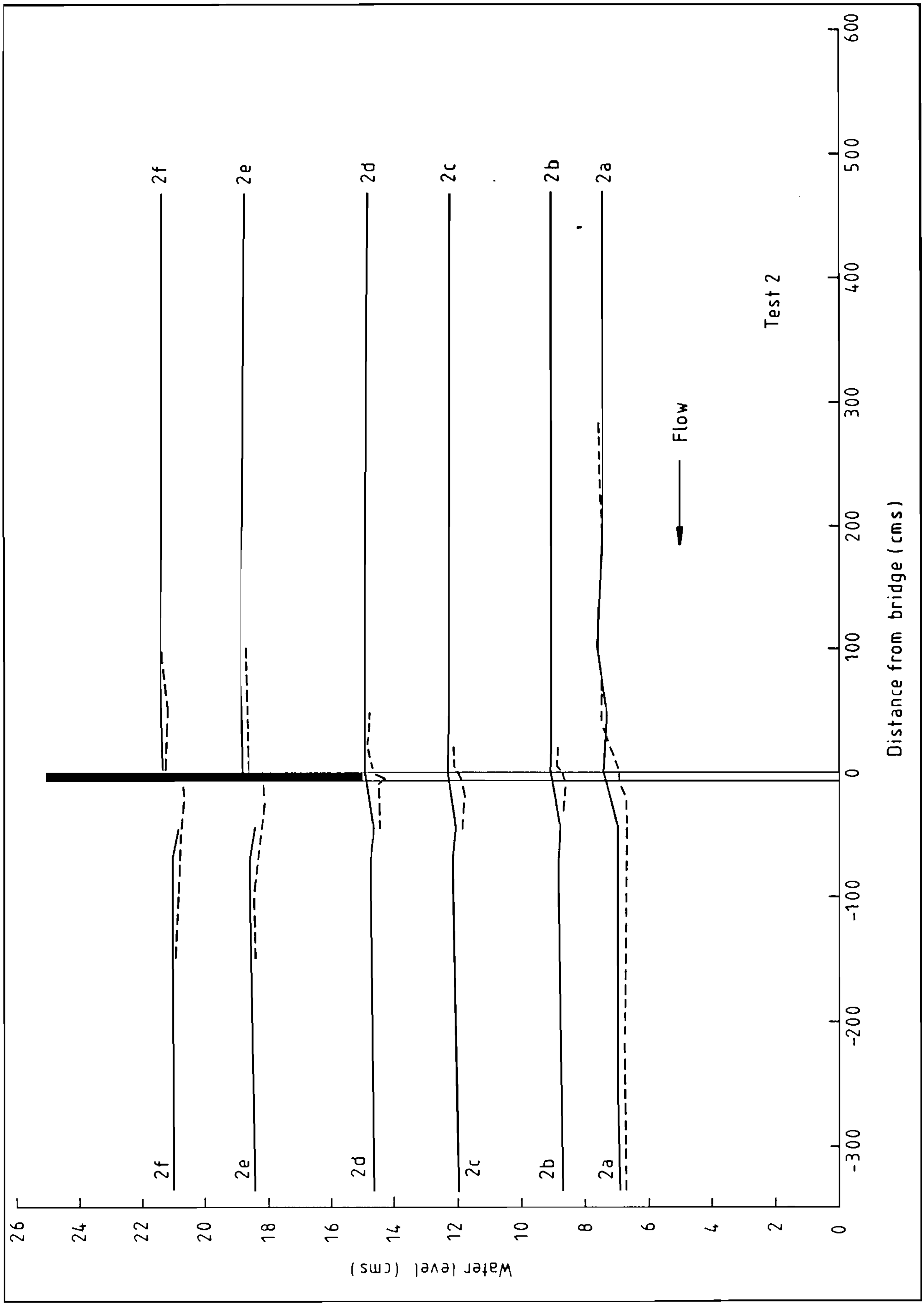

Fig 3 Water surface profiles, test 2, discharge 0·01 m^3/s

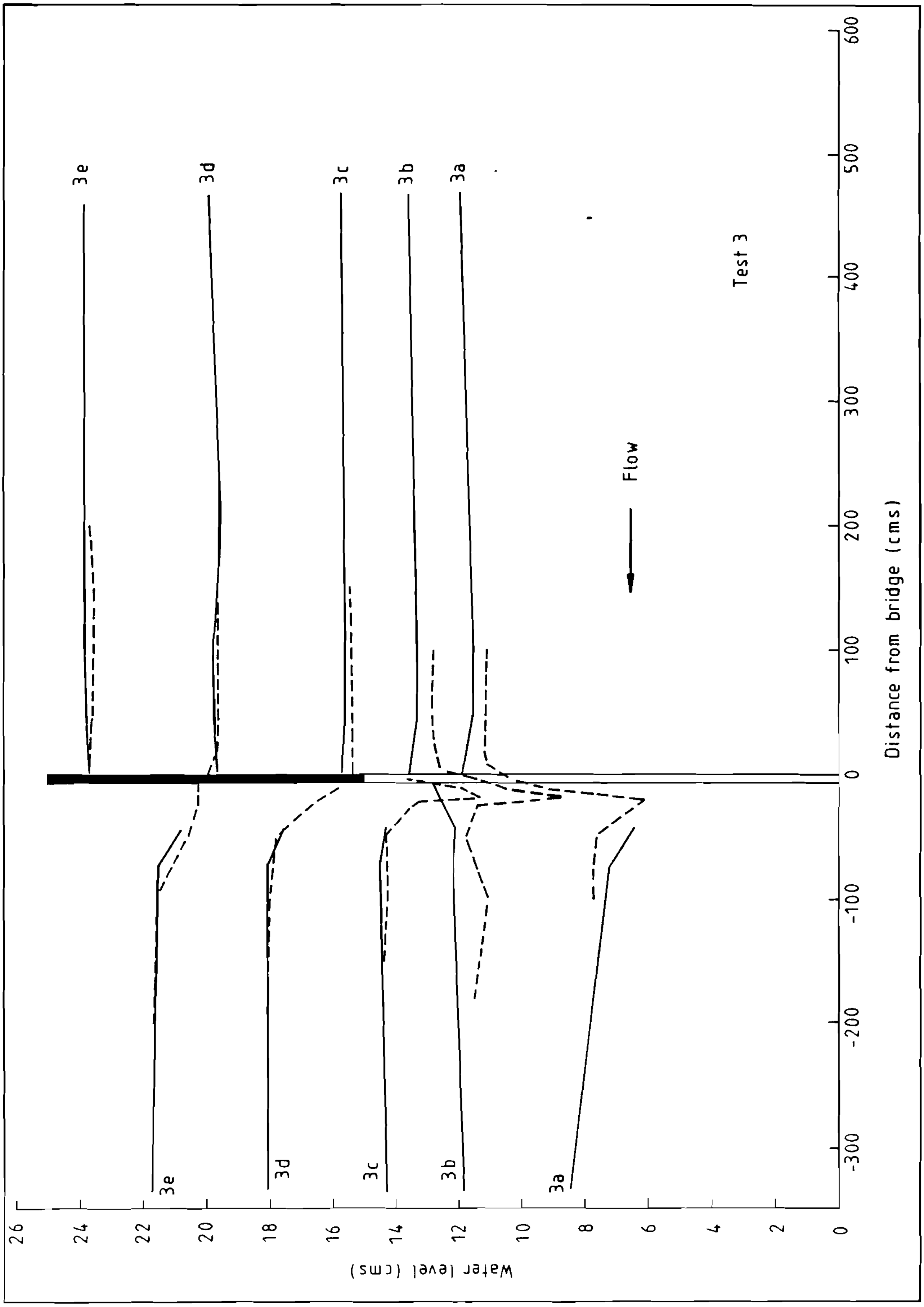

Fig 4 Water surface profiles, test 3, discharge 0·025 m^3/s

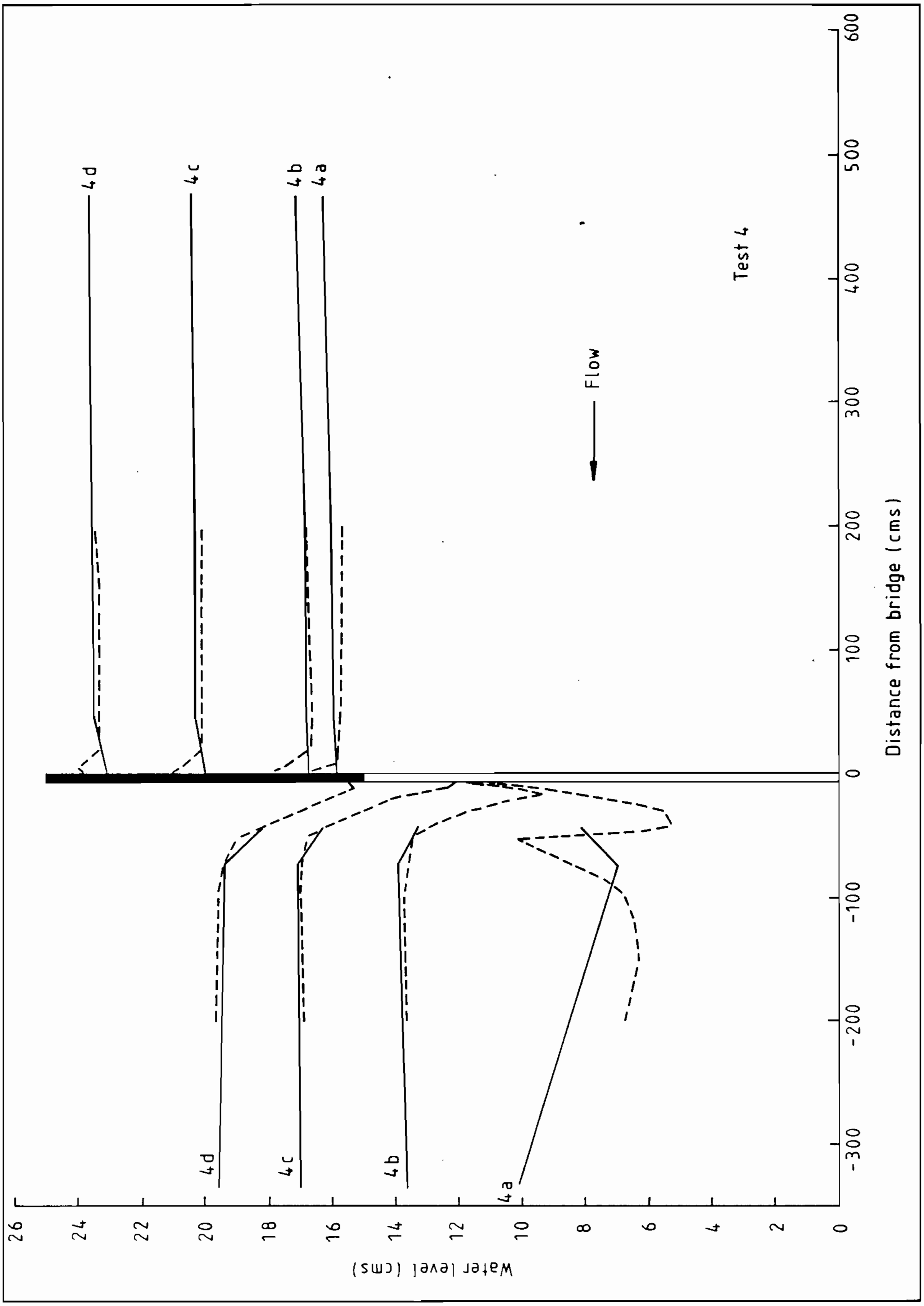

Fig 5 Water surface profiles, test 4, discharge 0·035 m^3/s

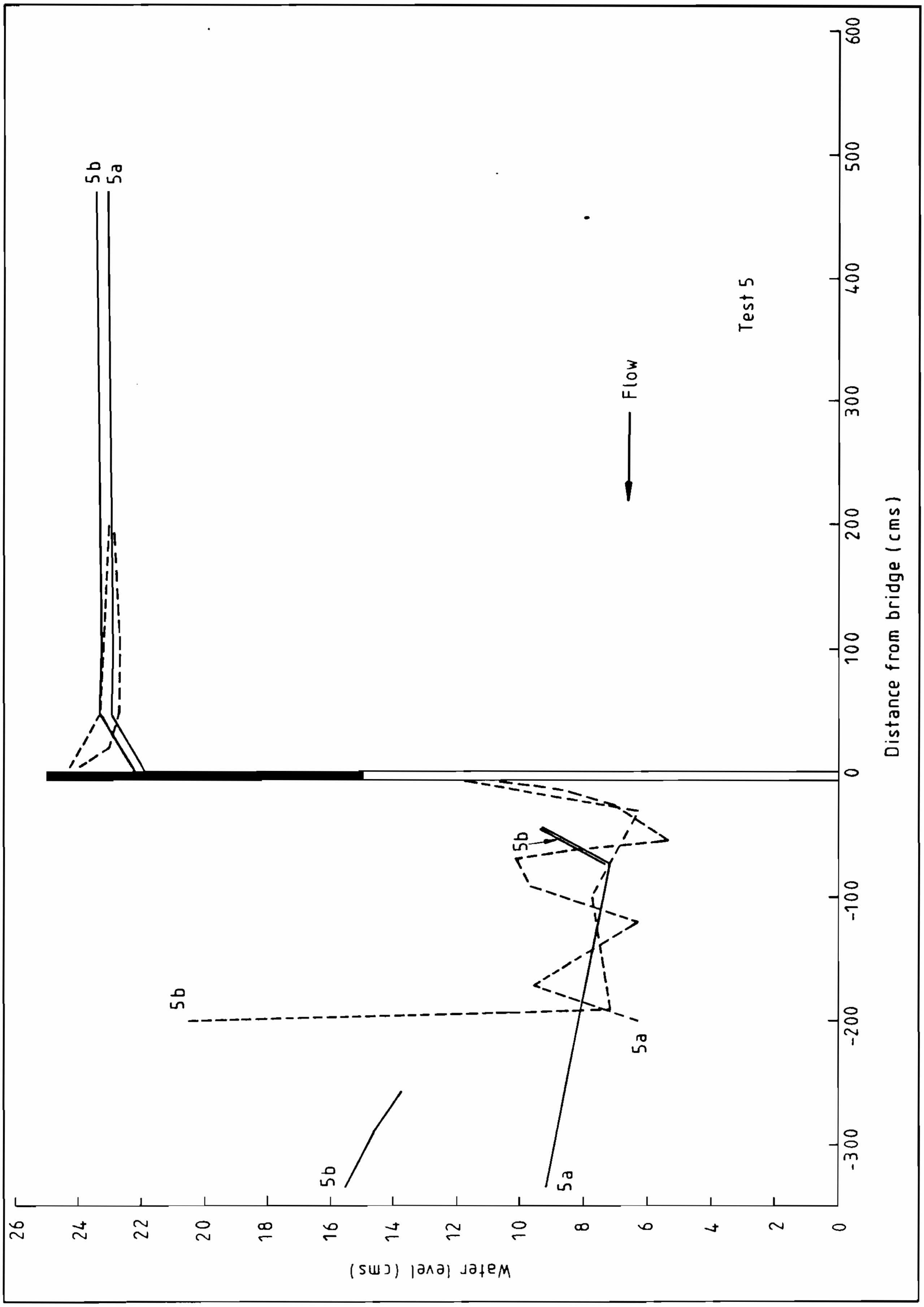

Fig 6 Water surface profiles, test 5, discharge 0·044 m^3/s

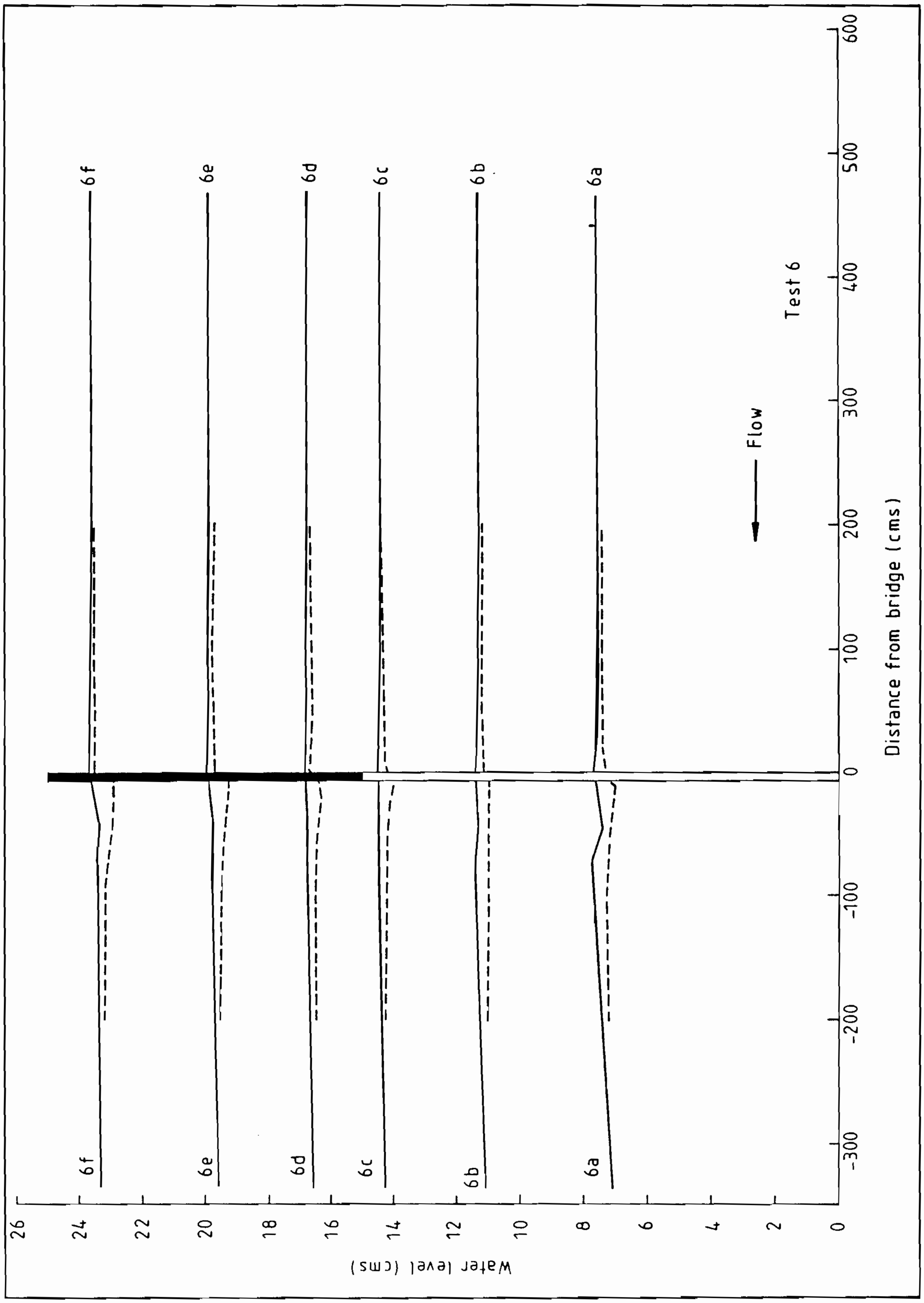

Fig 7 Water surface profiles, test 6, discharge 0·0098 m^3/s

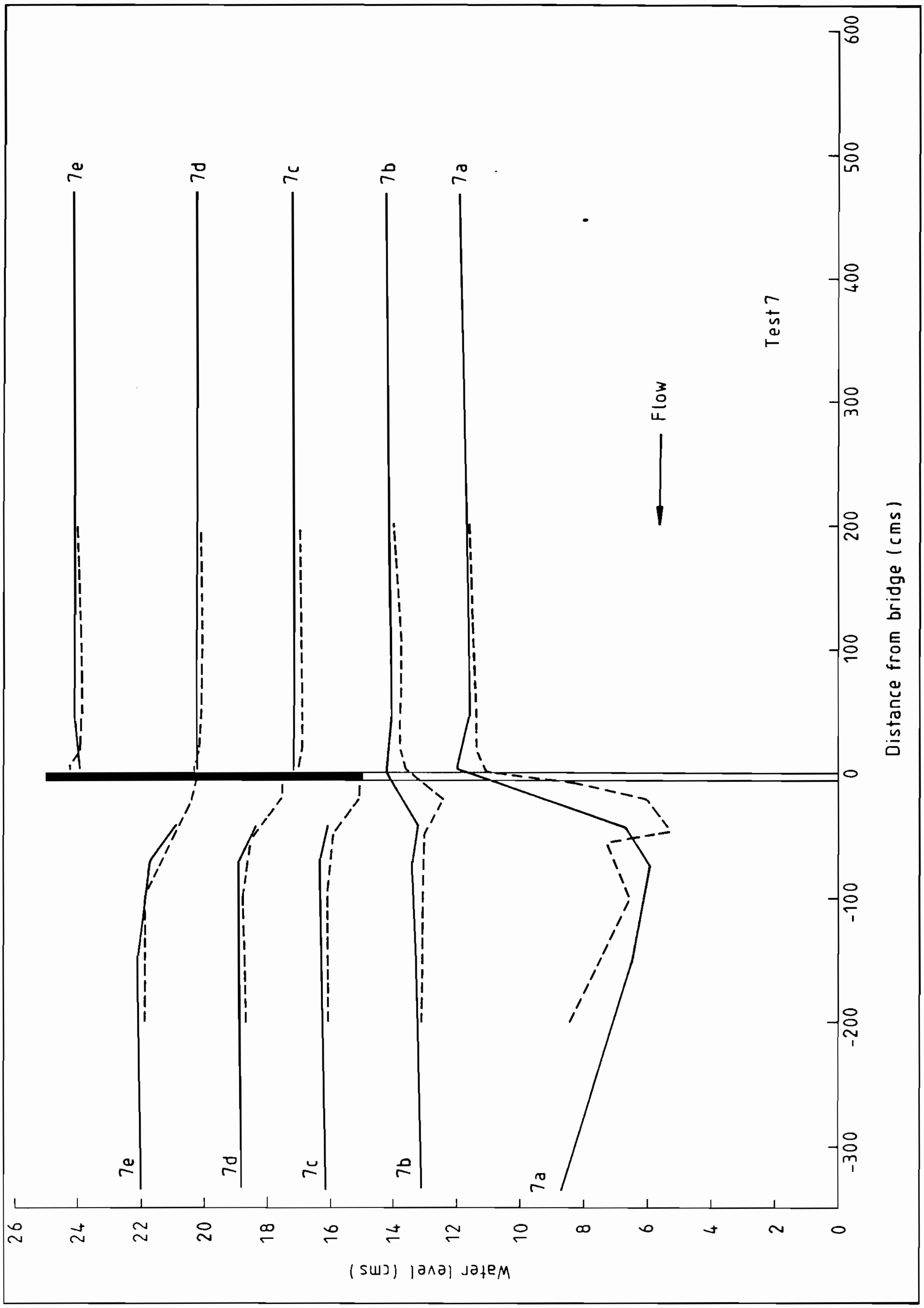

Fig 8 Water surface profiles, test 7, discharge 0·025 m^3/s

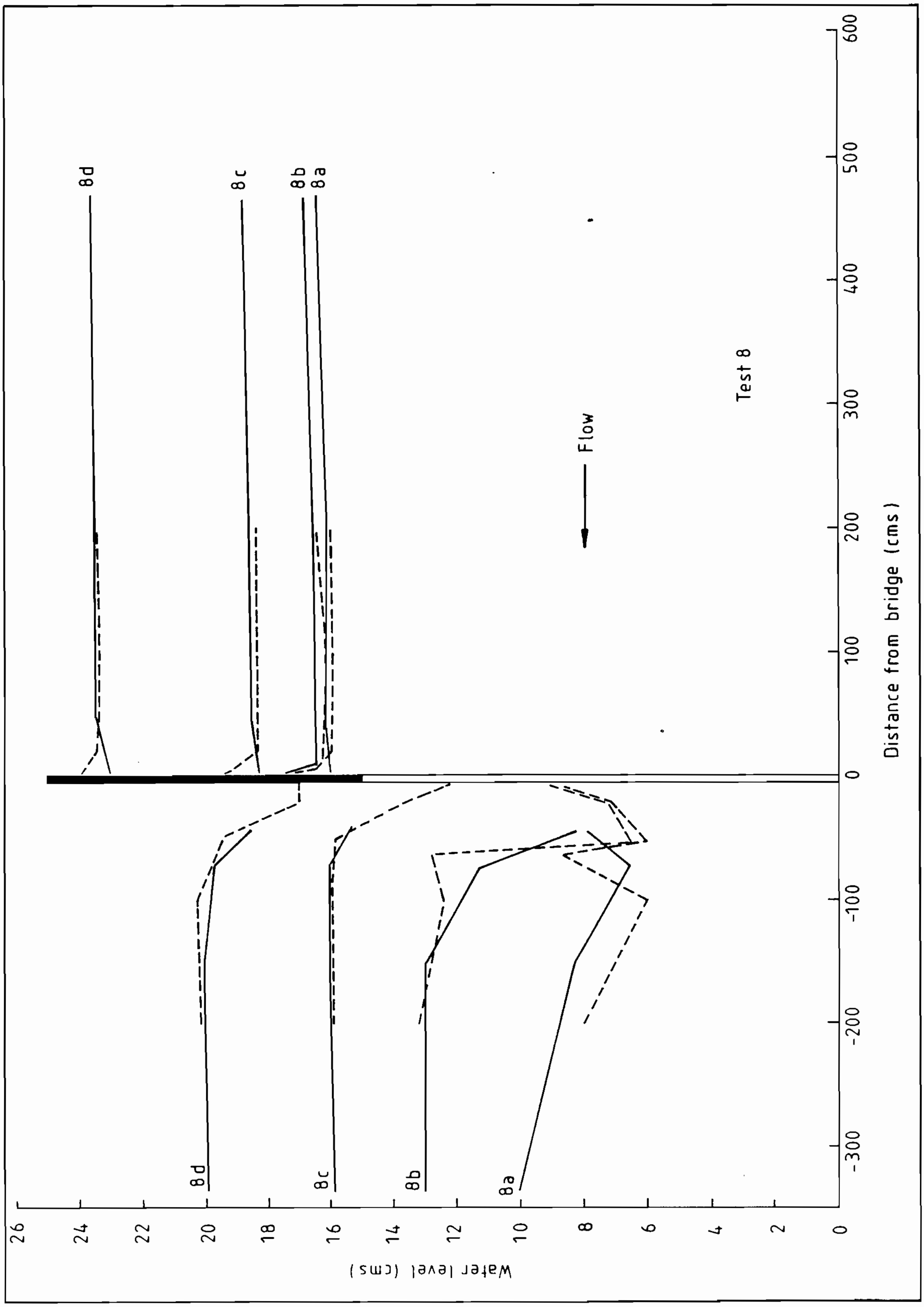

Fig 9 Water surface profiles, test 8, discharge 0·035 m^3/s

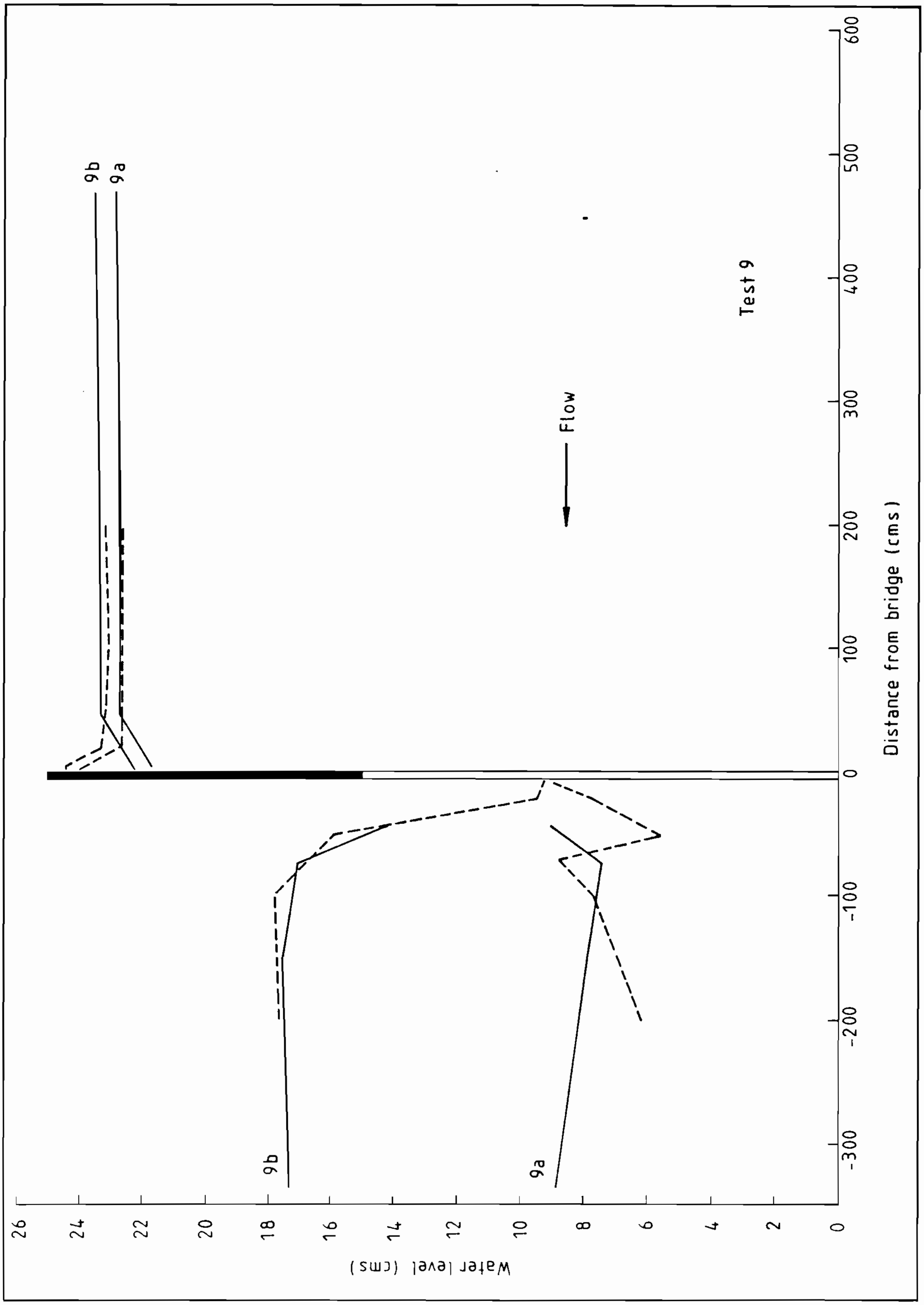

Fig 10 Water surface profiles, test 9, discharge 0·044 m^3/s

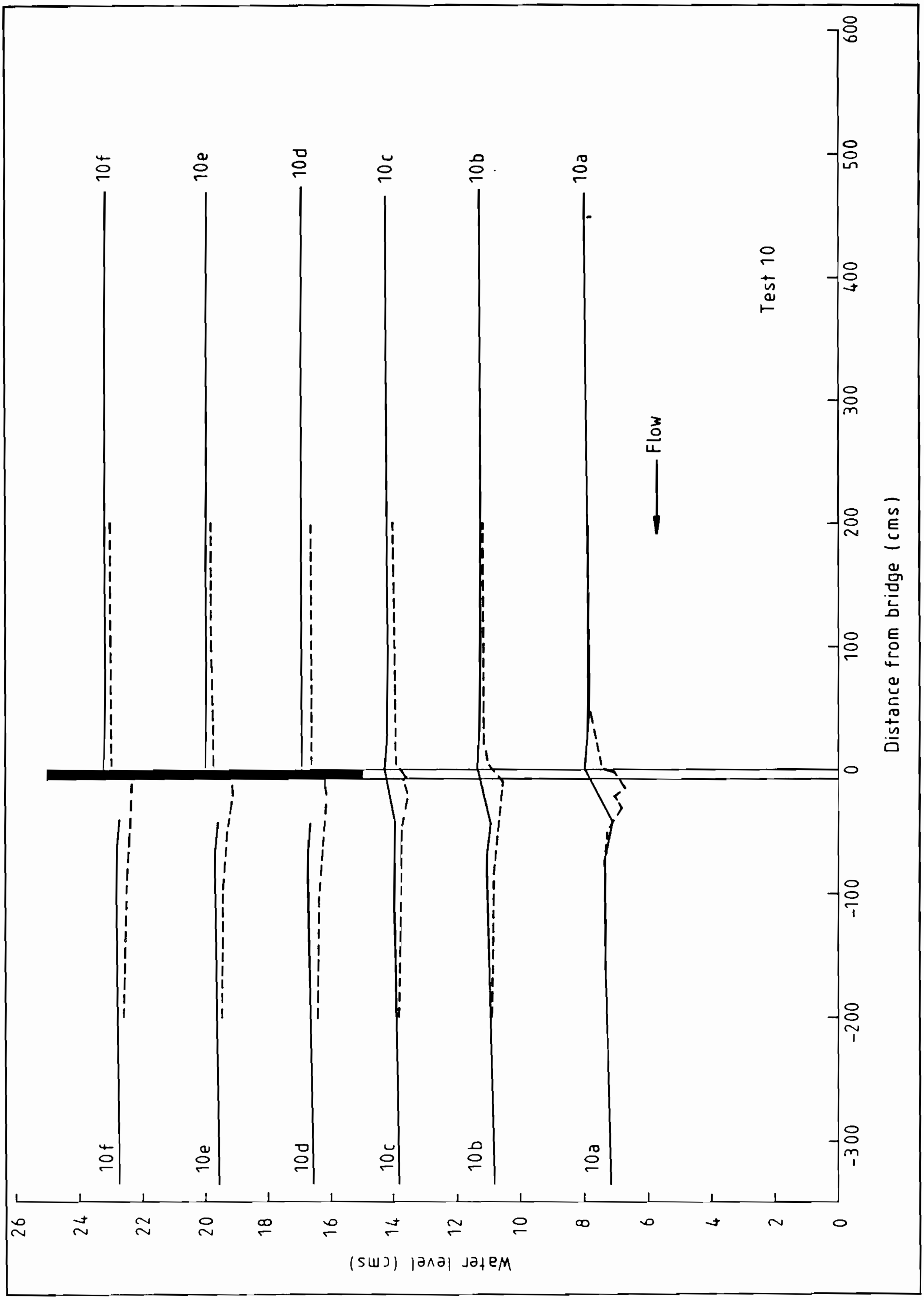

Fig 11 Water surface profiles, test 10, discharge 0·01 m³/s

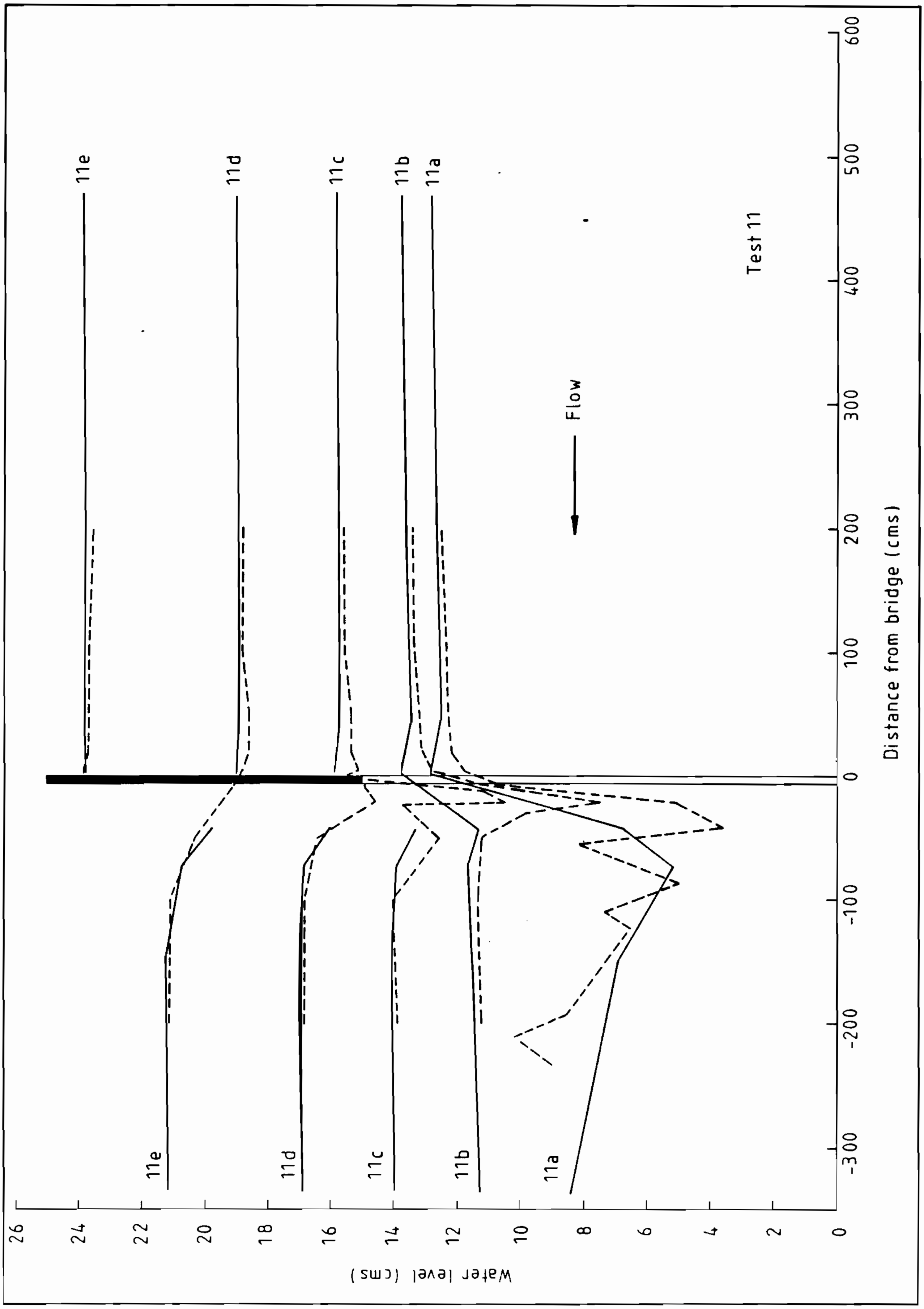

Fig 12 Water surface profiles, test 11, discharge $0{\cdot}025 m^3/s$

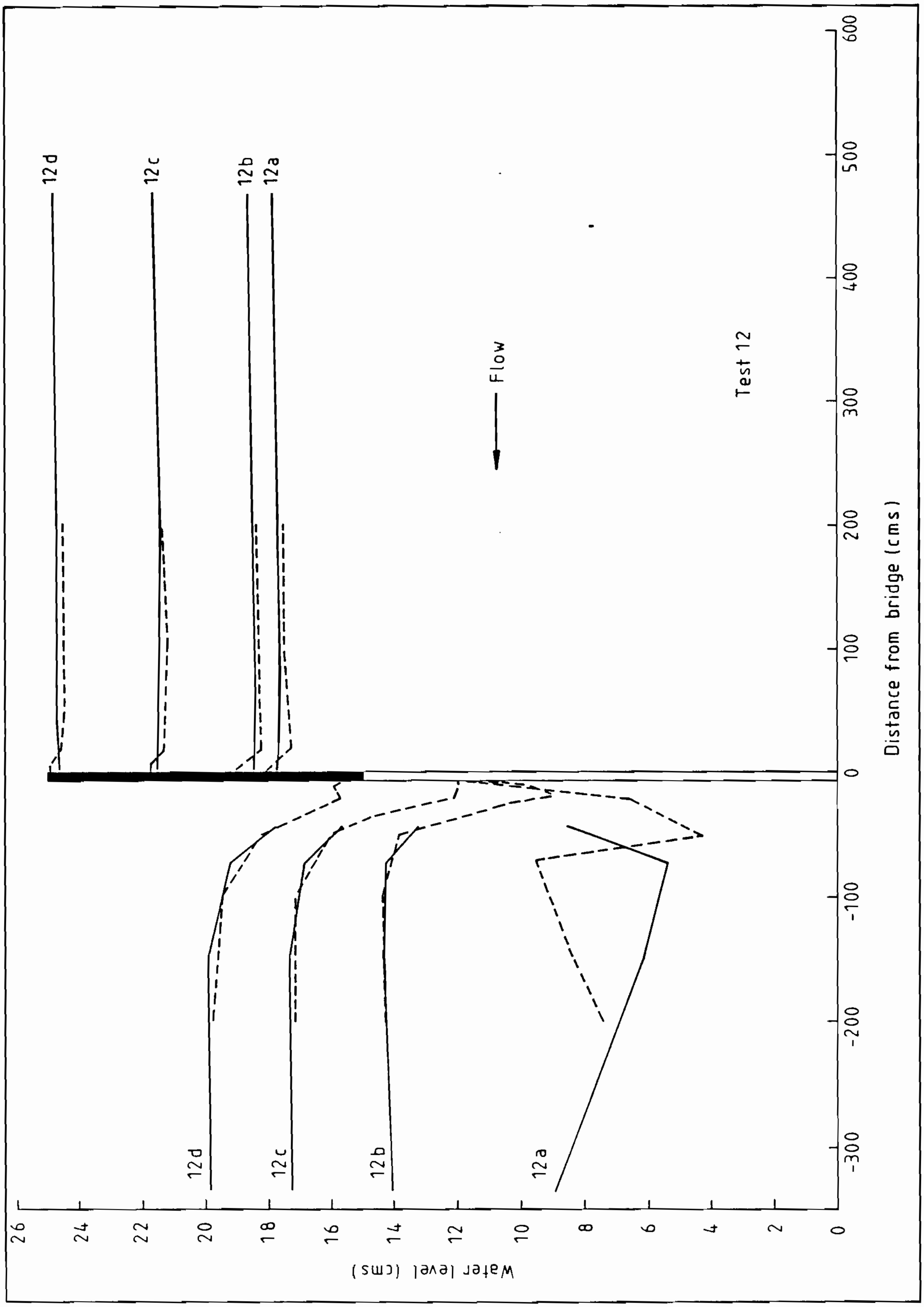

Fig 13 Water surface profiles, test 12, discharge 0·035 m^3/s

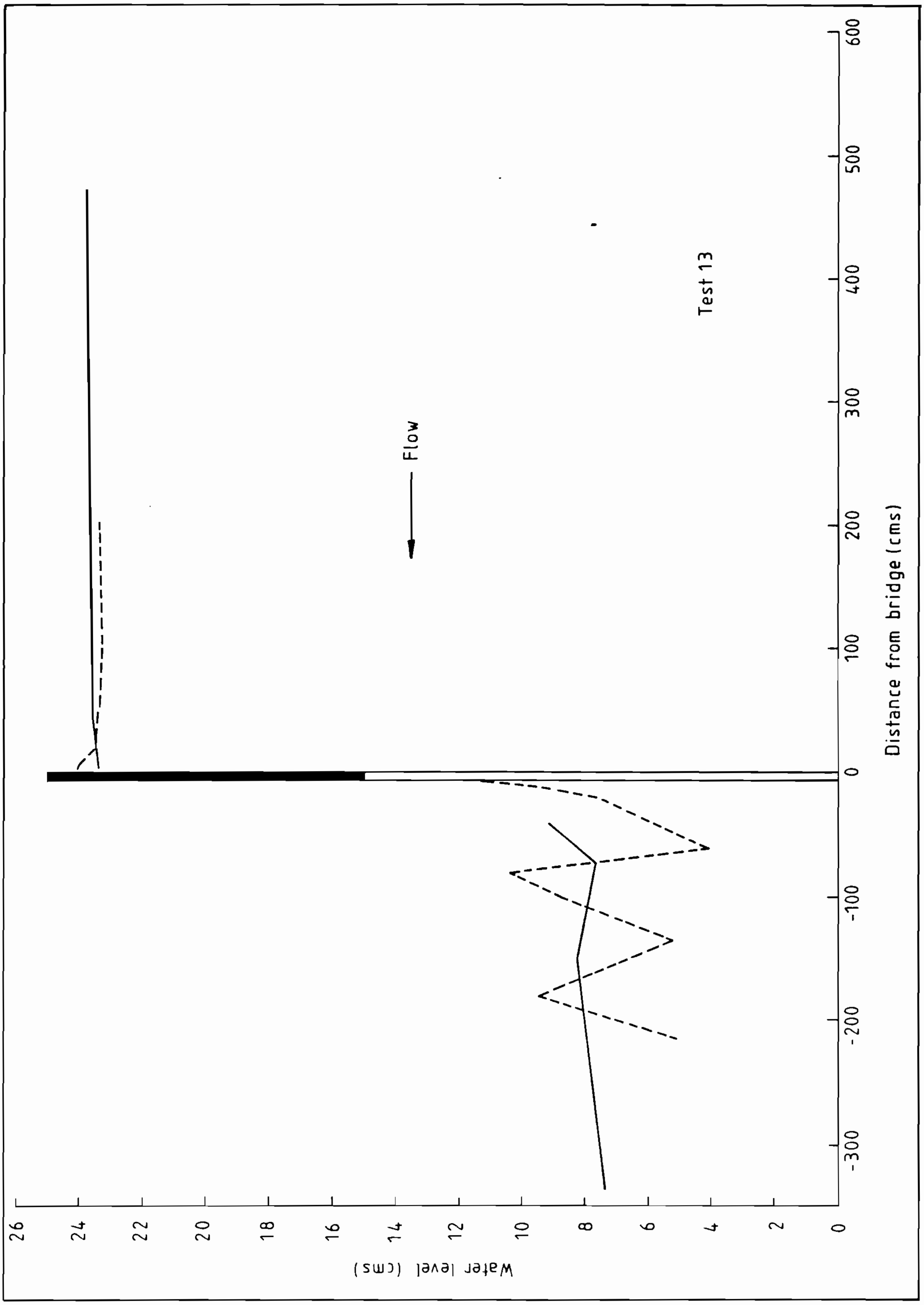

Fig 14 Water surface profiles, test 13, discharge 0·043 m^3/s

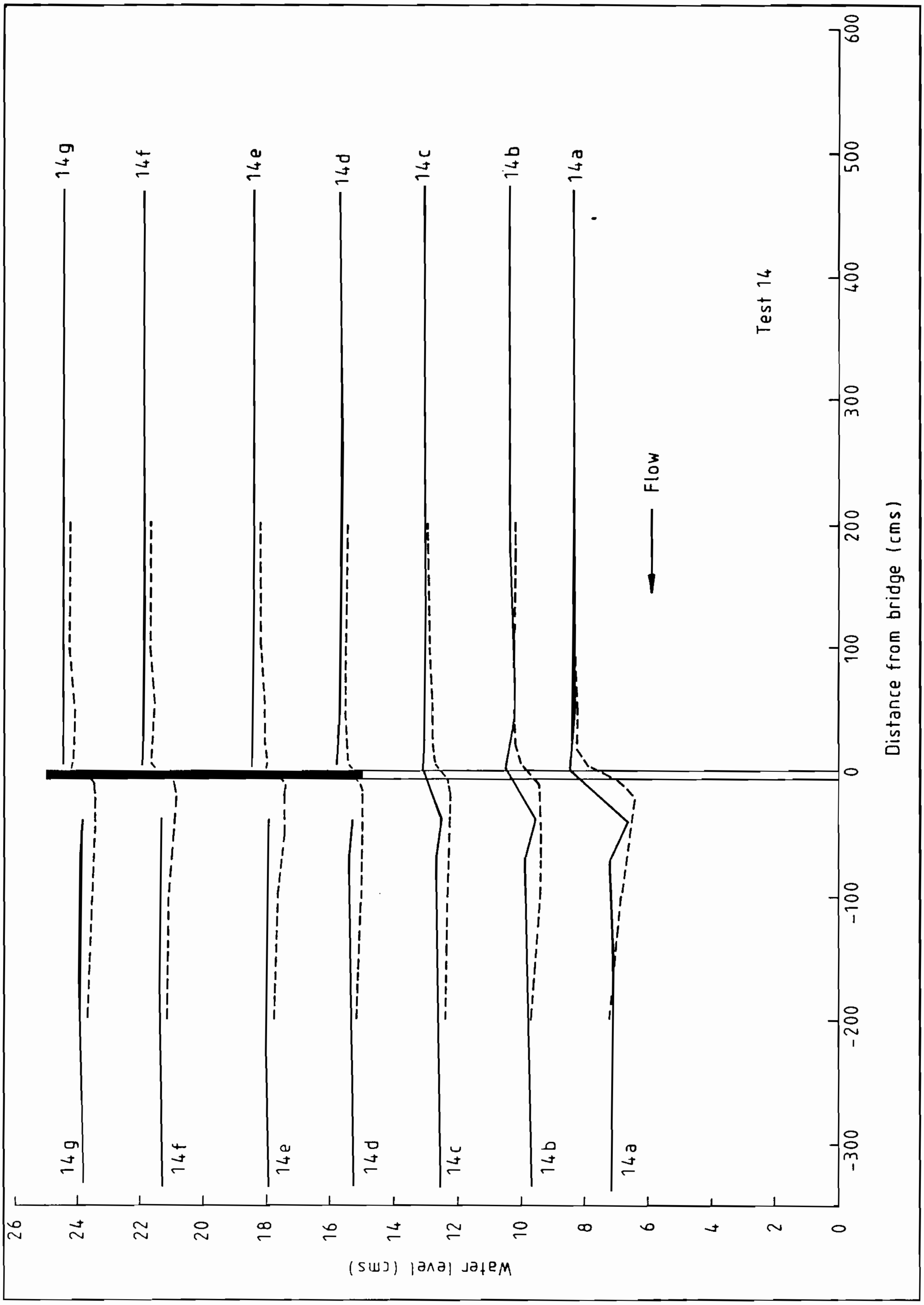

Fig 15 Water surface profiles, test 14, discharge 0·01 m³/s

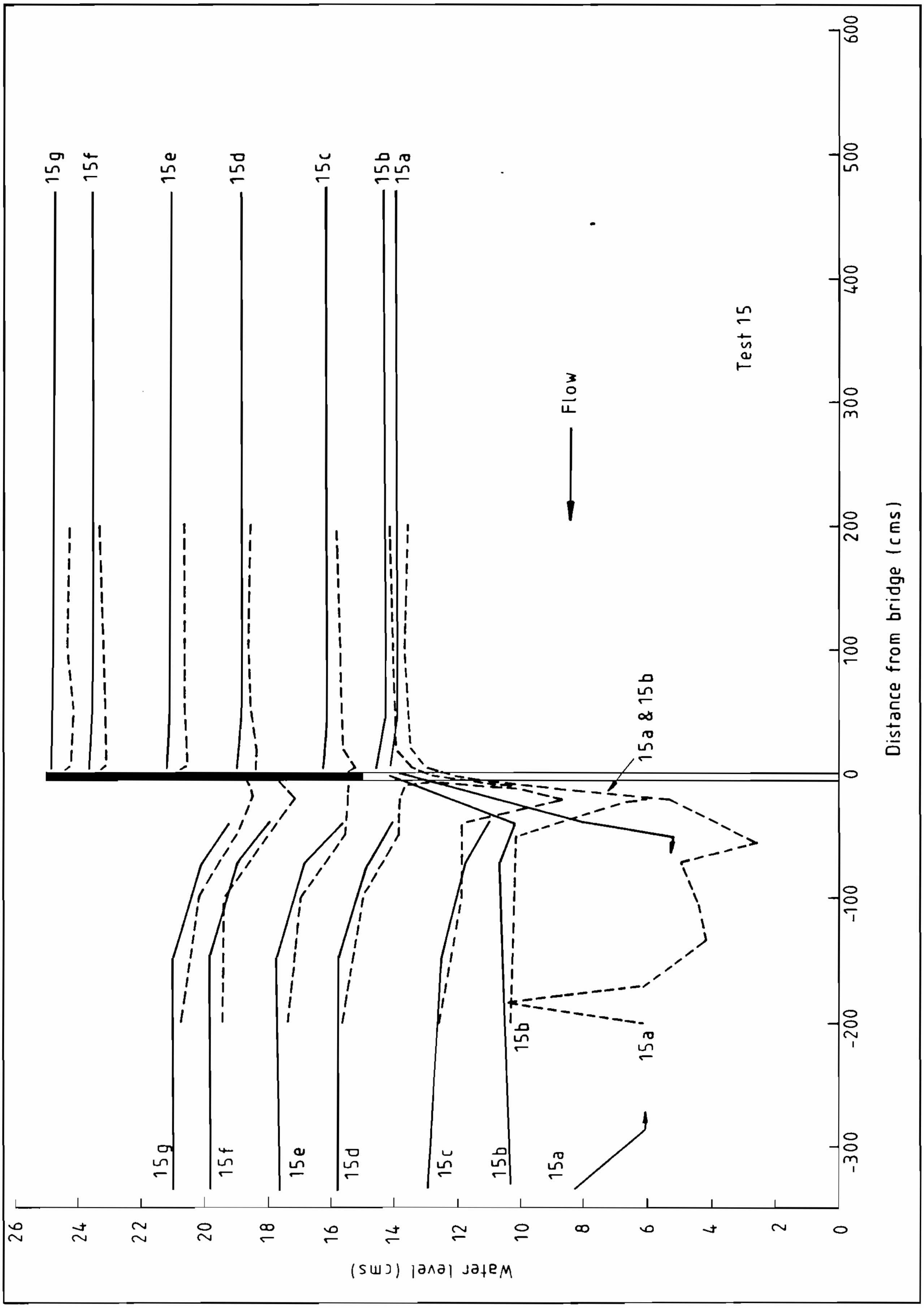

Fig 16 Water surface profiles, test 15, discharge $0{\cdot}026\ m^3/s$

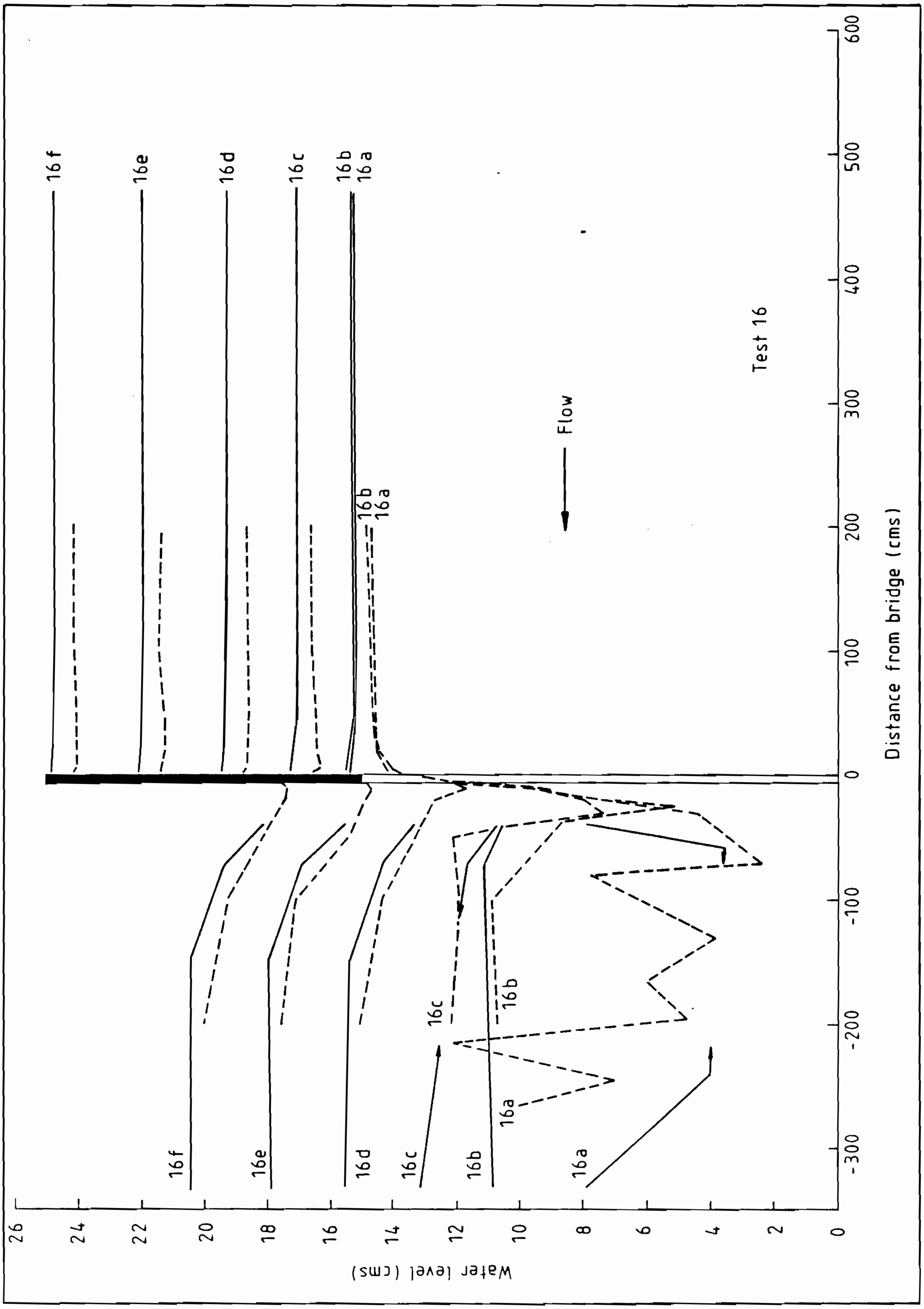

Fig 17 Water surface profiles, test 16, discharge 0·0285 m^3/s

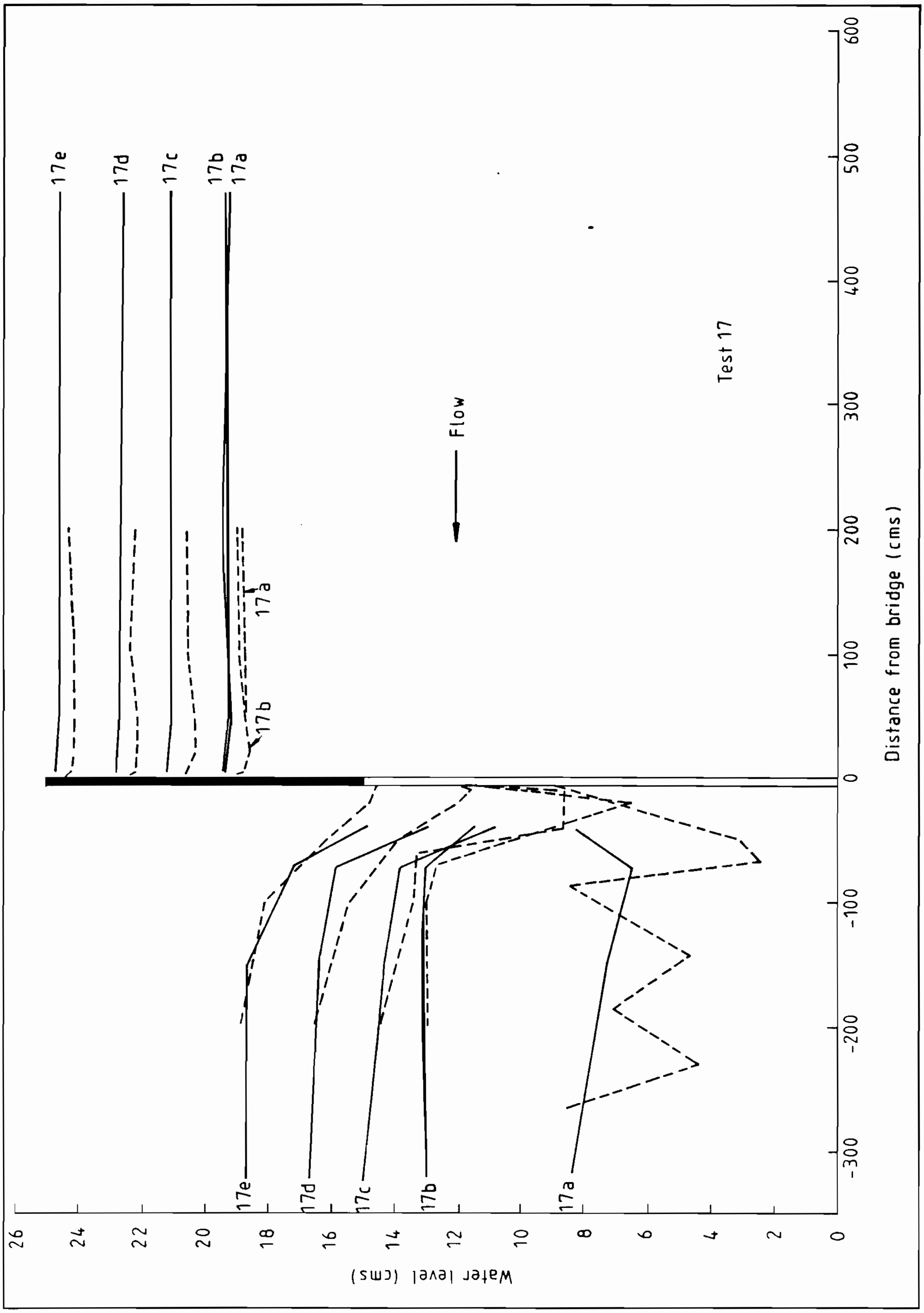

Fig 18 Water surface profiles, test 17, discharge $0{\cdot}035\,m^3/s$

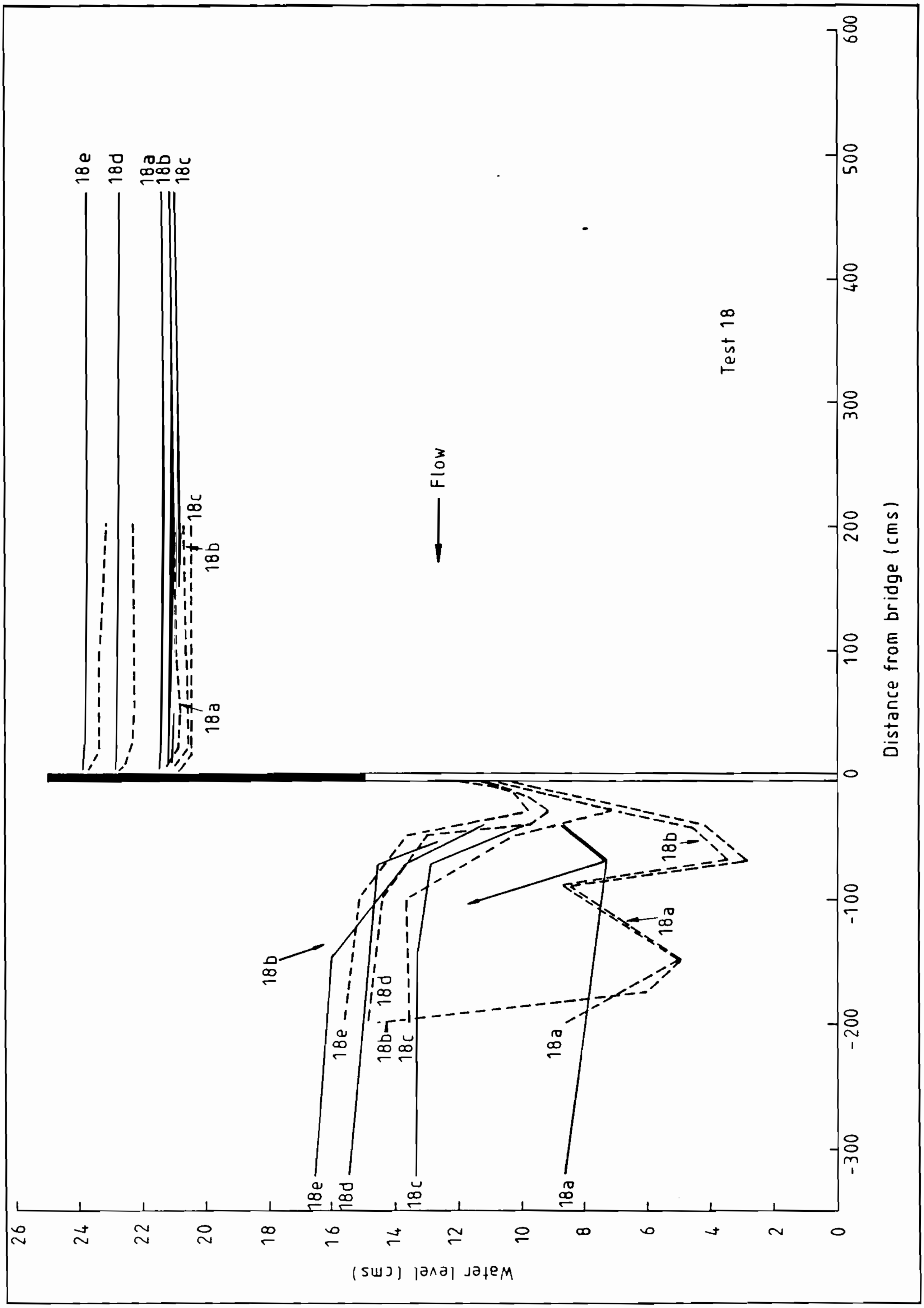

Fig 19 Water surface profiles, test 18, discharge 0·038 m^3/s

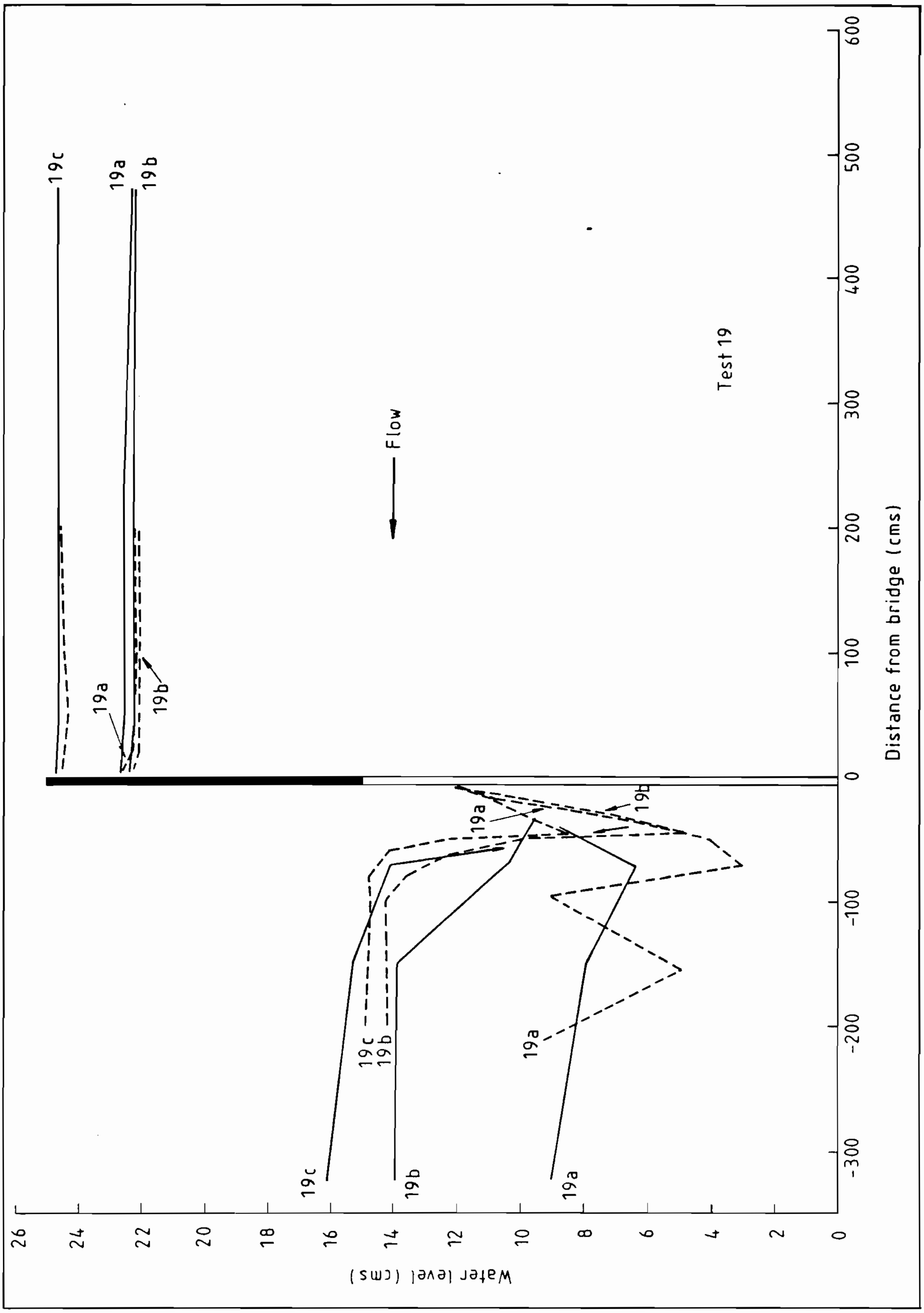

Fig 20 Water surface profiles, test 19, discharge 0·0397 m^3/s

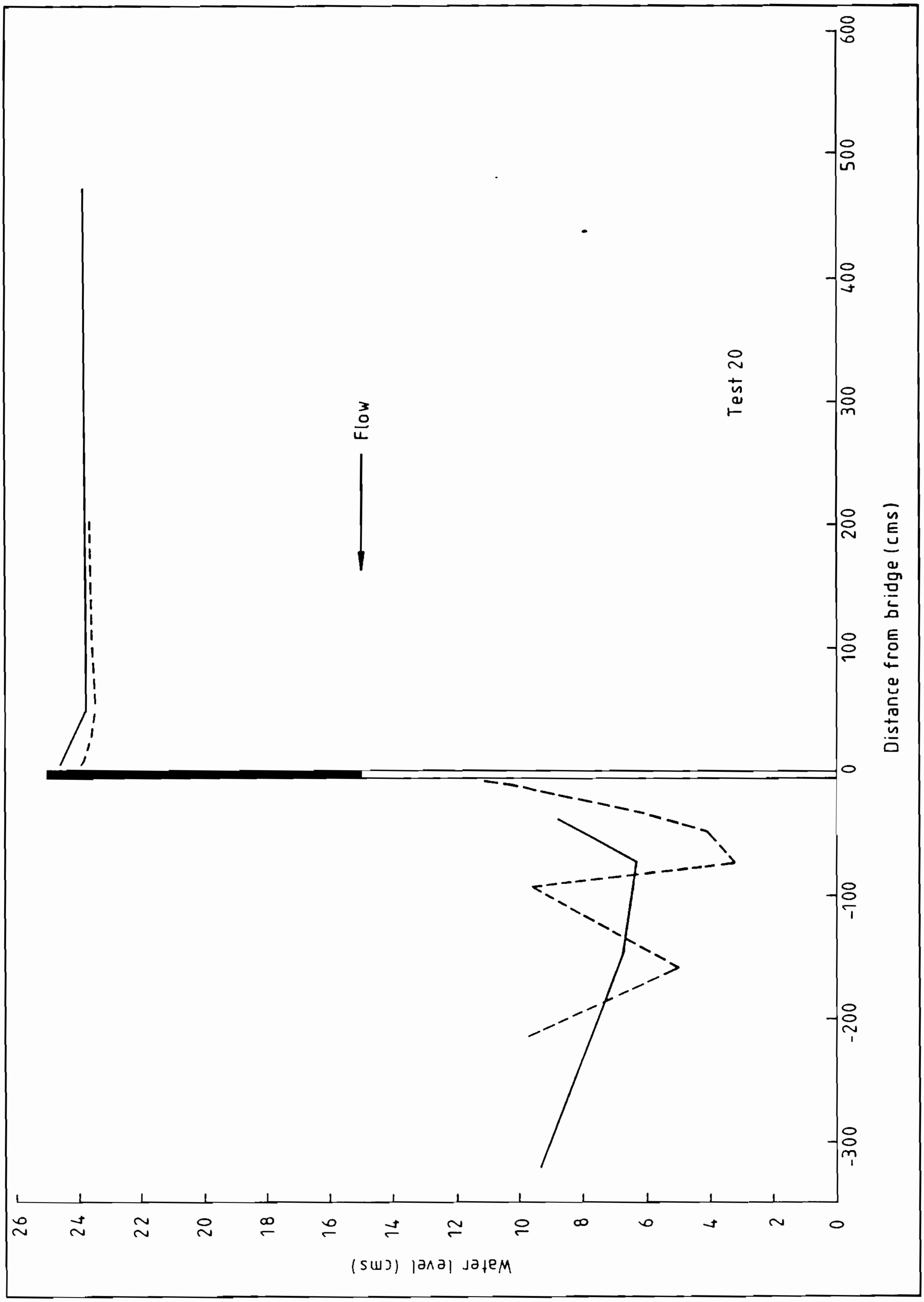

Fig 21 Water surface profiles, test 20, discharge 0·0412 m^3/s

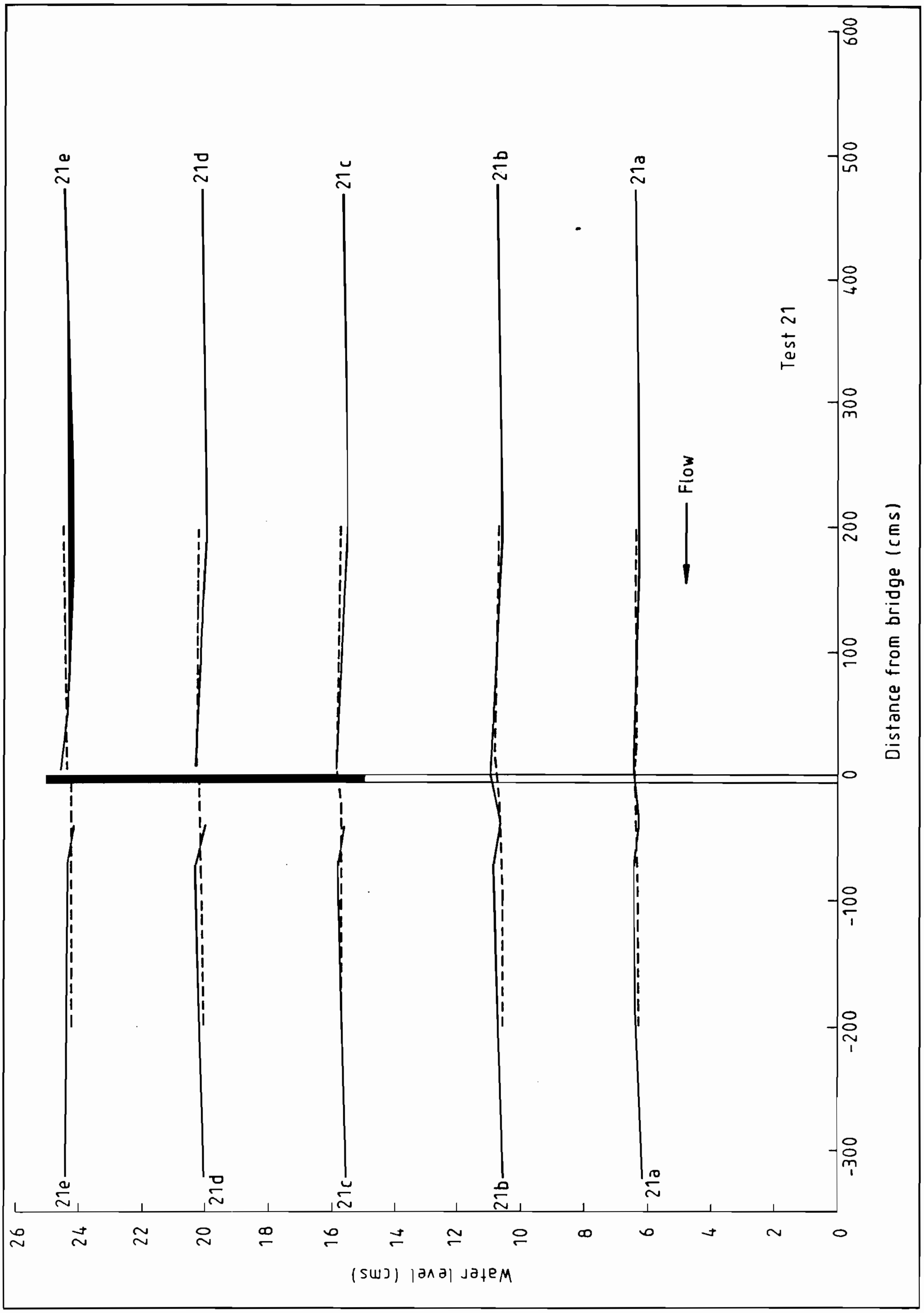

Fig 22 Water surface profiles, test 21, discharge 0·003 m^3/s

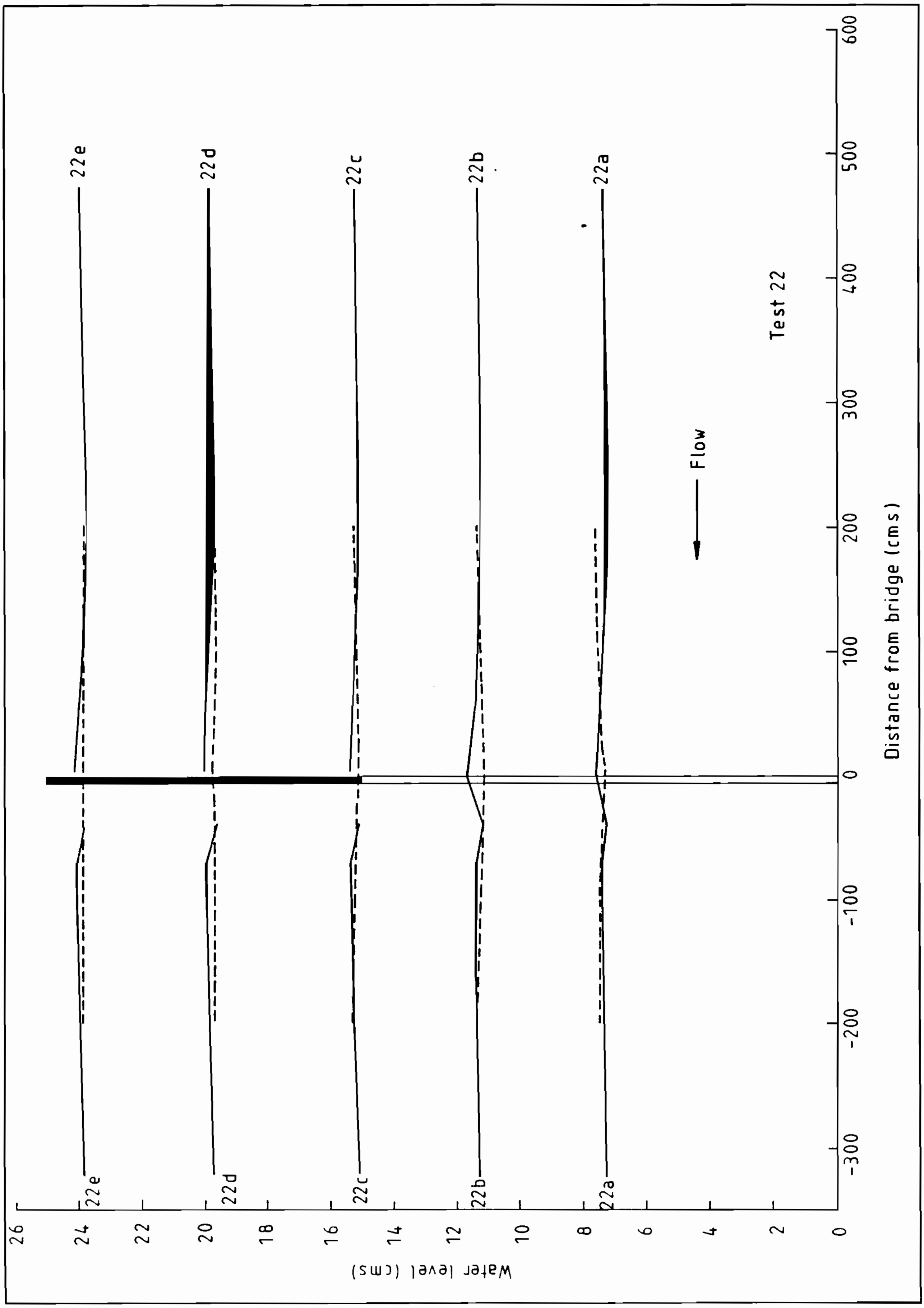

Fig 23 Water surface profiles, test 22, discharge 0·01 m^3/s

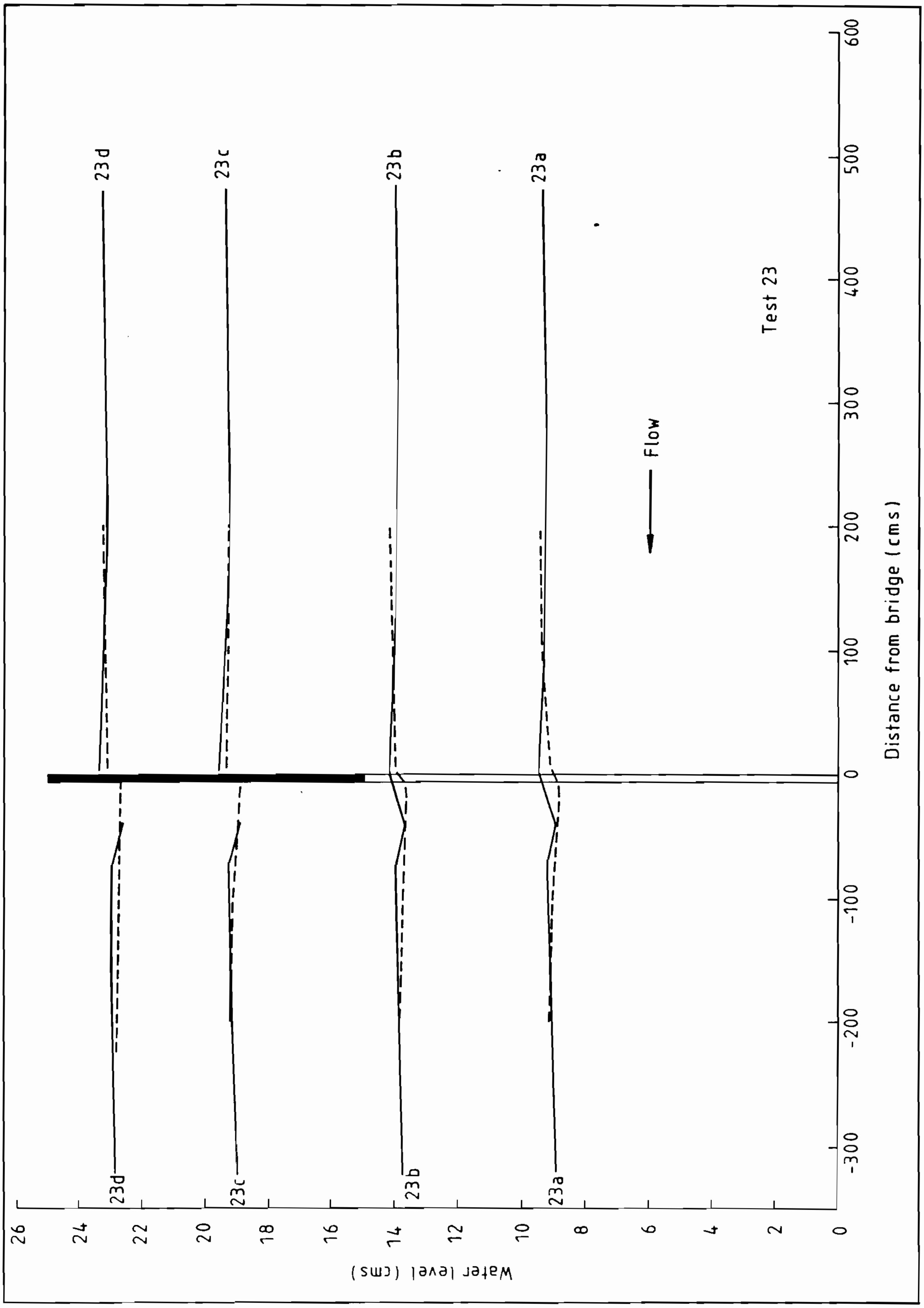

Fig 24 Water surface profiles, test 23, discharge 0·025 m^3/s

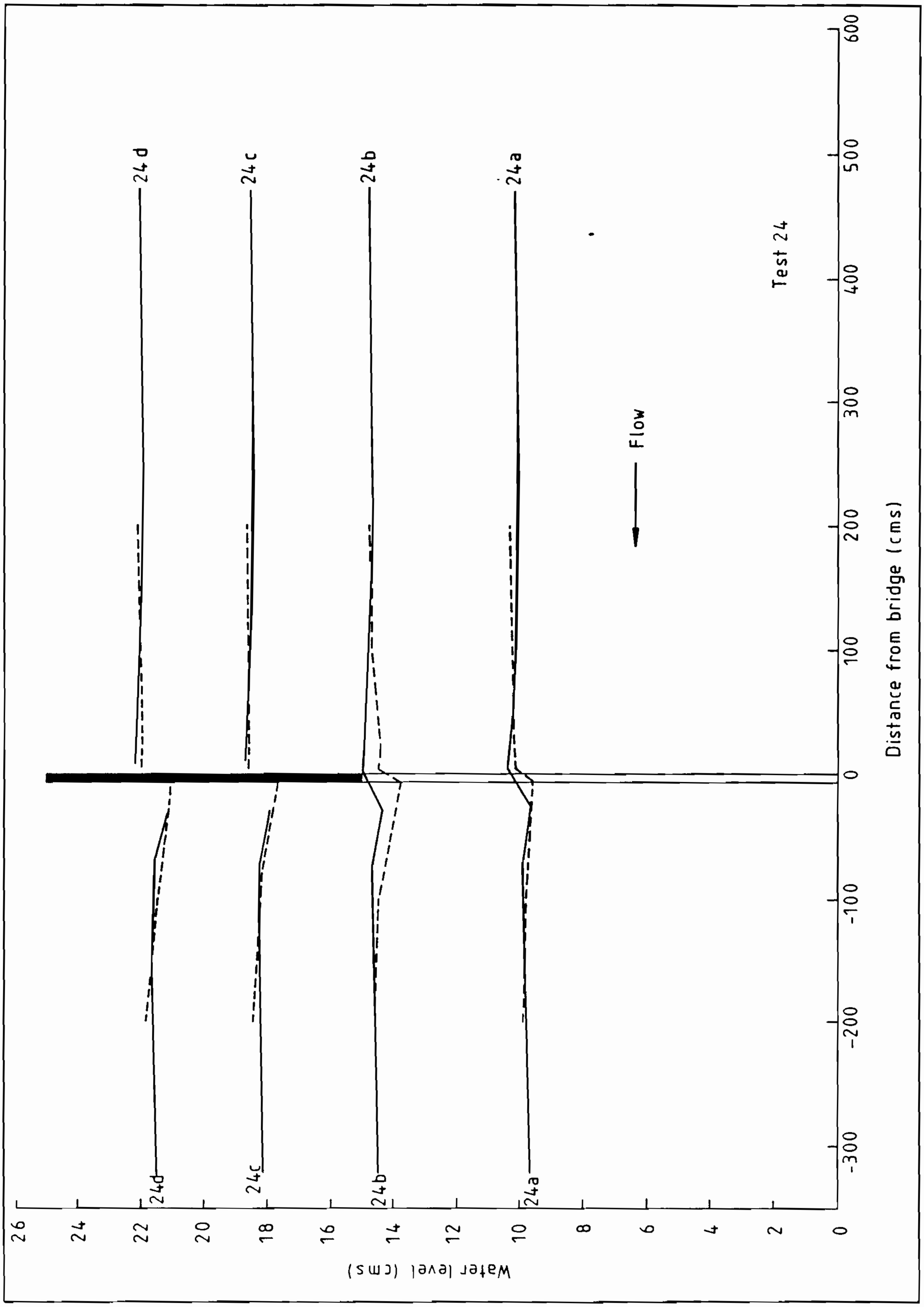

Fig 25 Water surface profiles, test 24, discharge $0{\cdot}035\,m^3/s$

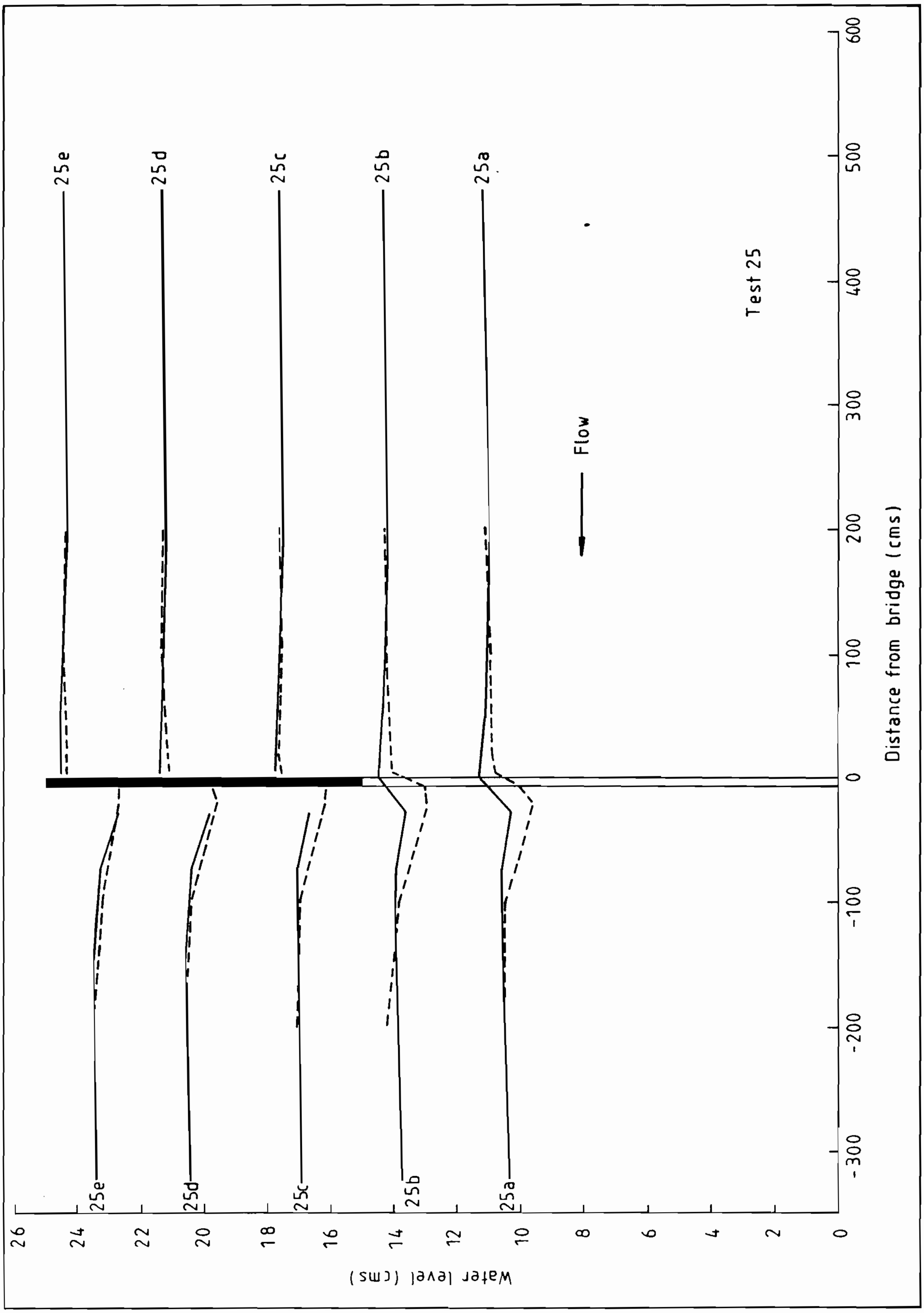

Fig 26 Water surface profiles, test 25, discharge 0·044 m^3/s

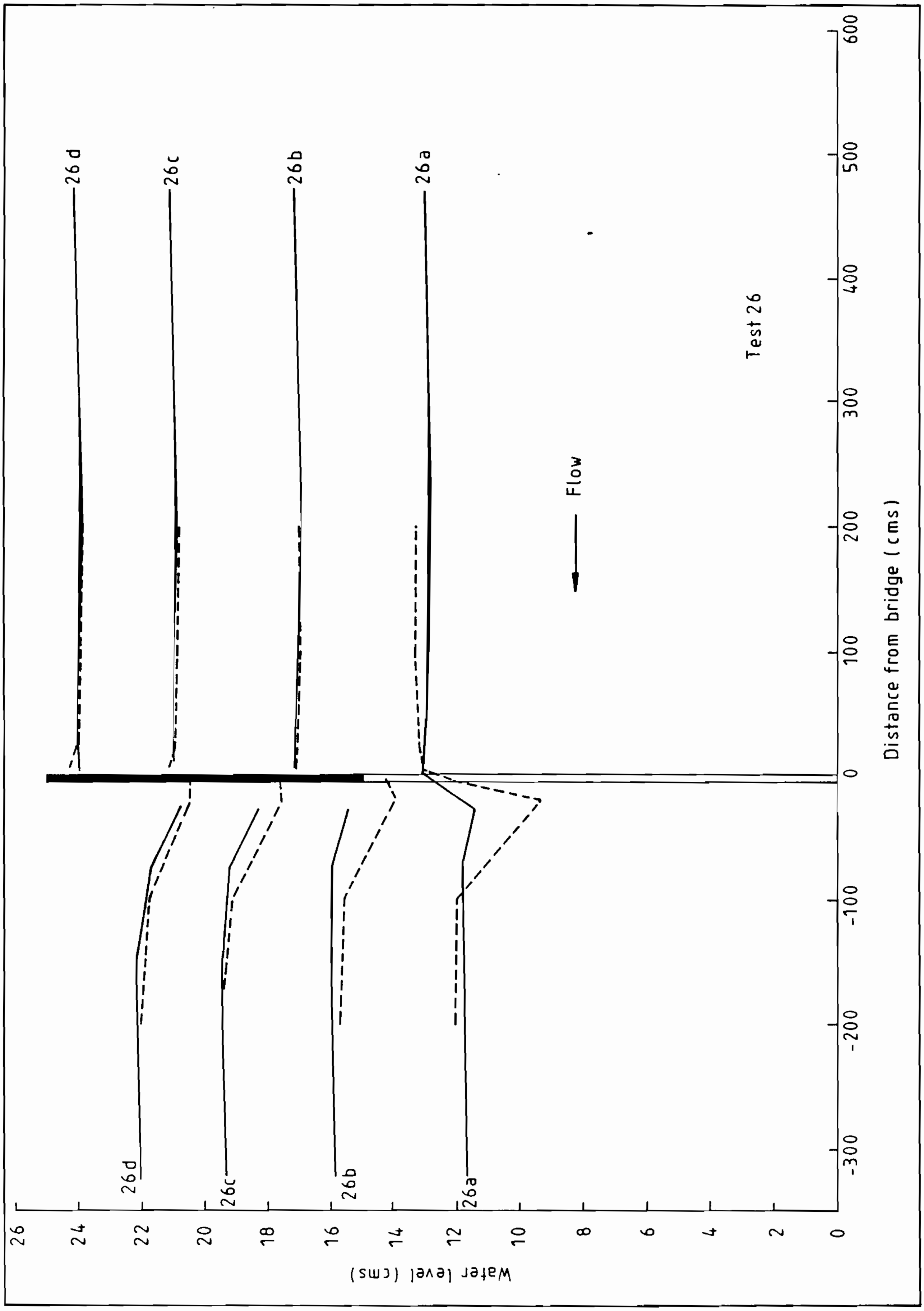

Fig 27 Water surface profiles, test 26, discharge 0·06 m^3/s

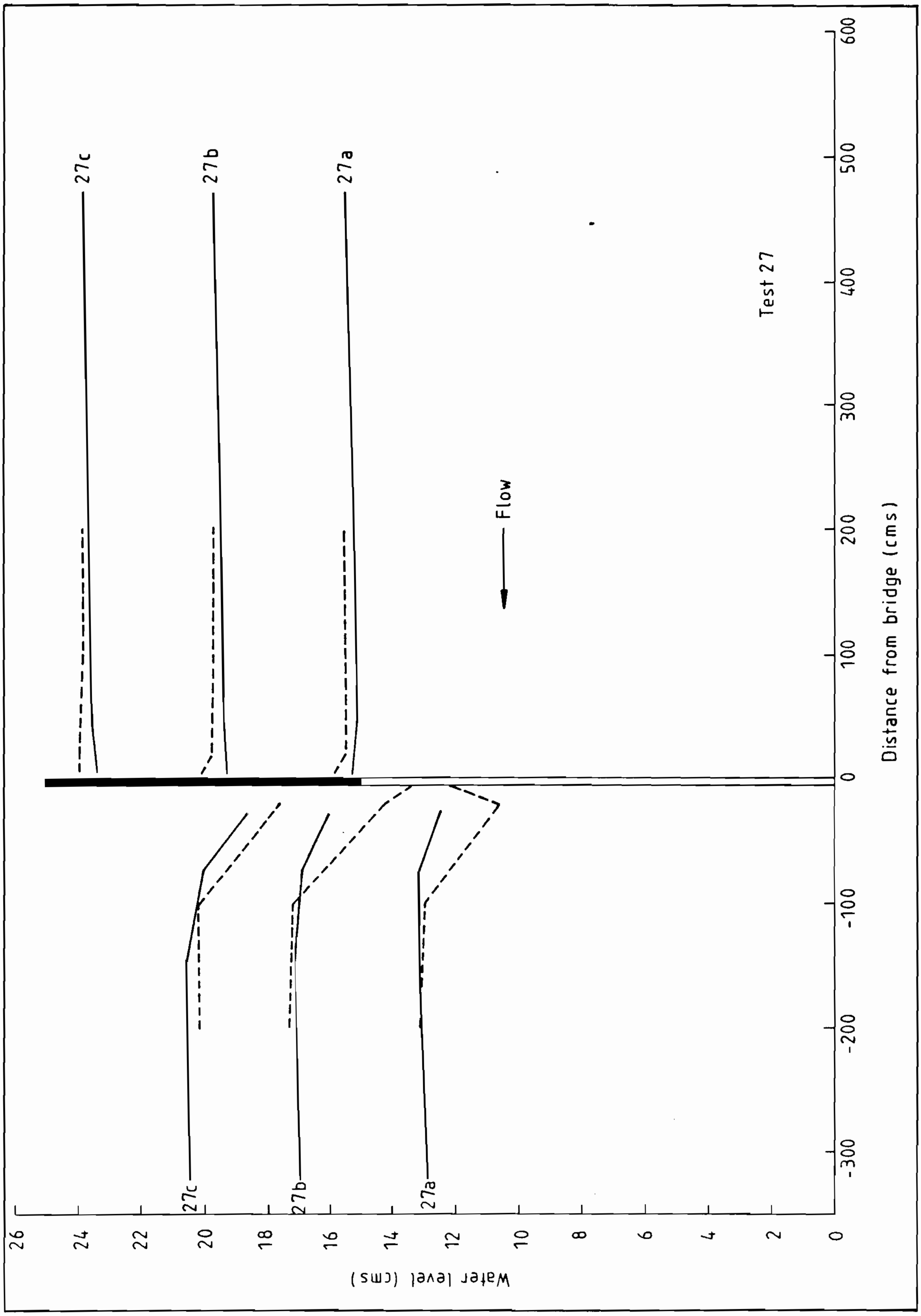

Fig 28 Water surface profiles, test 27, discharge 0·08 m^3/s

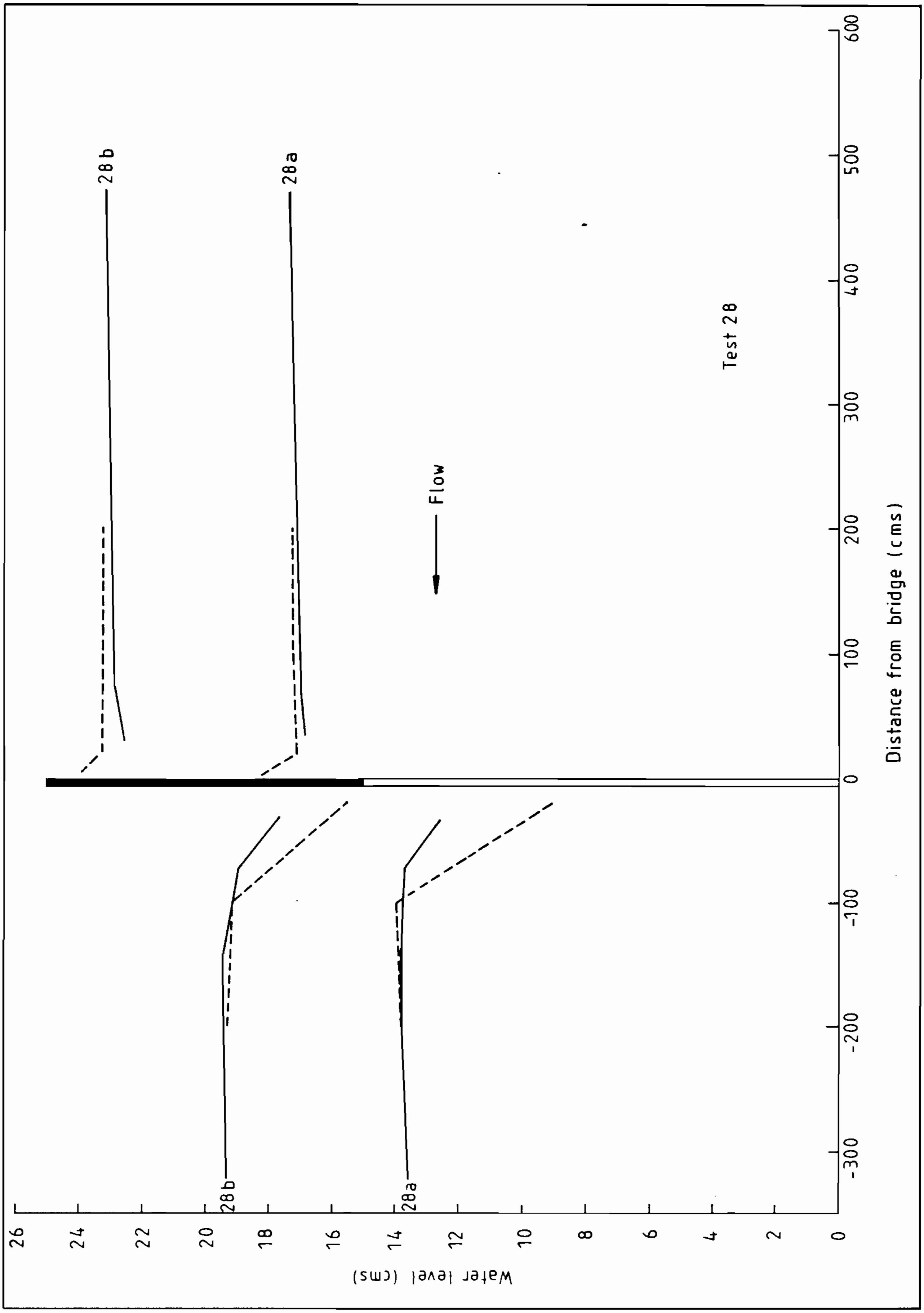

Fig 29 Water surface profiles, test 28, discharge 0·09 m^3/s

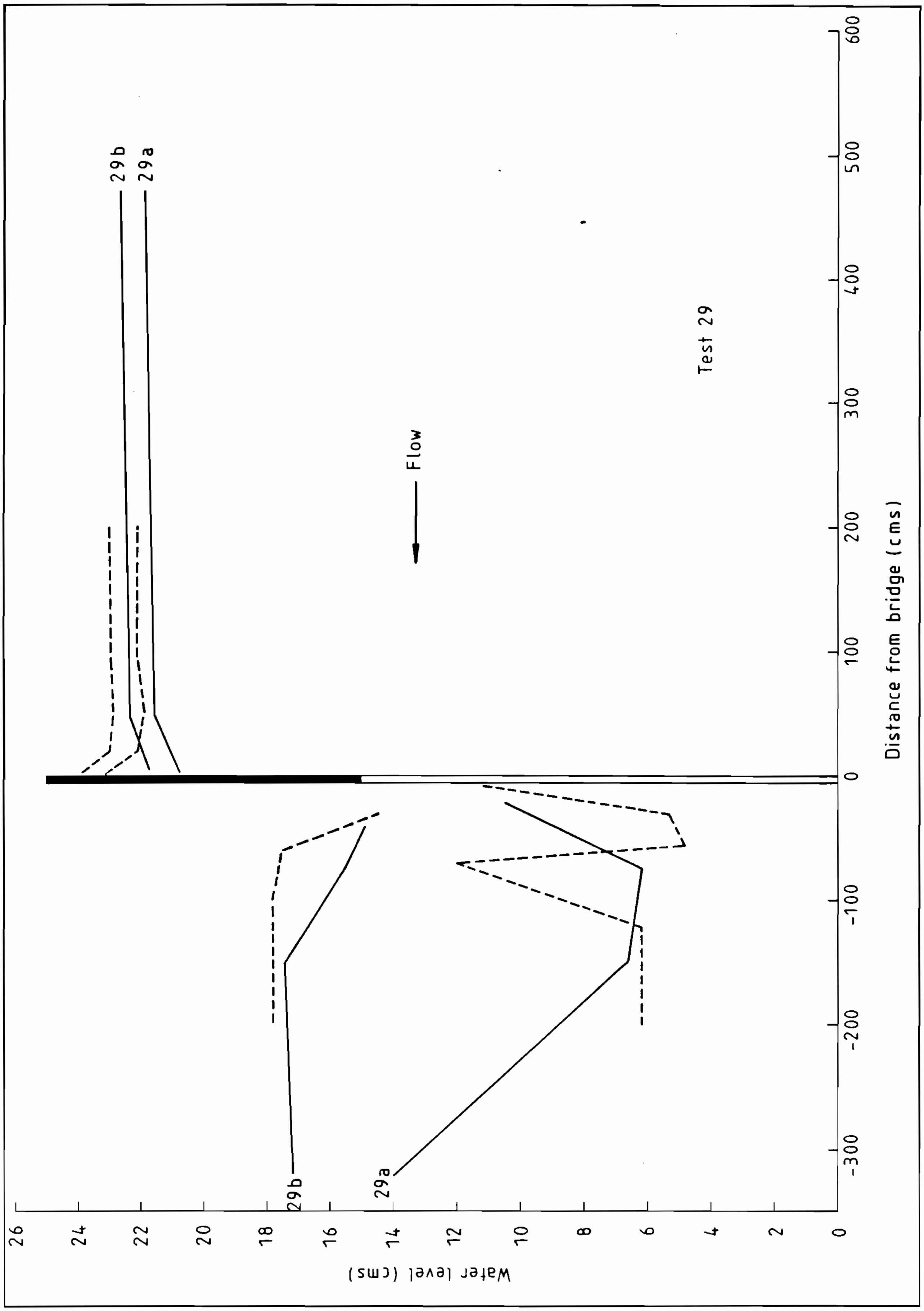

Fig 30 Water surface profiles, test 29, discharge $0{\cdot}11\ m^3/s$

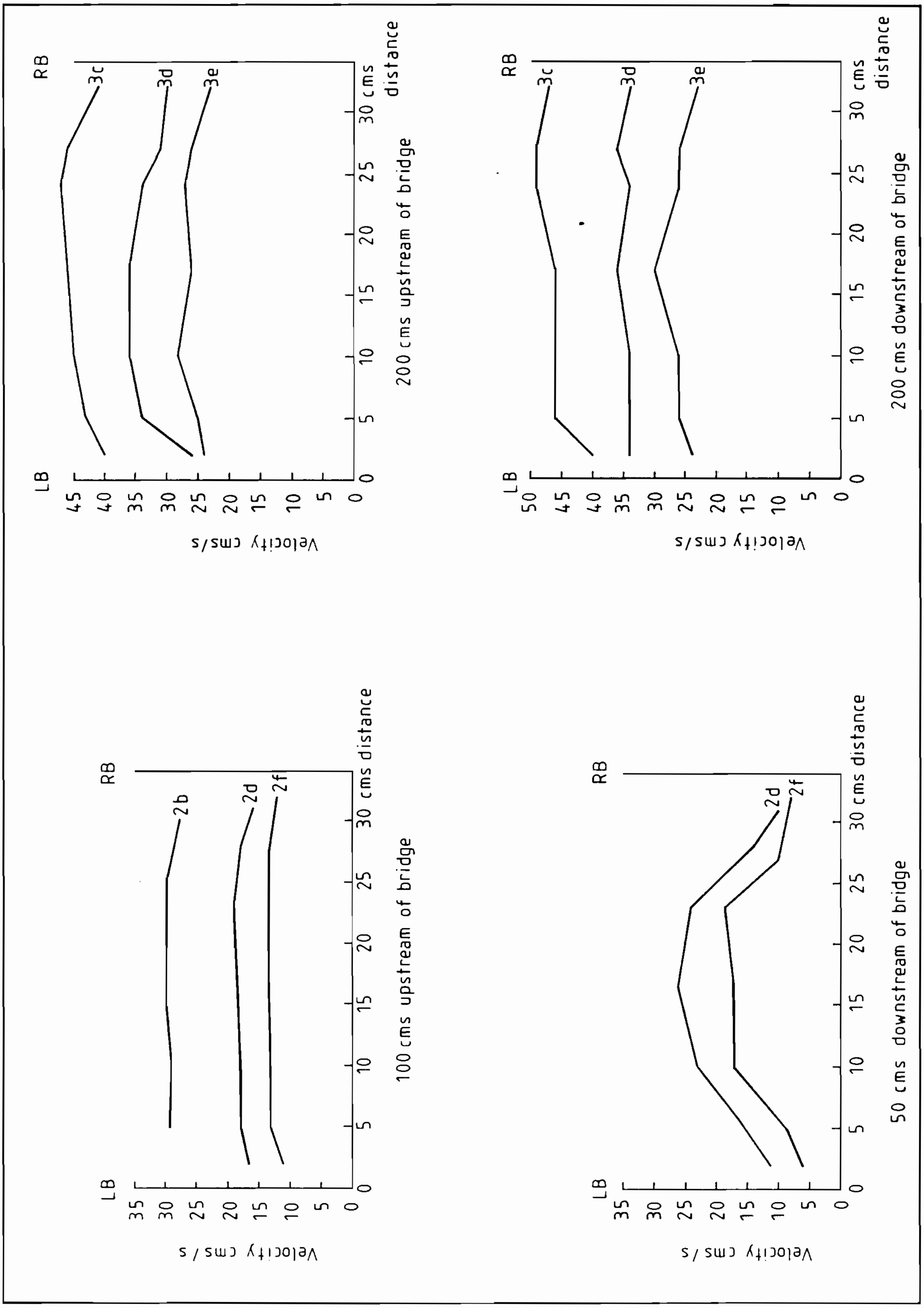

Fig 31 Mid depth velocities, tests 2 to 3

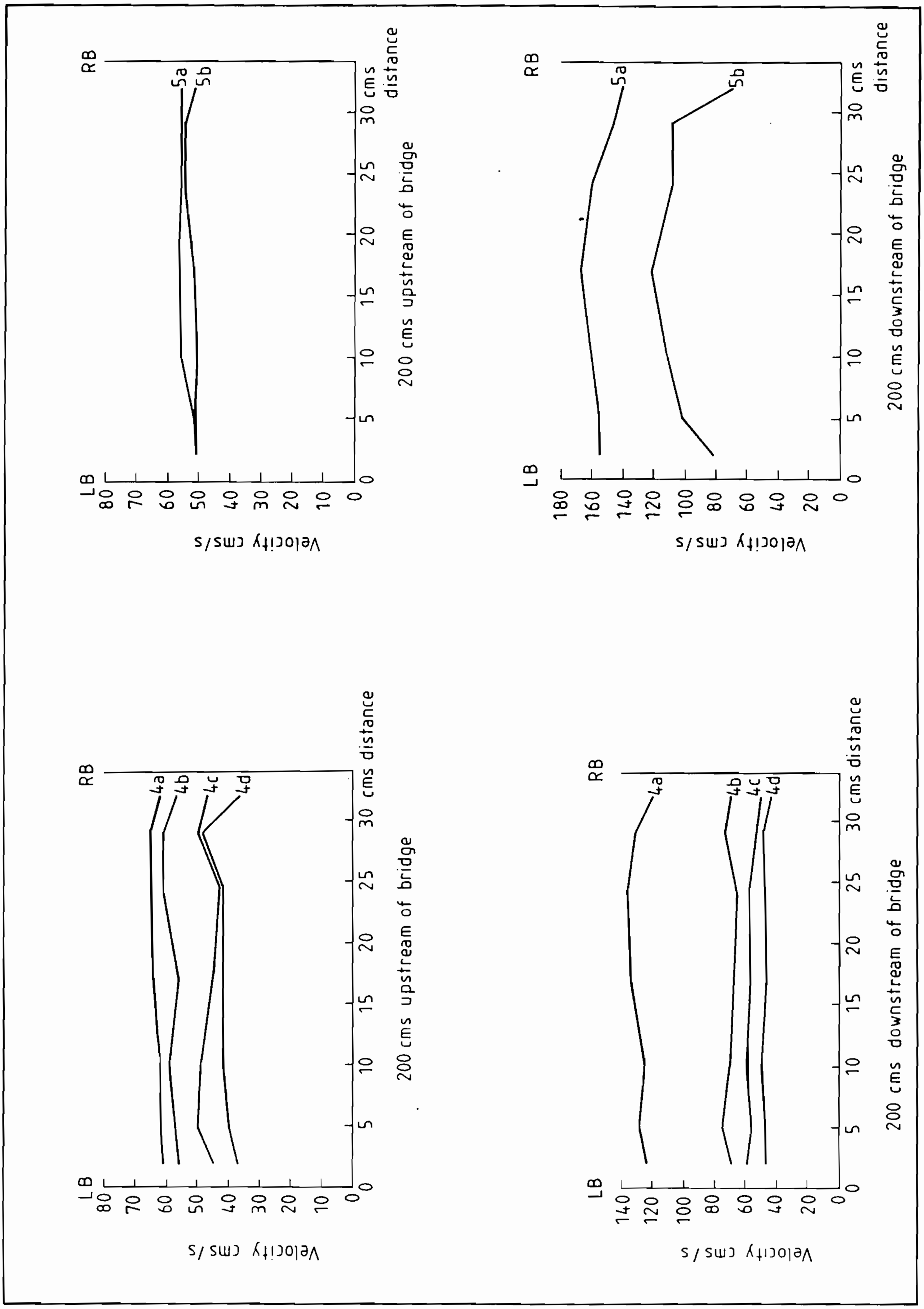

Fig 32 Mid depth velocities, tests 4 to 5

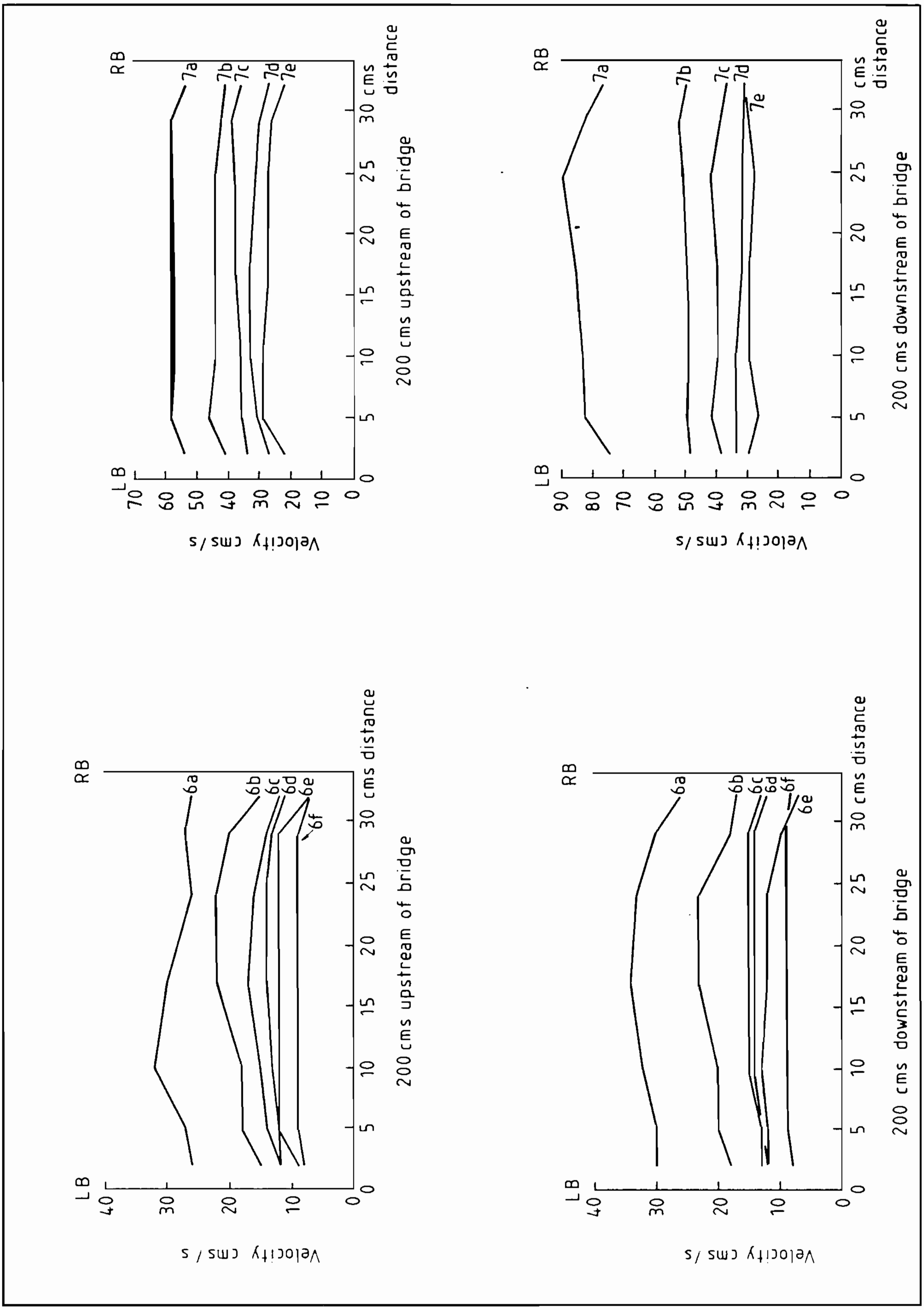

Fig 33 Mid depth velocities, tests 6 to 7

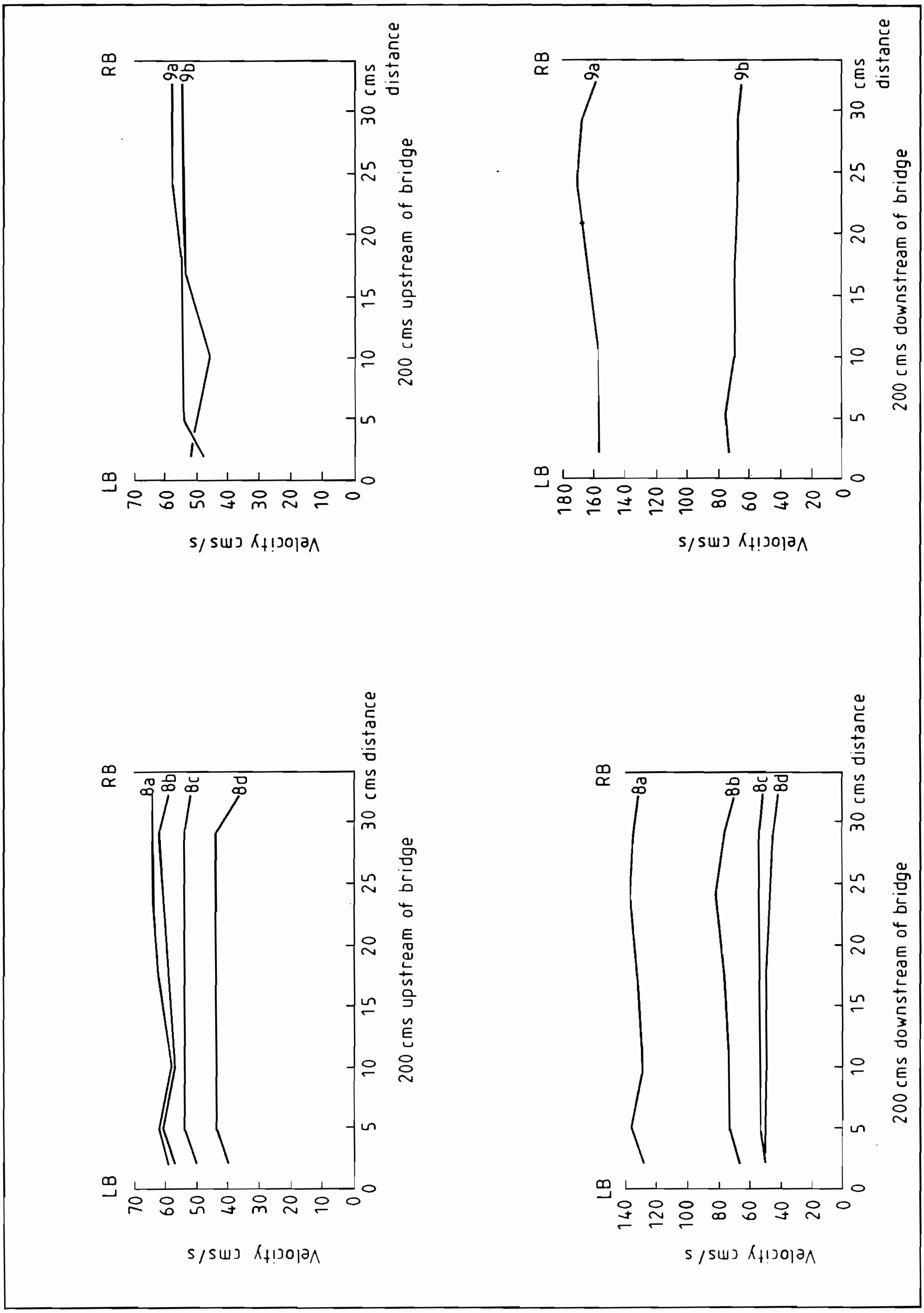

Fig 34 Mid depth velocities, tests 8 to 9

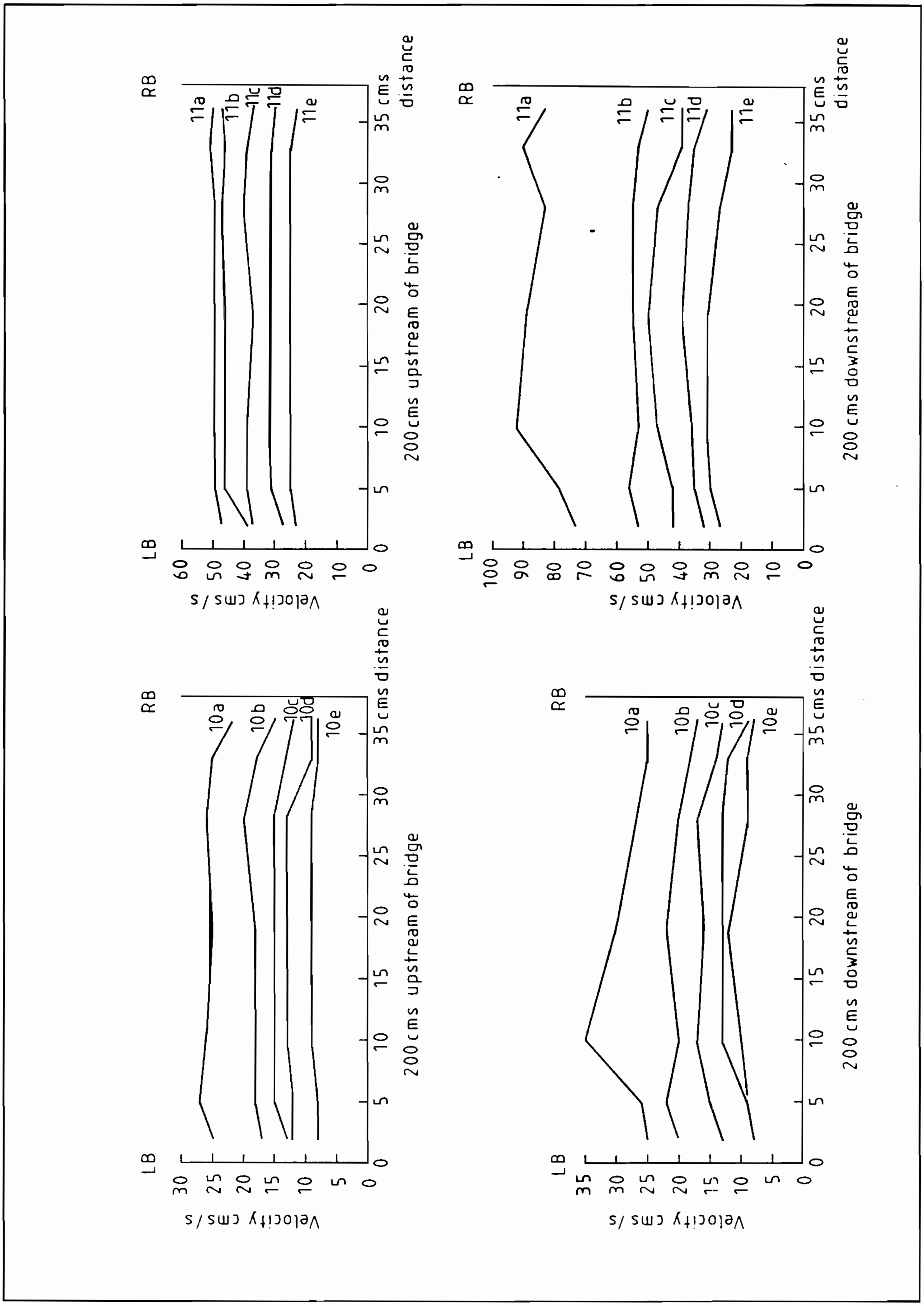

Fig 35 Mid depth velocities, tests 10 to 11

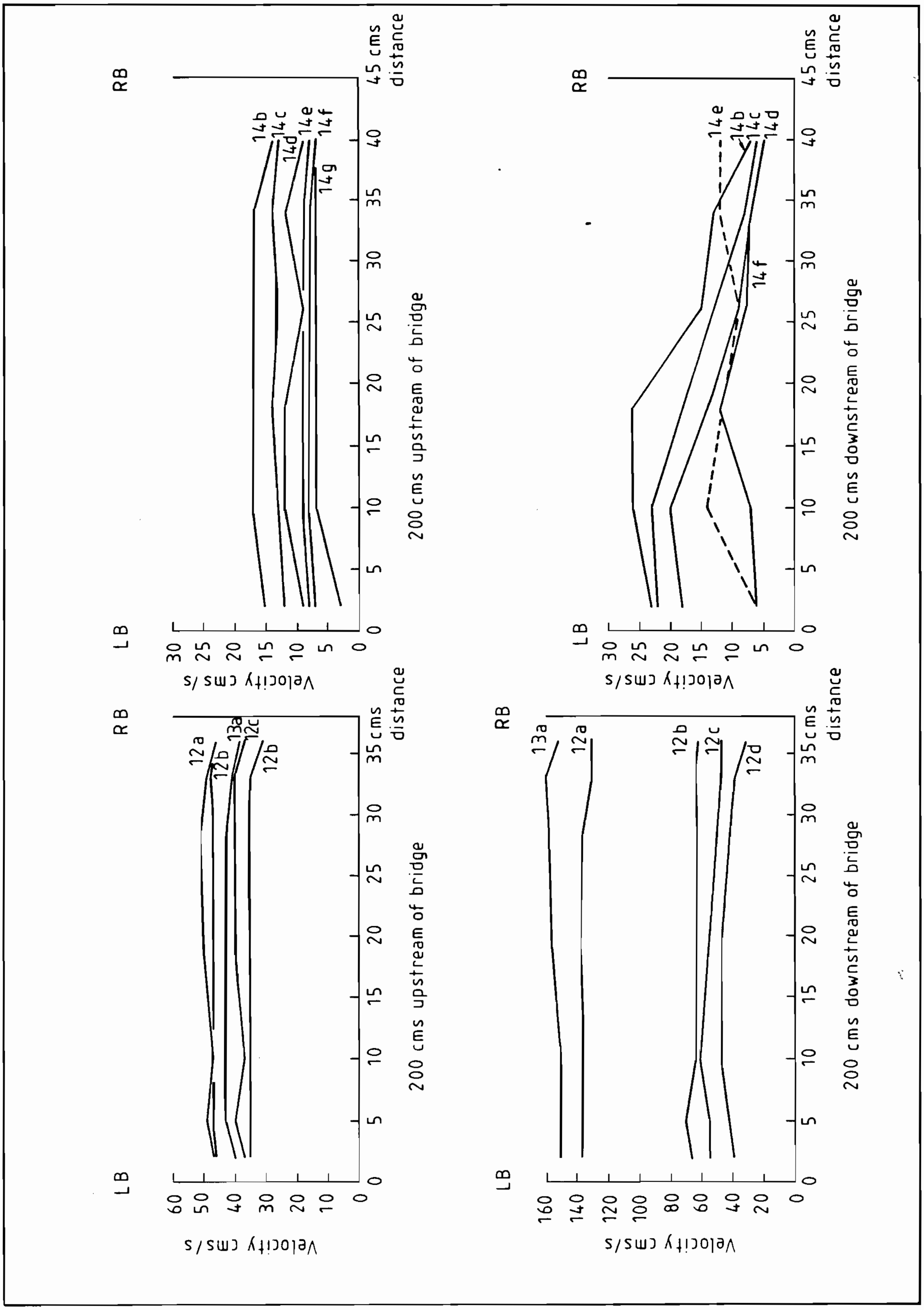

Fig 36 Mid depth velocities, tests 12 to 14

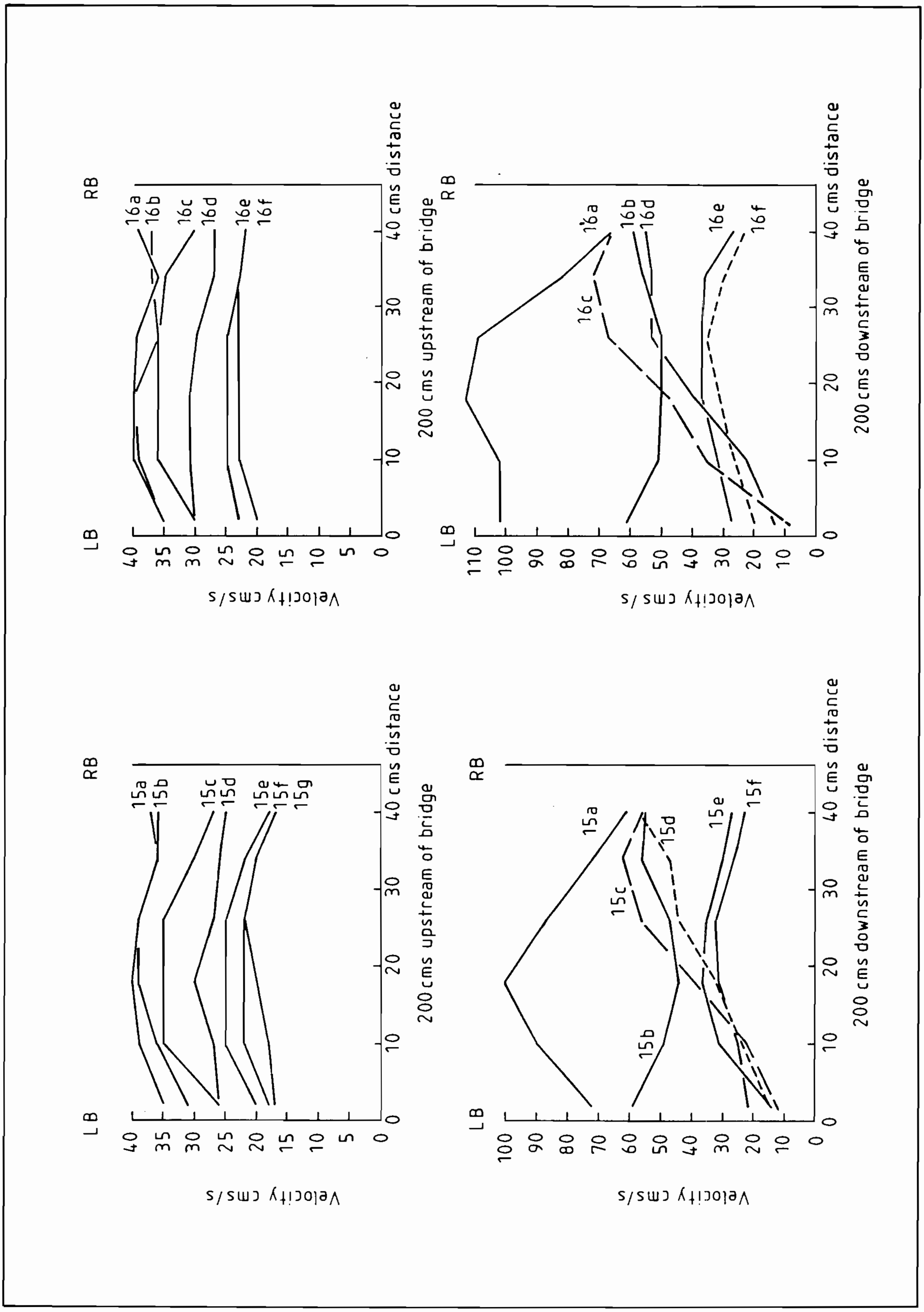

Fig 37 Mid depth velocities, tests 15 to 16

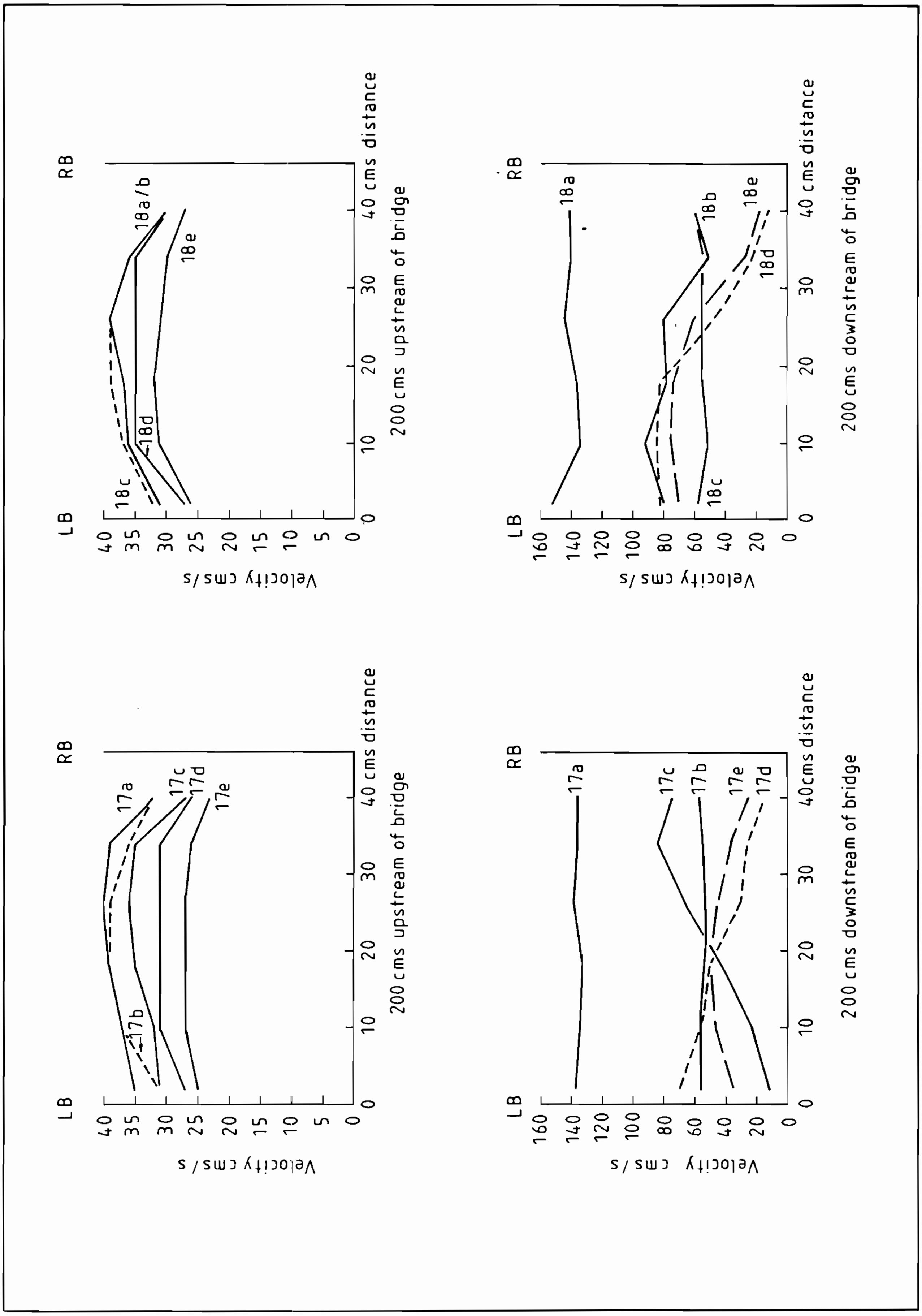

Fig 38 Mid depth velocities, tests 17 to 18

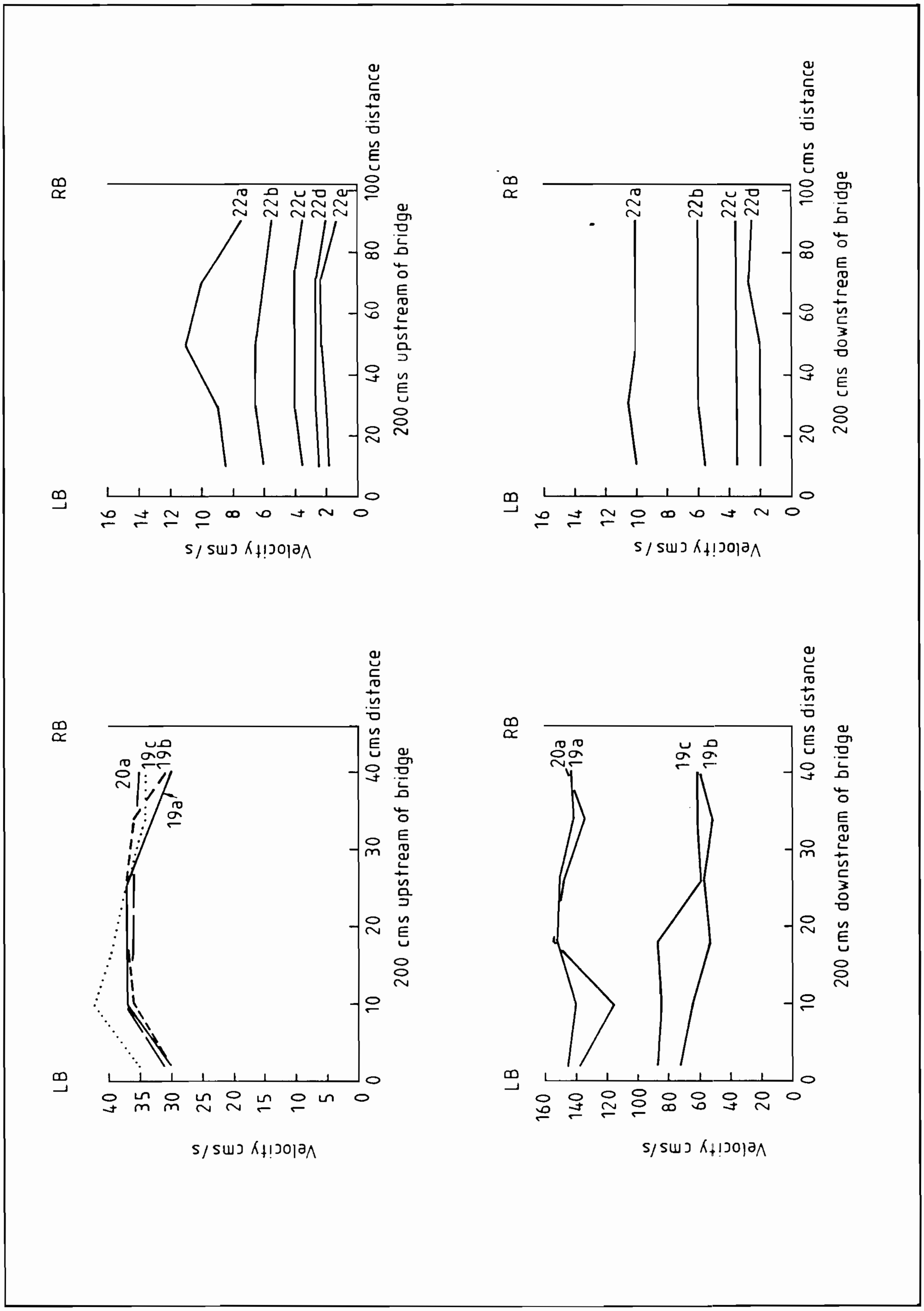

Fig 39 Mid depth velocities, tests 19 to 22

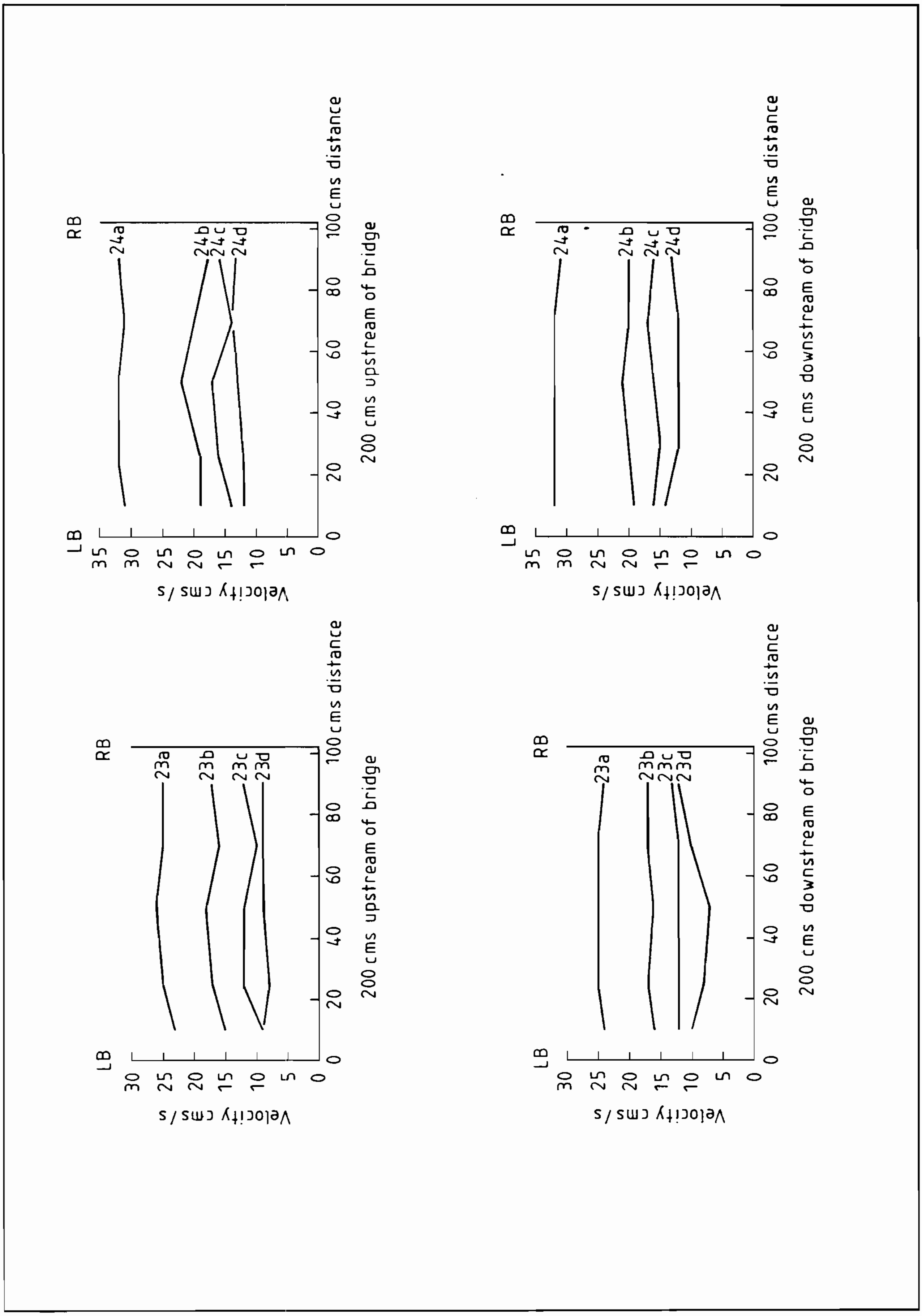

Fig 40 Mid depth velocities, tests 23 to 24

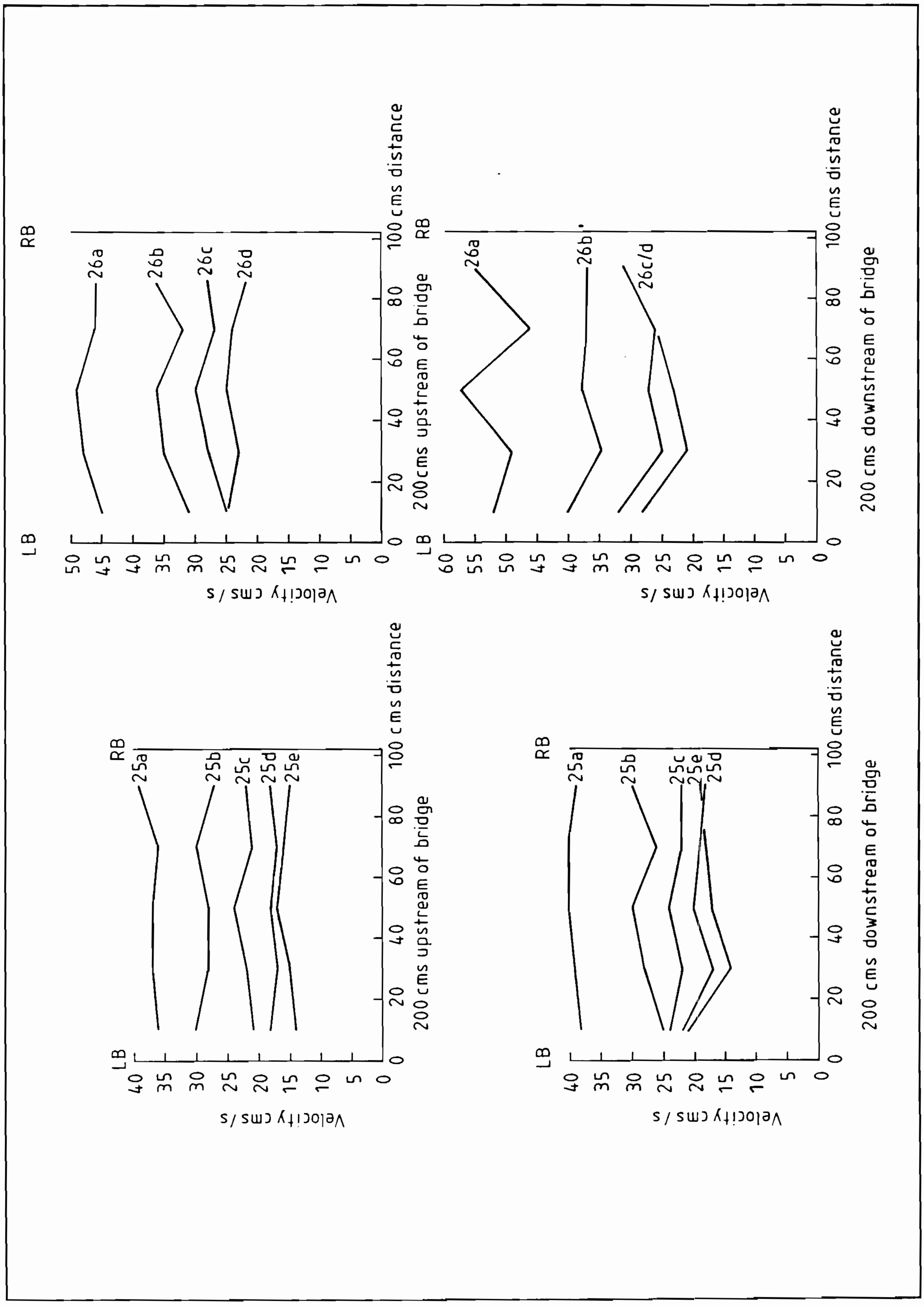

Fig 41 Mid depth velocities, tests, 25 to 26

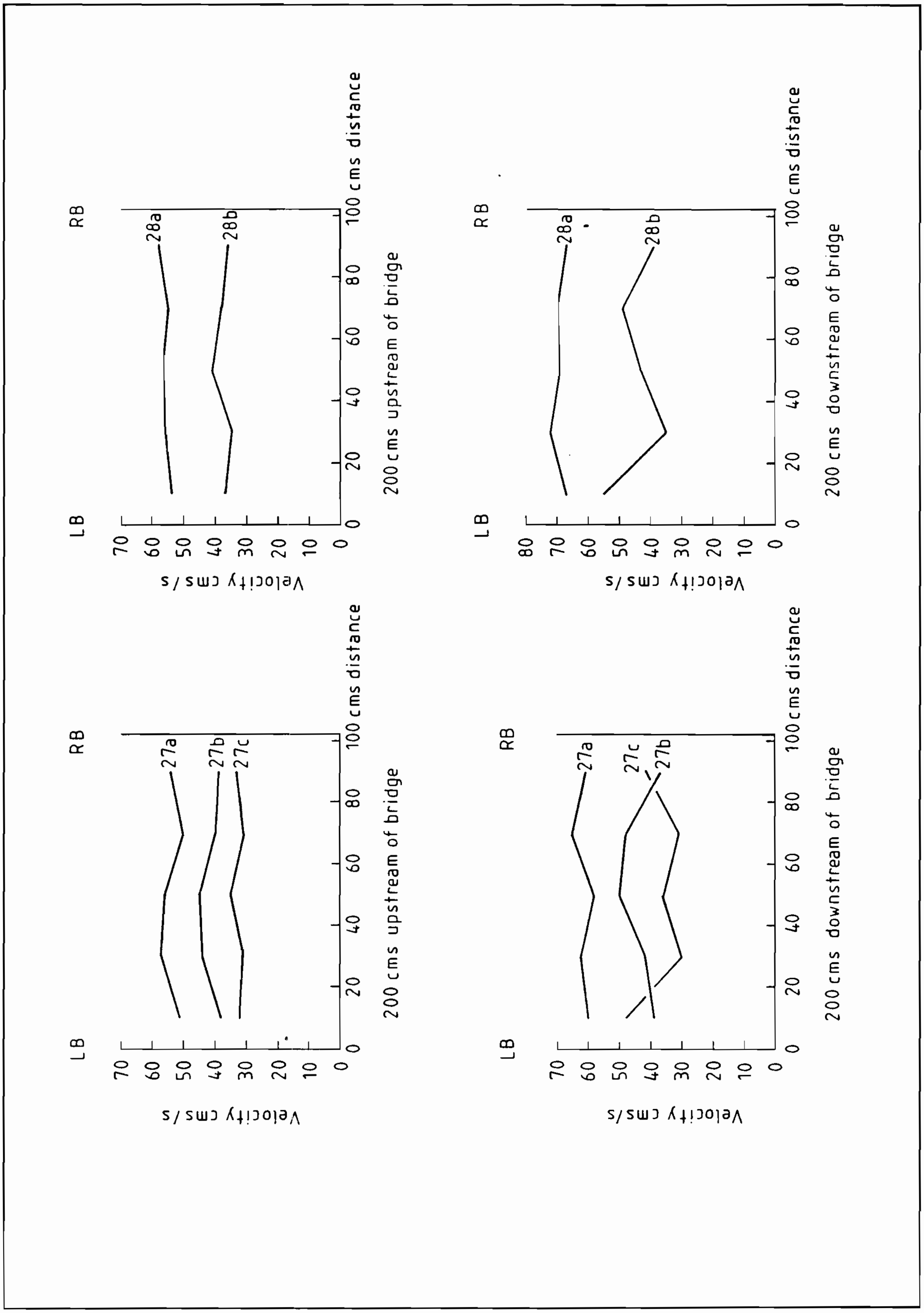

Fig 42 Mid depth velocities, tests 27 to 28

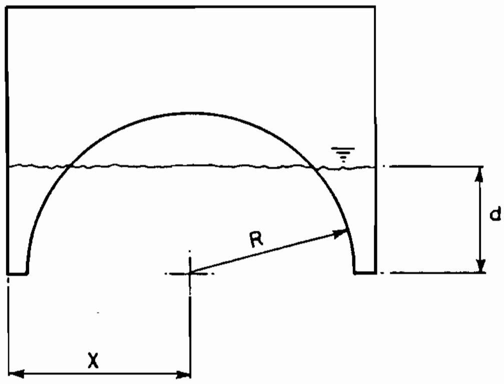

Basic bridge unit

Total blockage area, B, beneath water surface =

$$2\left[Xd - (R^2 - d^2)^{1/2}\ \frac{d}{2} - \frac{\sin^{-1}\ d/R}{360}\ \pi R^2\right]$$

Blockage ratio $J = \frac{B}{2Xd}$

Fig 43 Calculation of blockage ratio

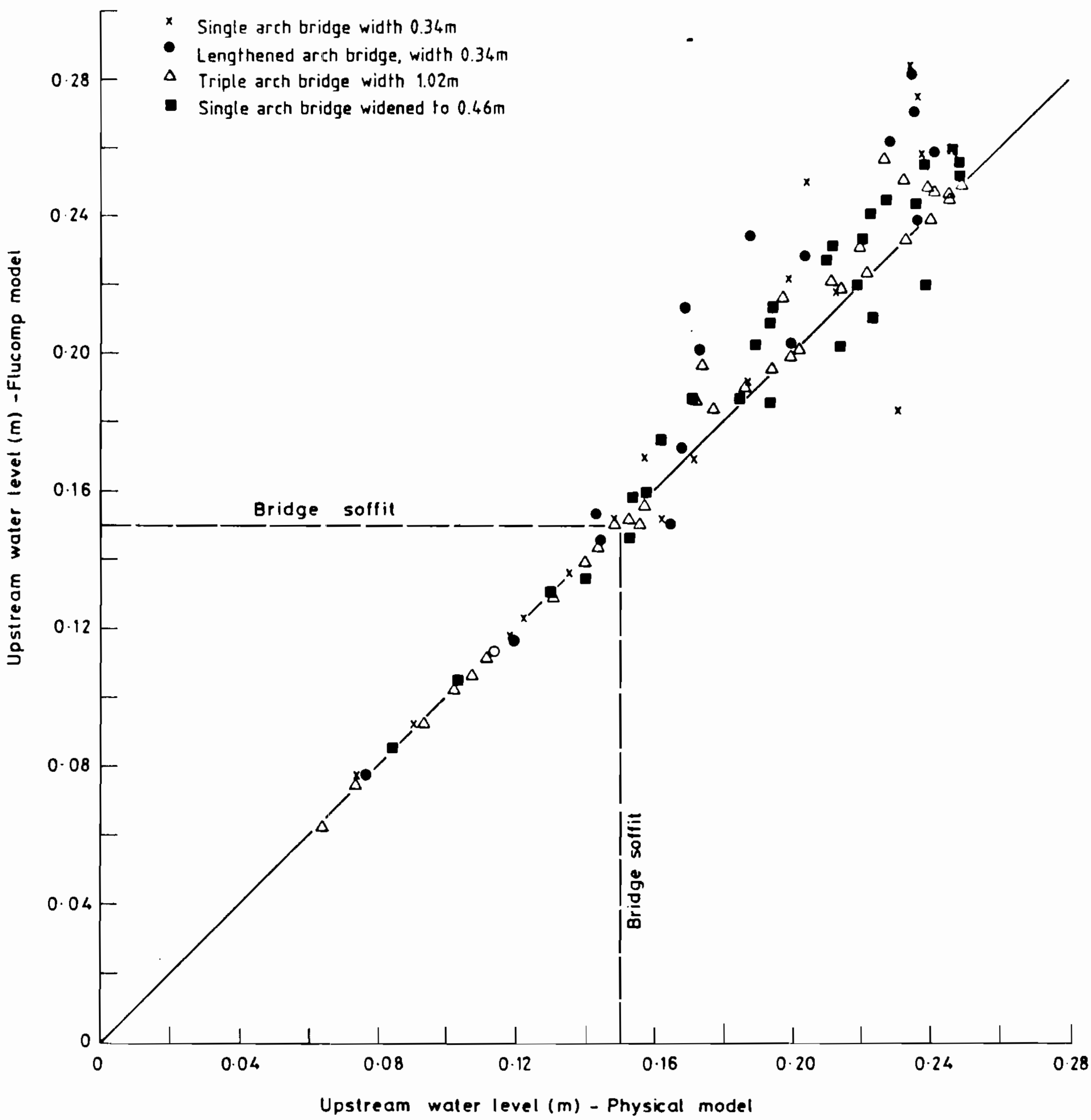

Fig 44 Comparison between mathematical and physical models

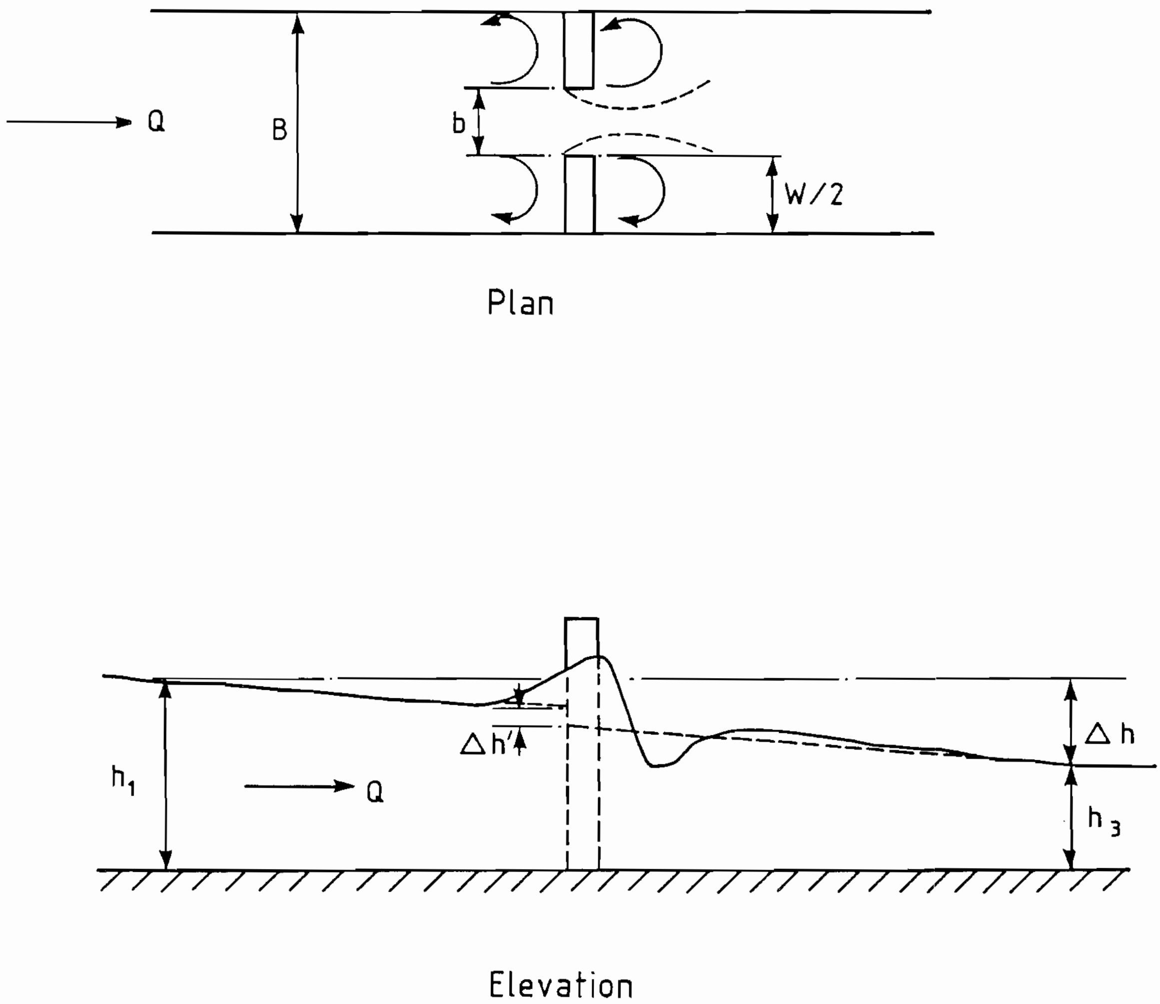

Fig 45 Effect of a channel constriction on the water surface profile

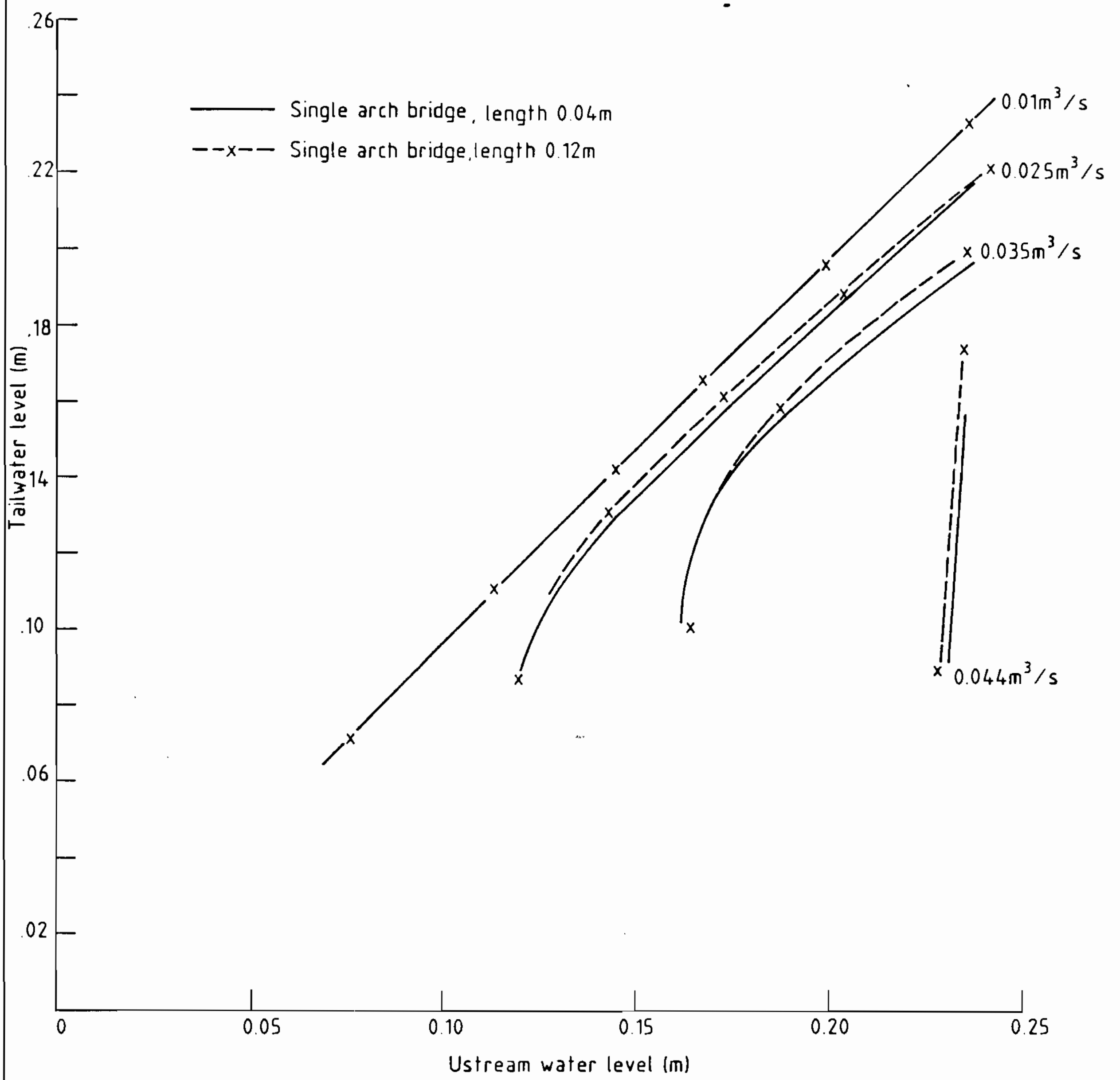

Fig 46 Effect on afflux of longer bridge

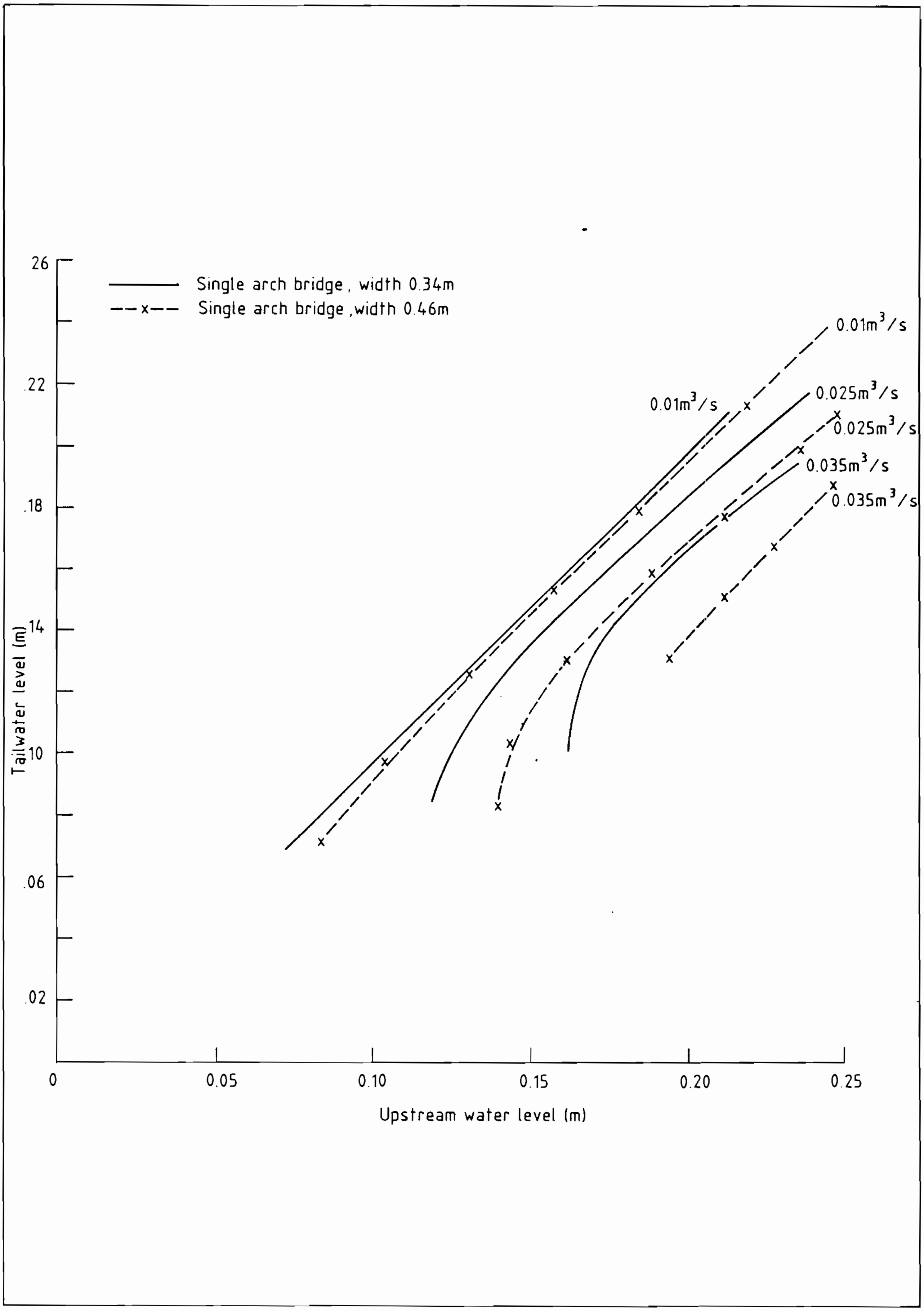

Fig 47 Effect on afflux of wider bridge

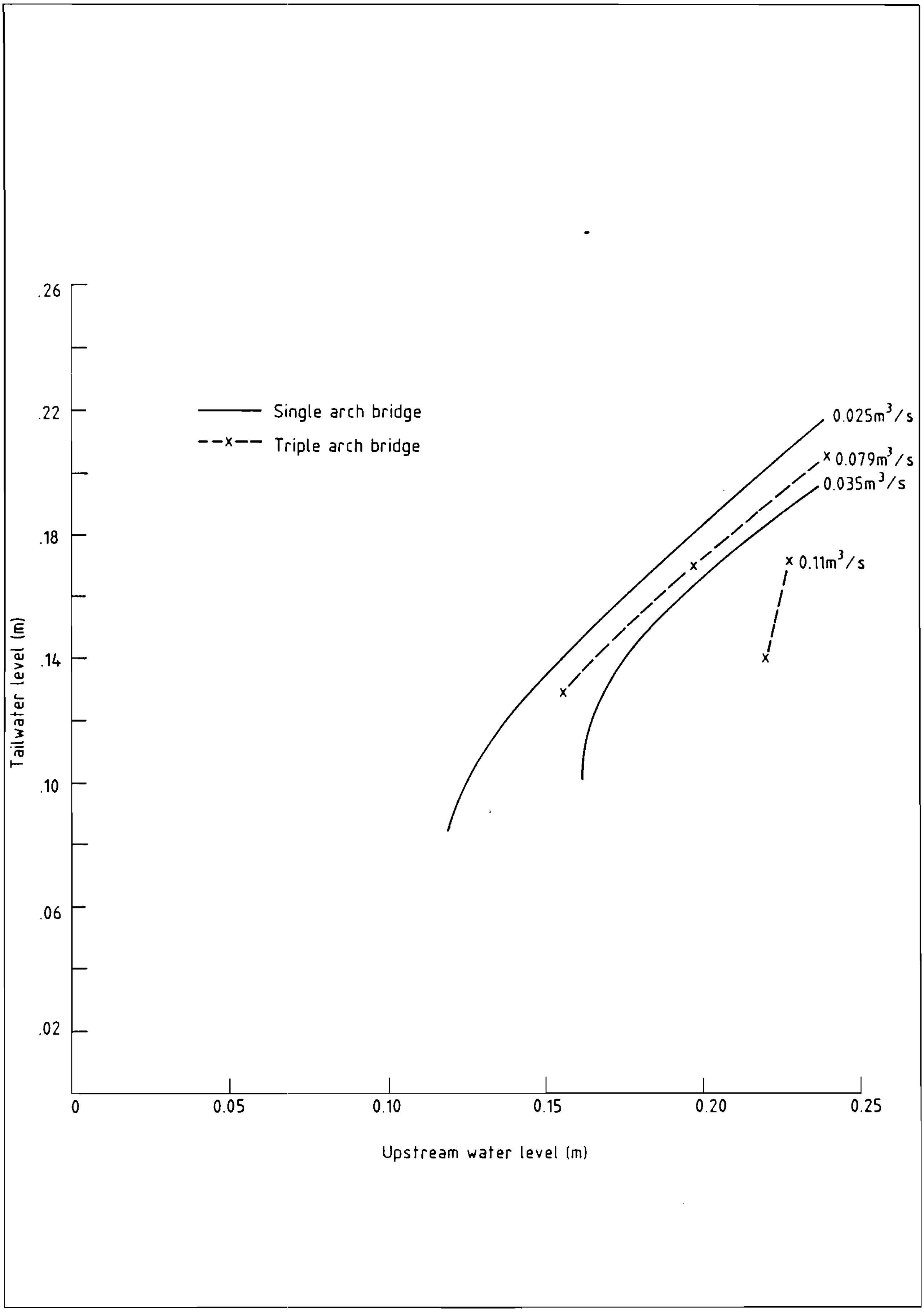

Fig 48 Effect on afflux of three arch bridge

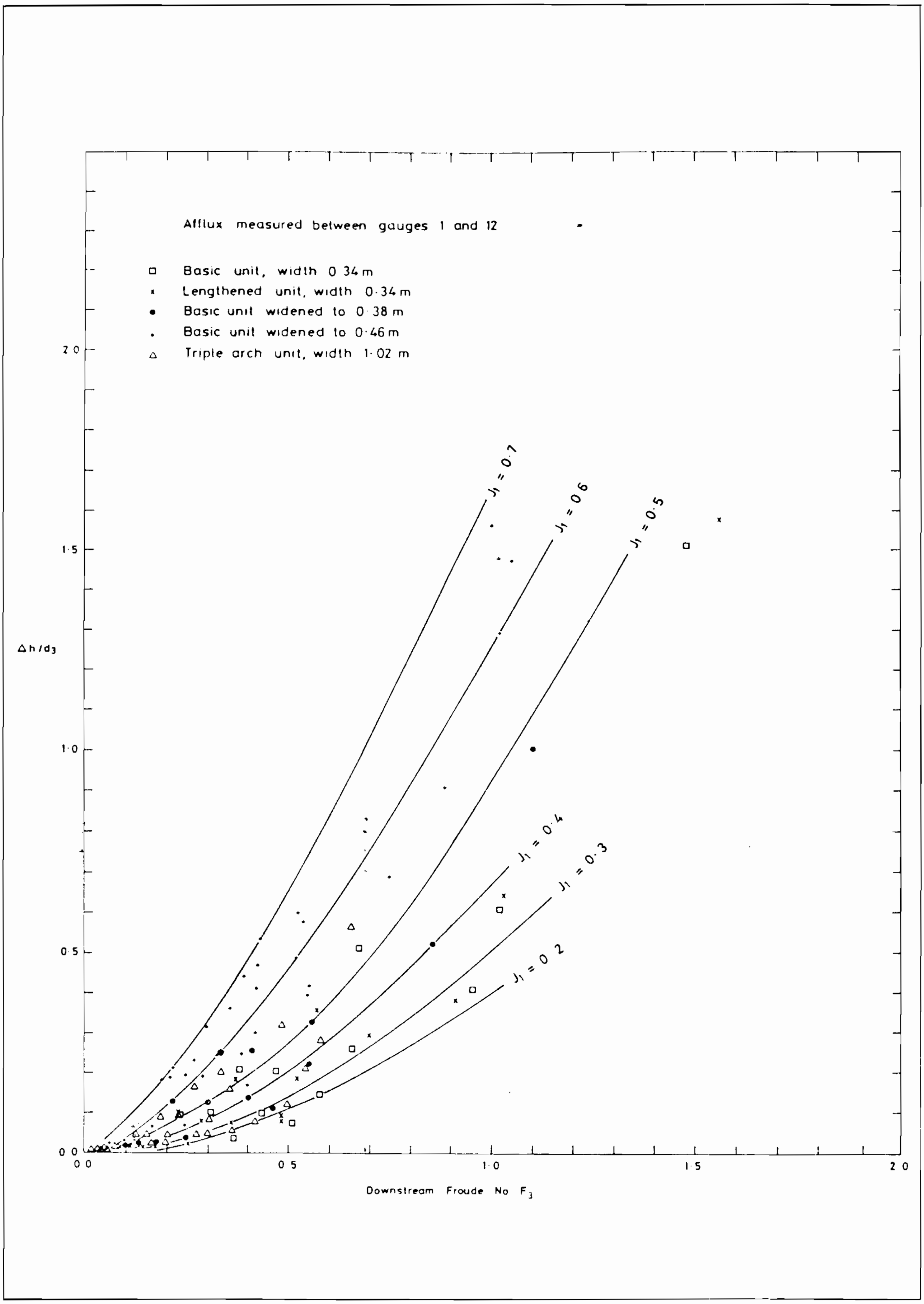

Fig 49 $\Delta h/d_3$ v F_3 and J_1

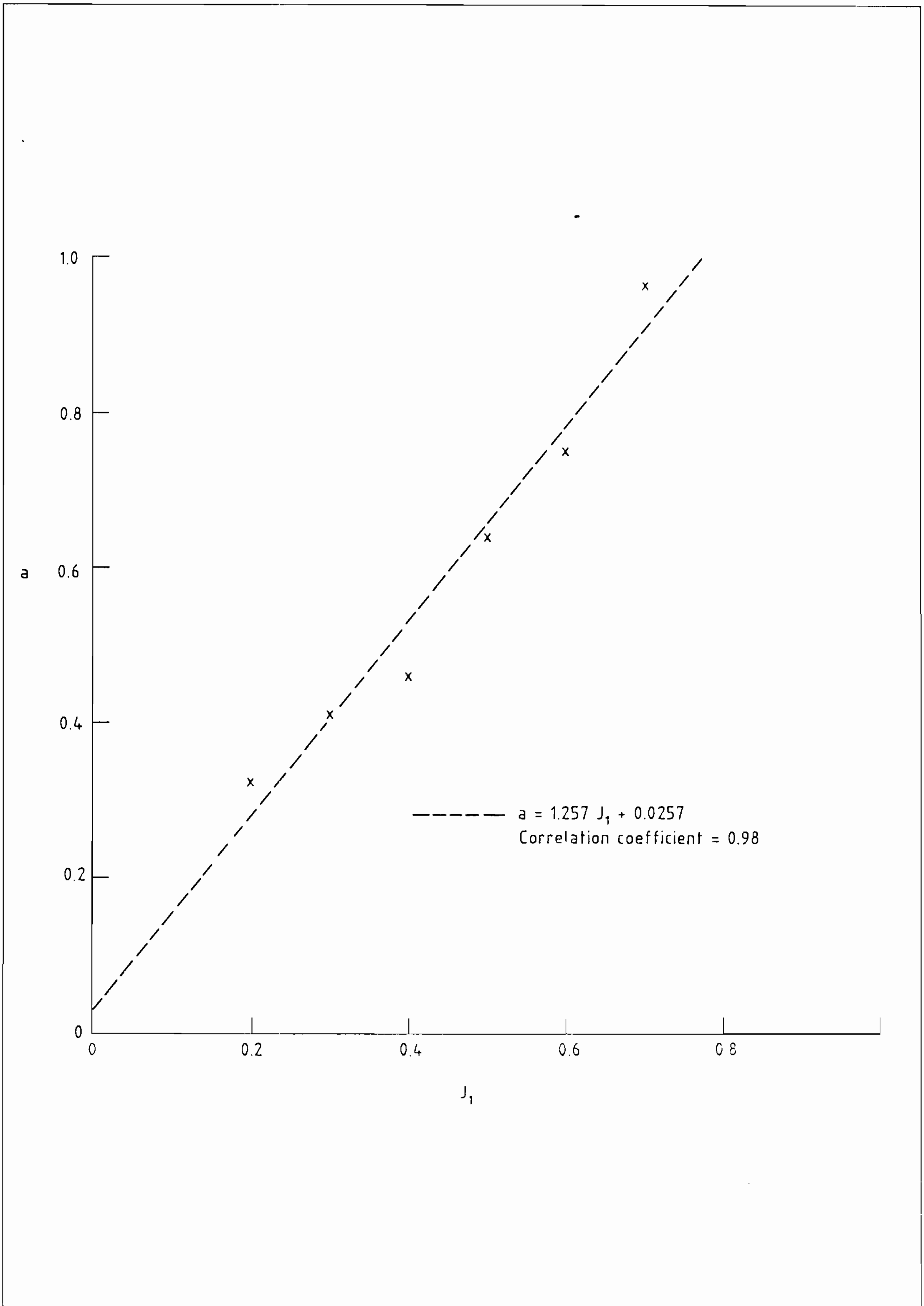

Fig 50 Plot of F_3^2 coefficient against J_1, from curves of Fig 49

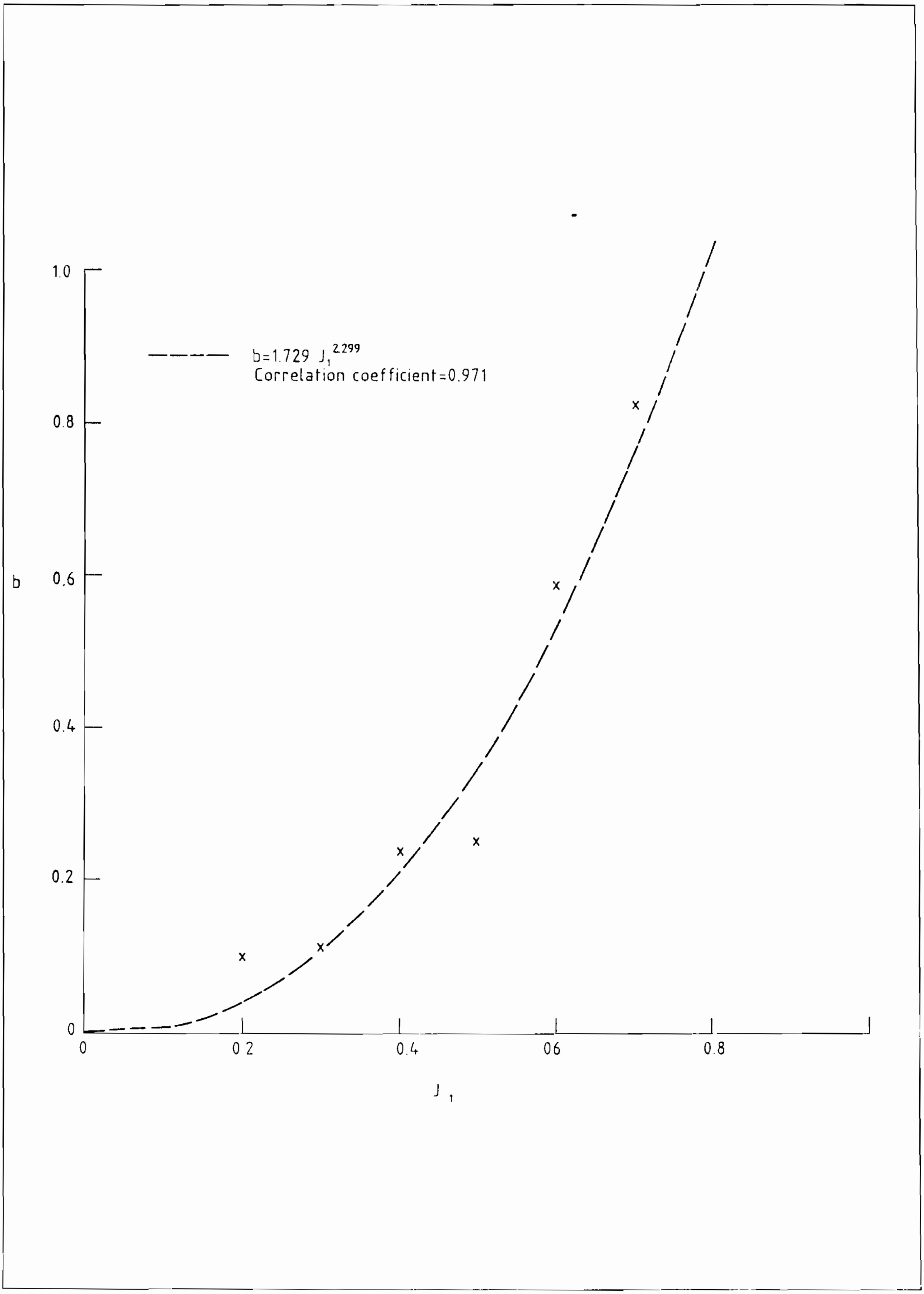

Fig 51 Plot of F_3 coefficient against J_1, from curves of Fig 49

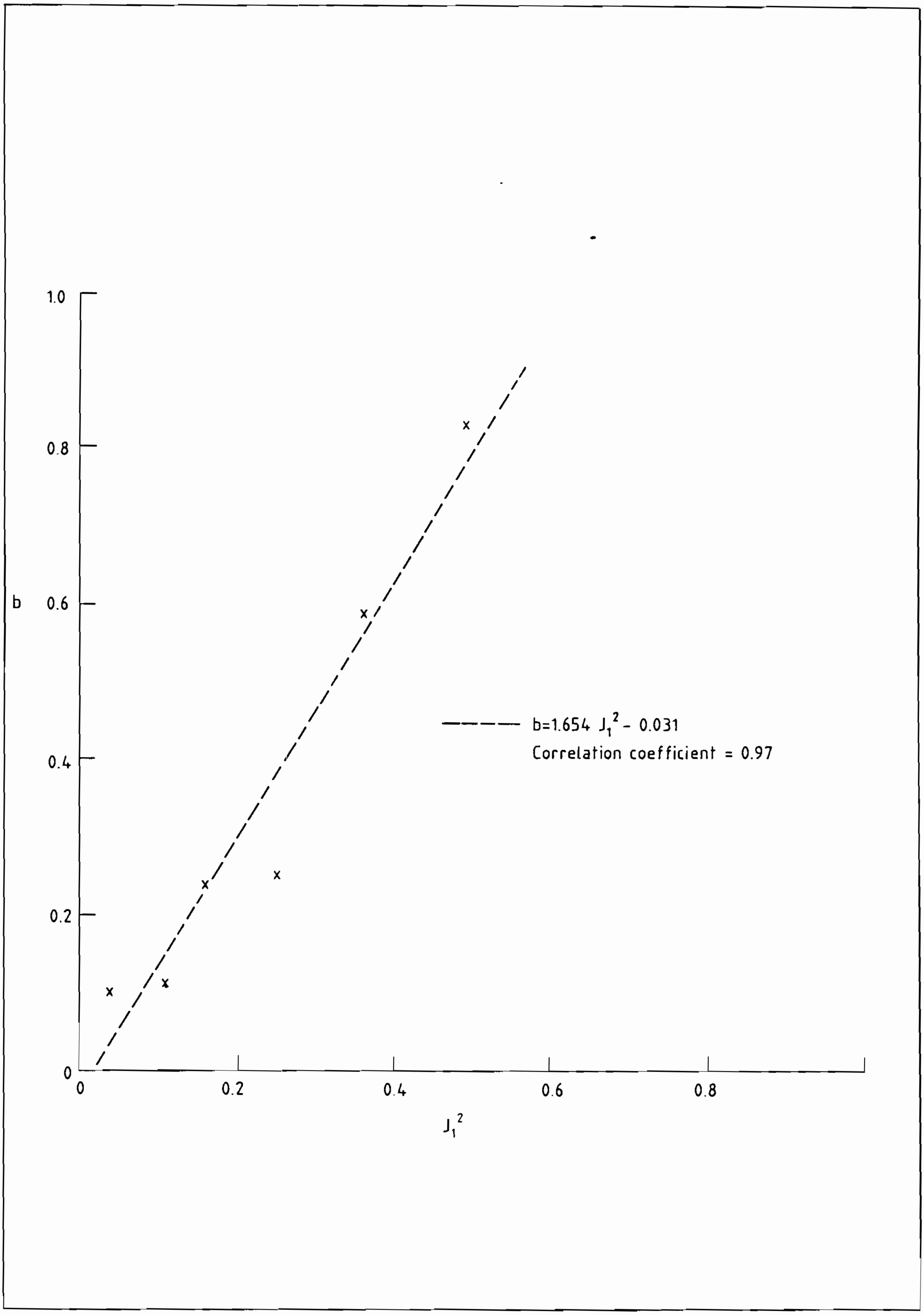

Fig 52 Plot of F_3 coefficient against J_1^2

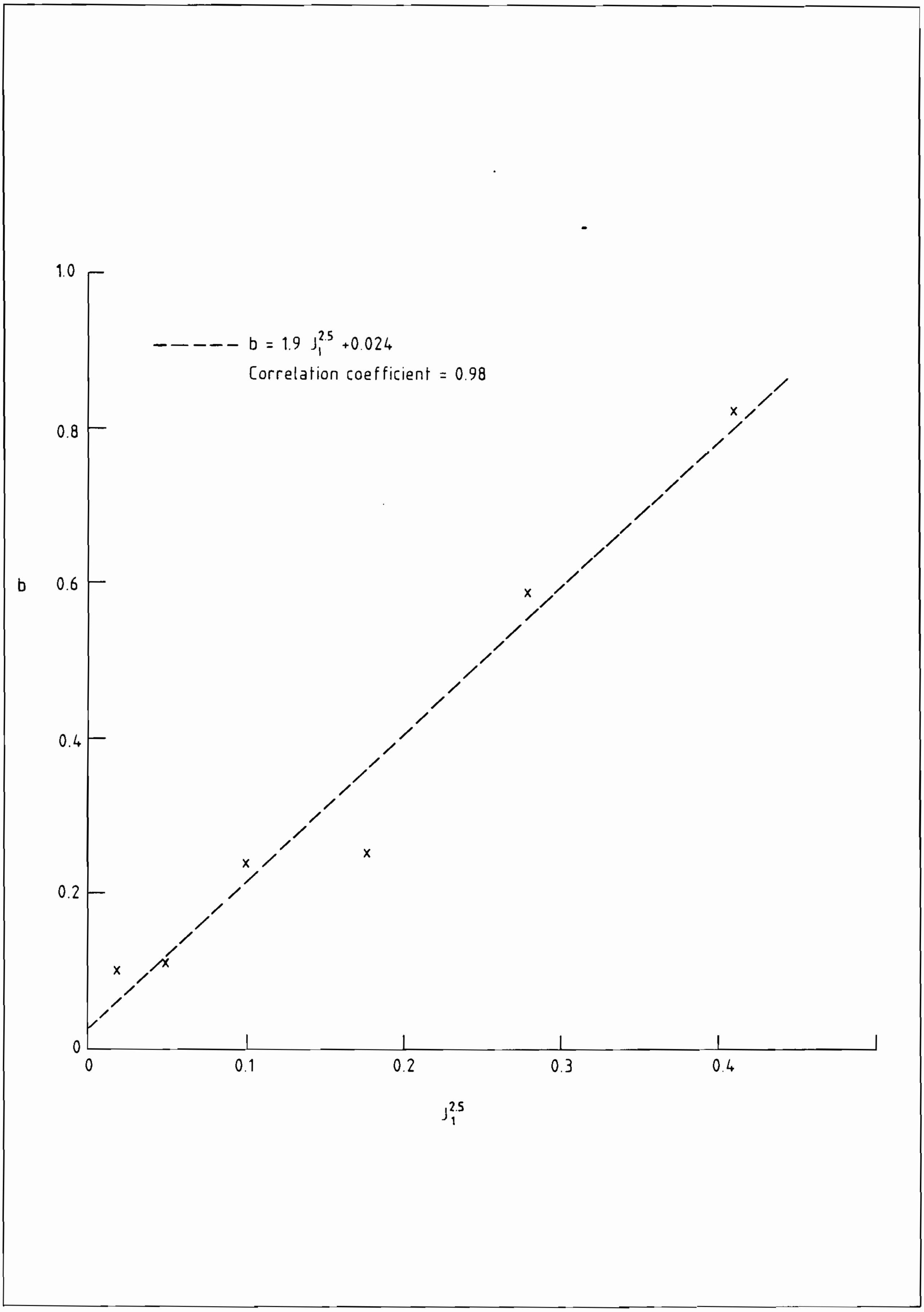

Fig 53 Plot of F_3 coefficient against $J_1^{2.5}$

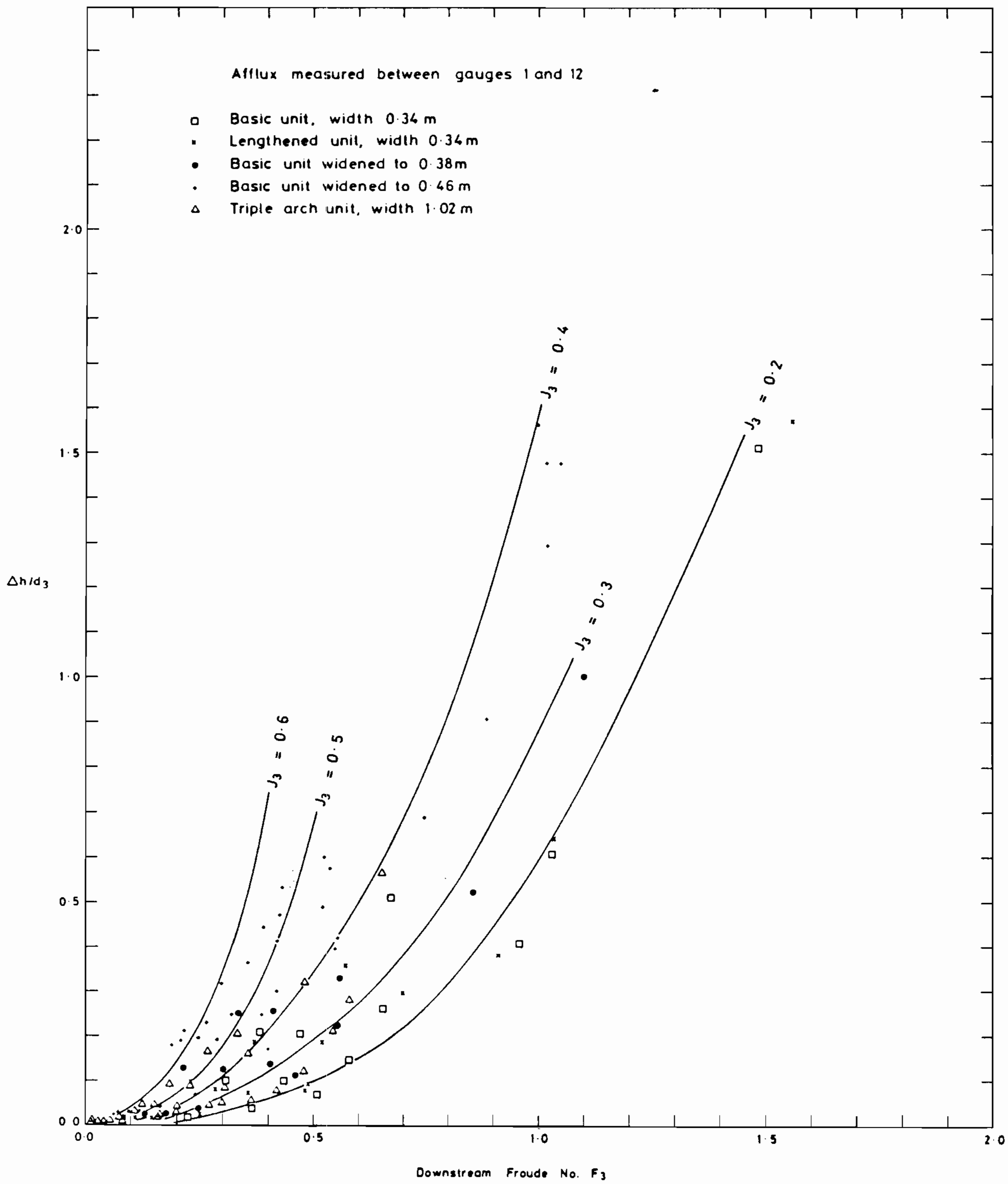

Fig 54 $\Delta h/d_3$ v F_3 and J_3

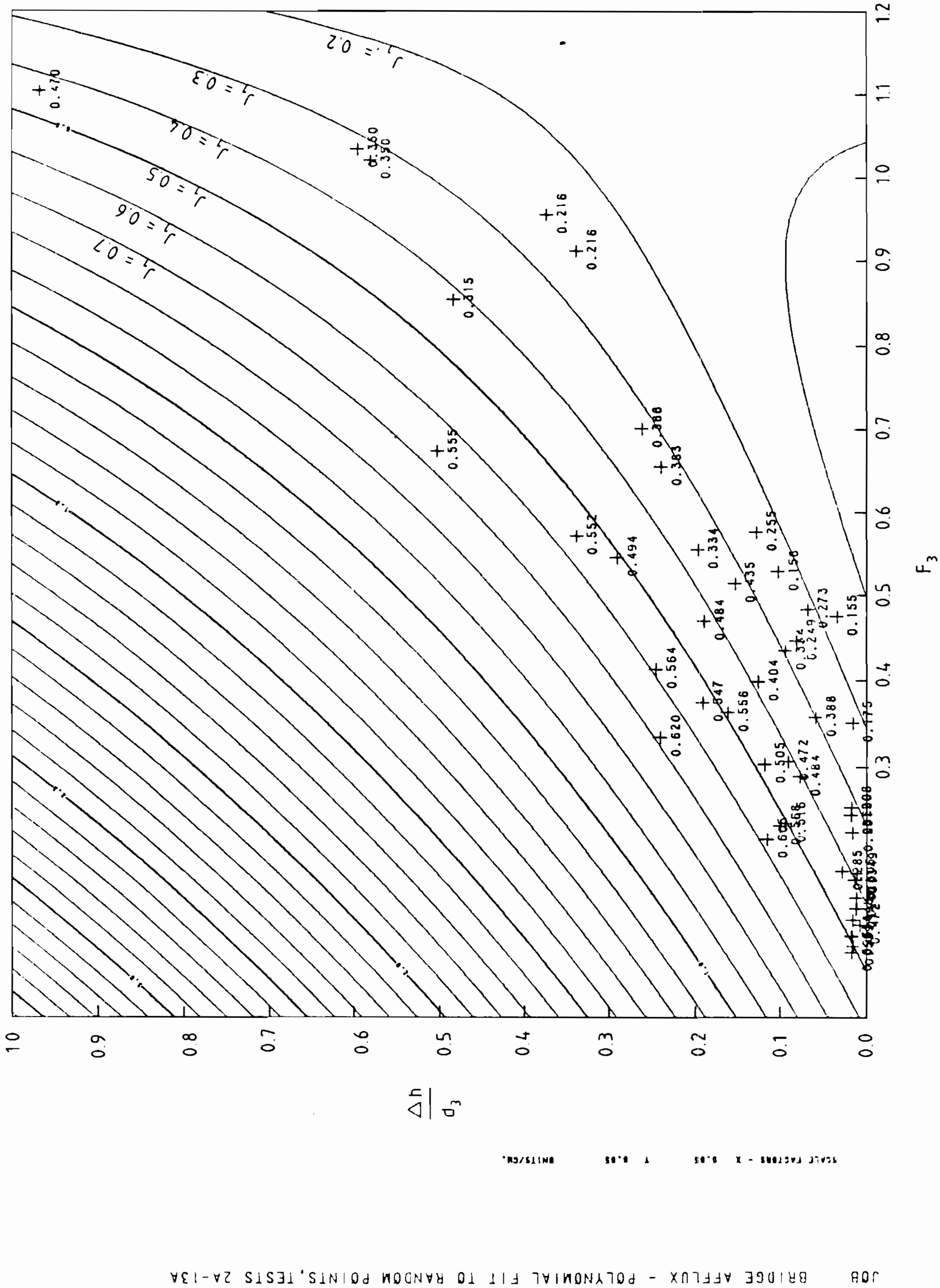

Fig 55 Computer fitted surface of $J_1 = f\left(\frac{\Delta h}{d_3}, F_3\right)$

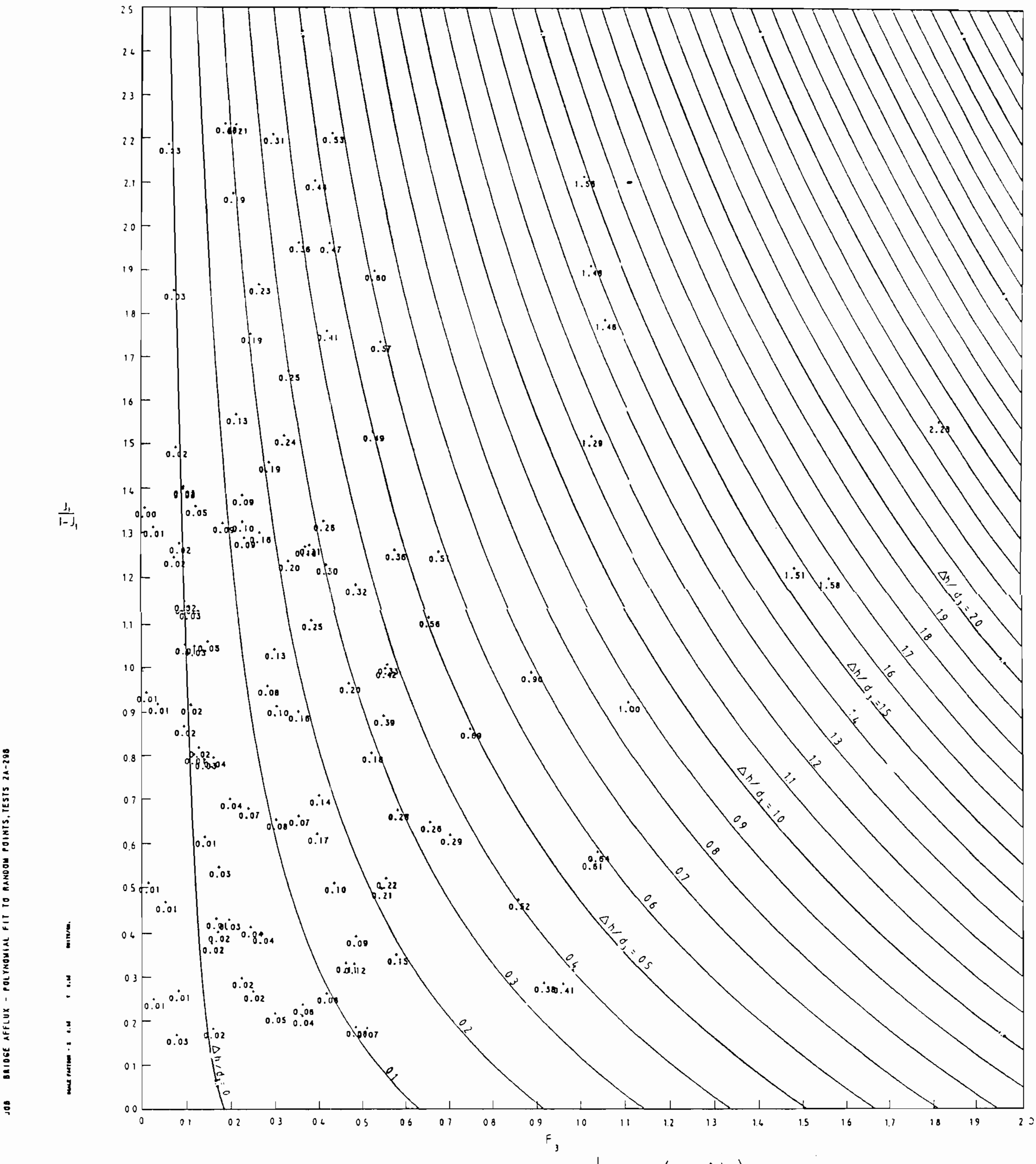

Fig 56 Computer fitted surface $\frac{J_1}{1-J_1} = f\left(F_3, \frac{\Delta h}{d_3}\right)$

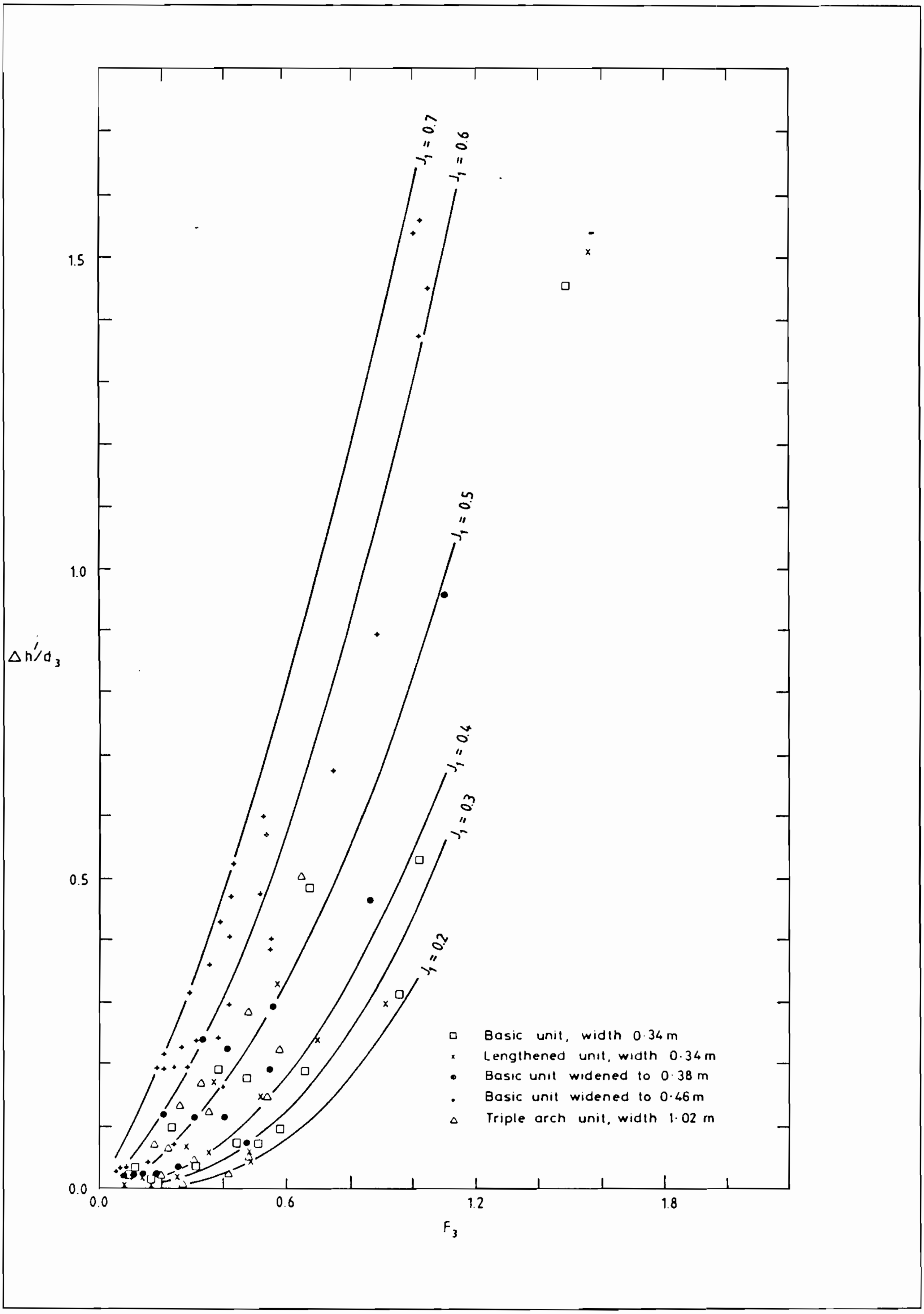

Fig 57 Relation between extrapolated afflux ratio $\Delta h'/d_3$, and J_1

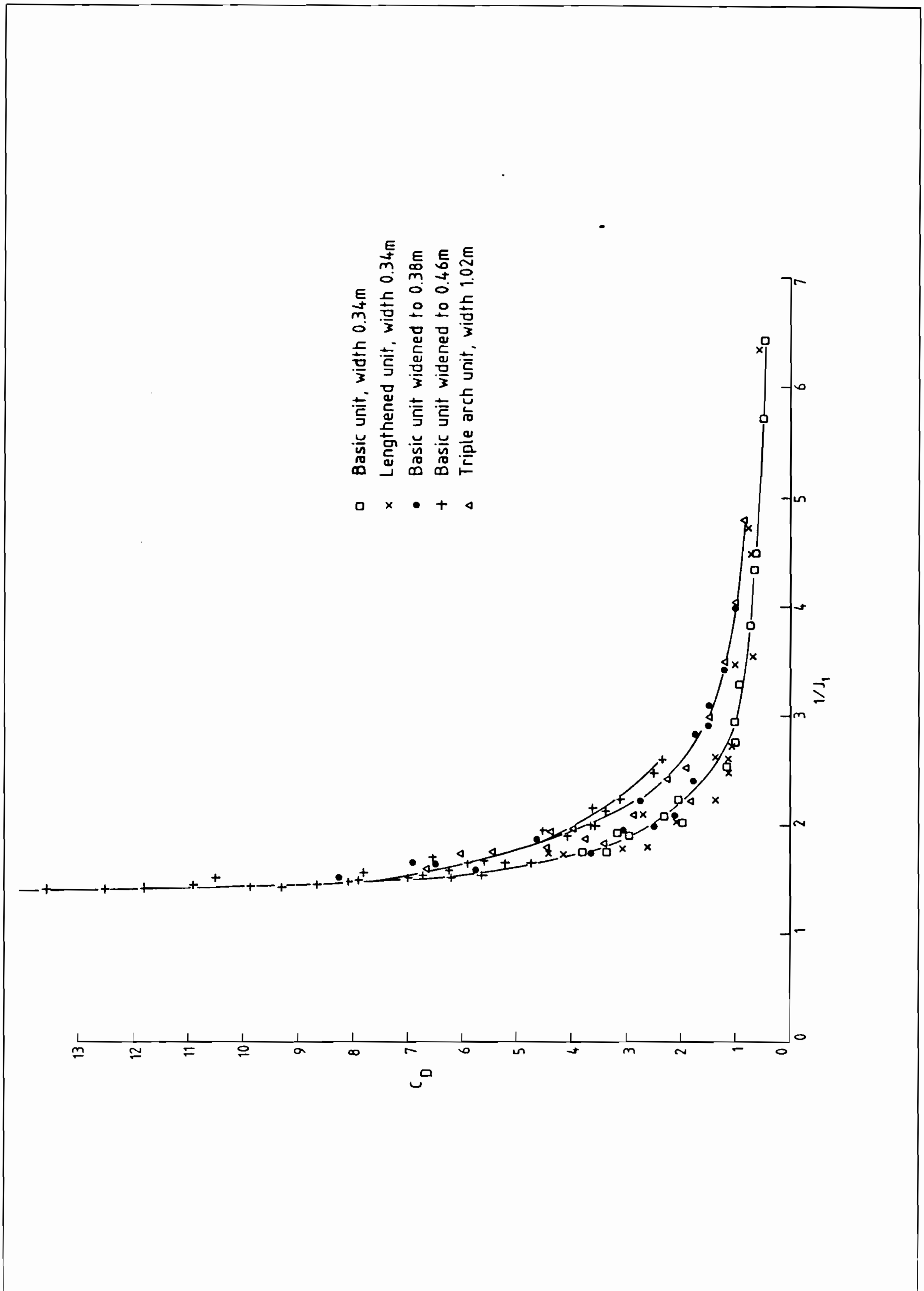

Fig 58 Plot of C_D against $1/J_1$

PLATES.

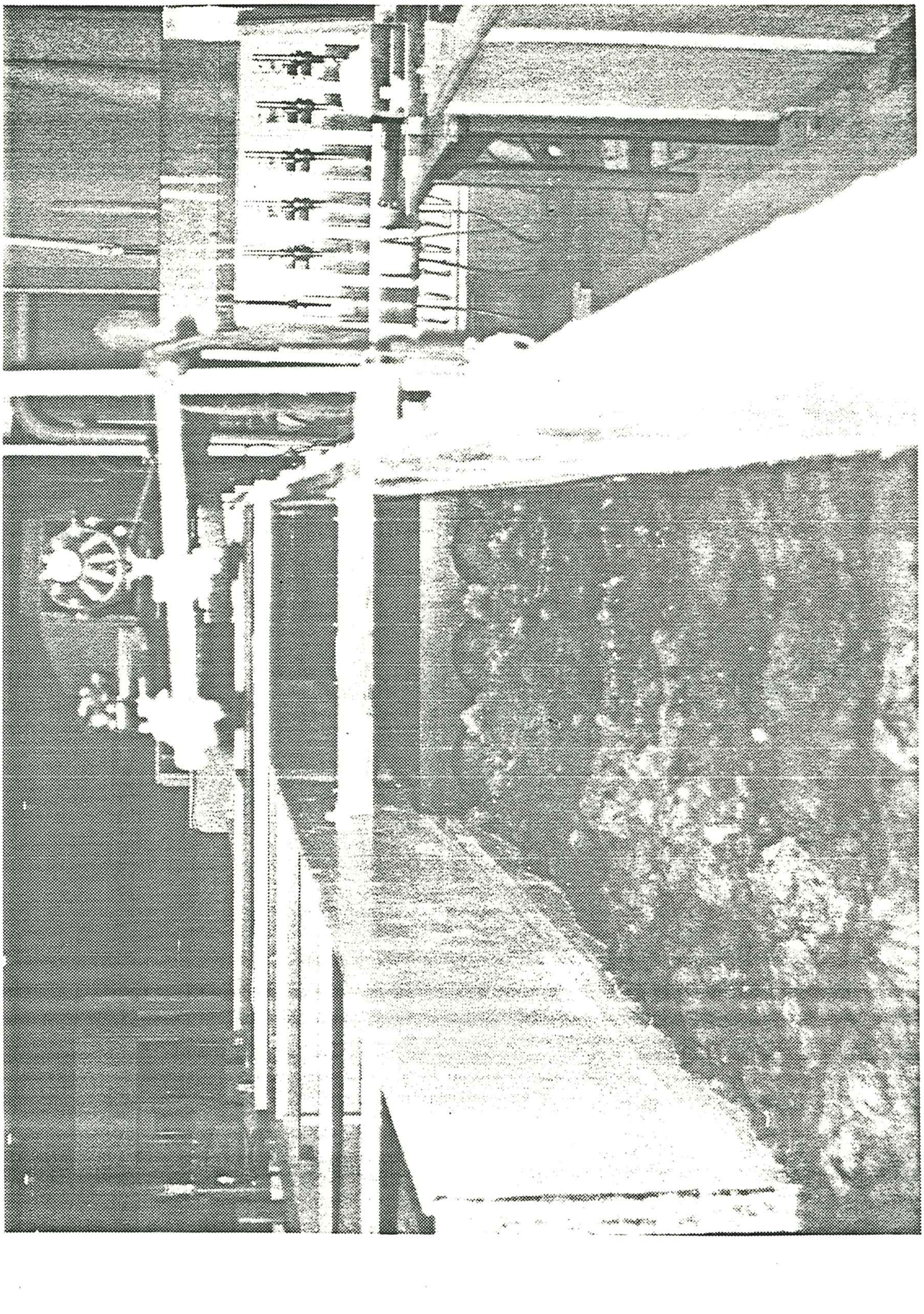

PLATE 1 Layout of flume

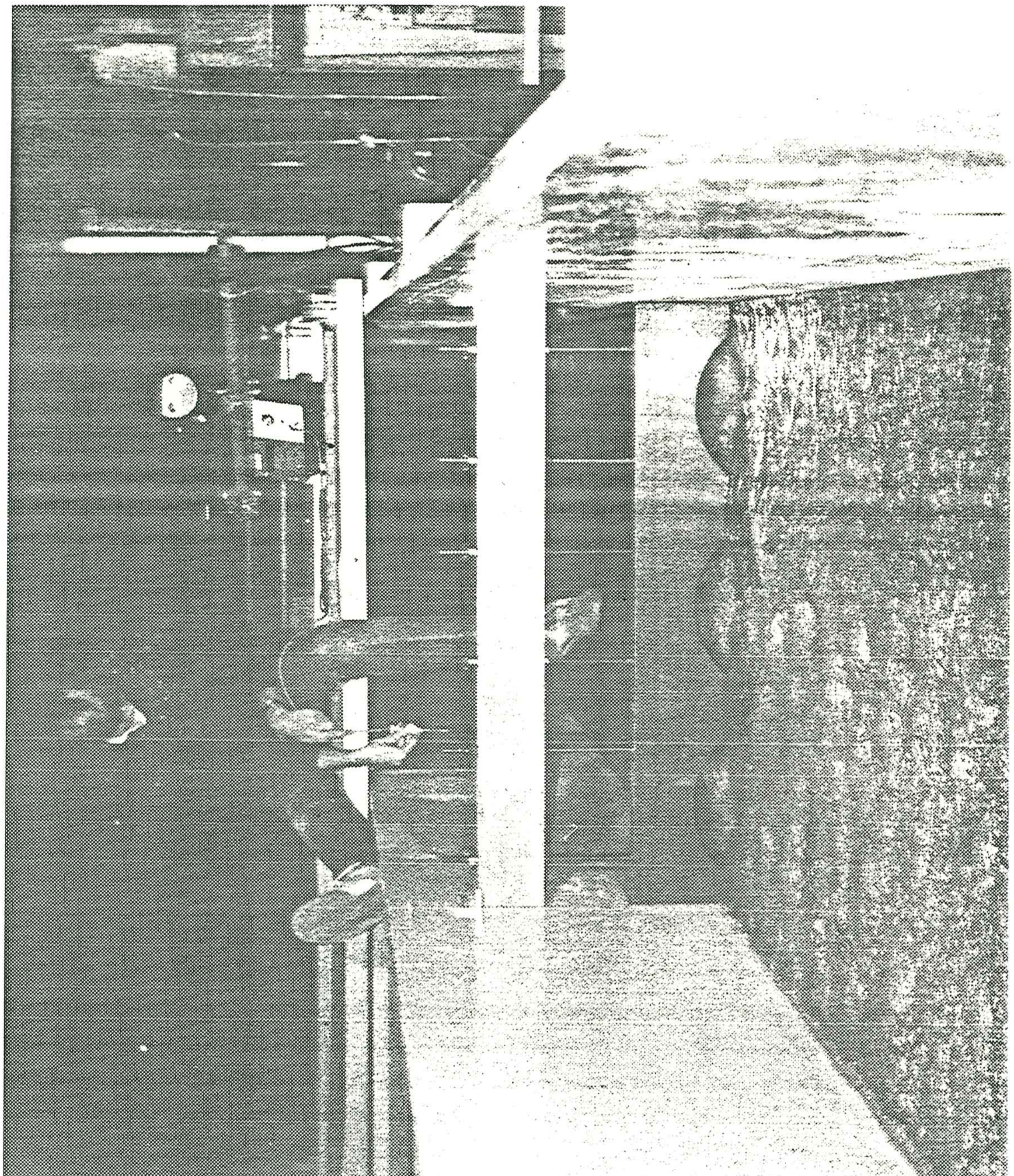

PLATE 2 Velocity measurements with miniature current meter

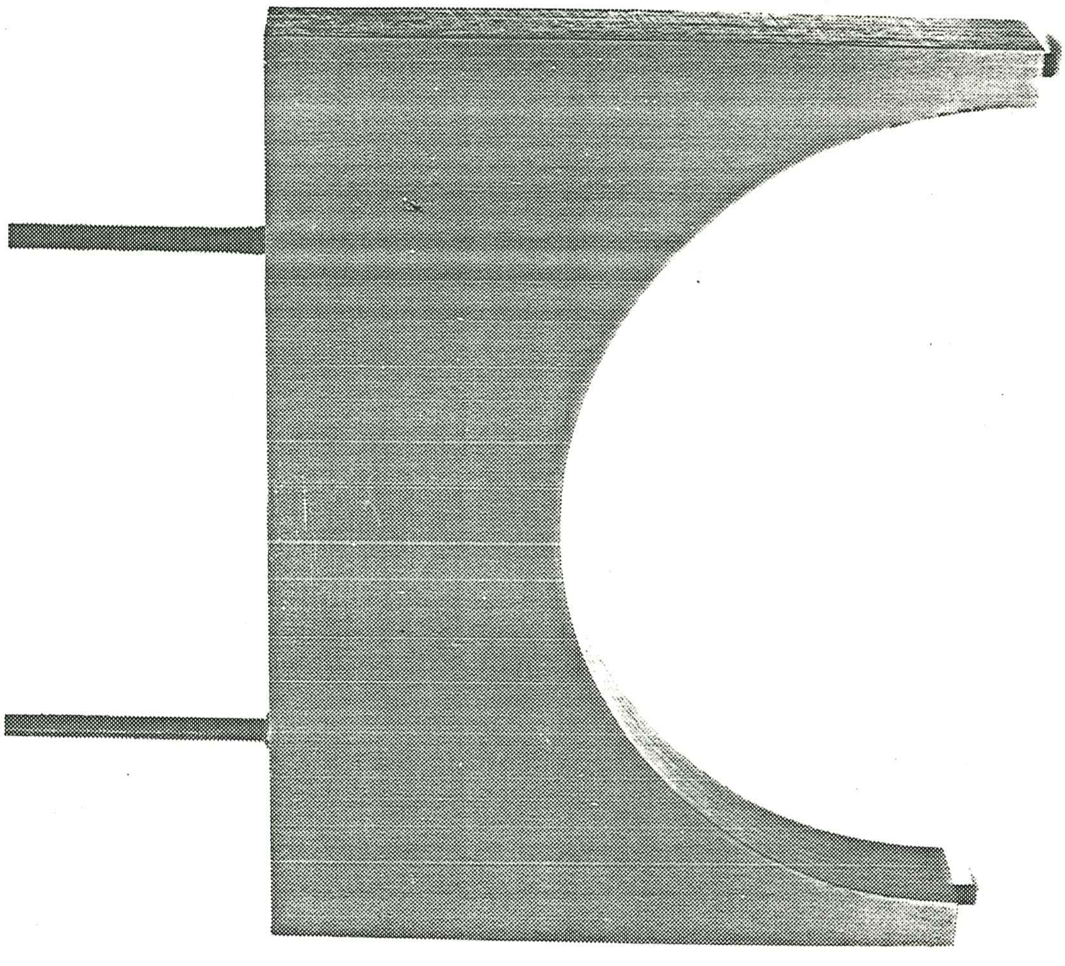

PLATE 3 Basic semi-circular arched bridge

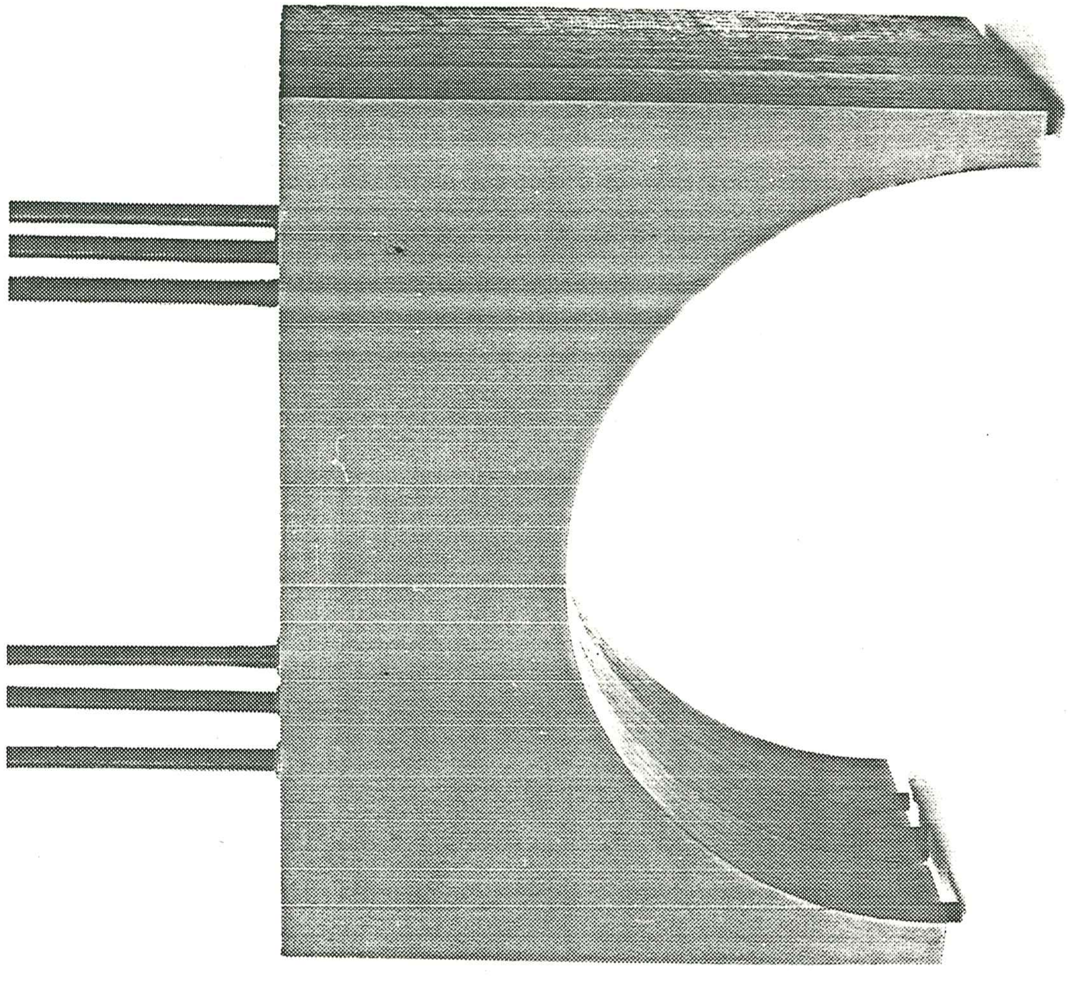

PLATE 4 Basic bridge lengthened in direction of flow

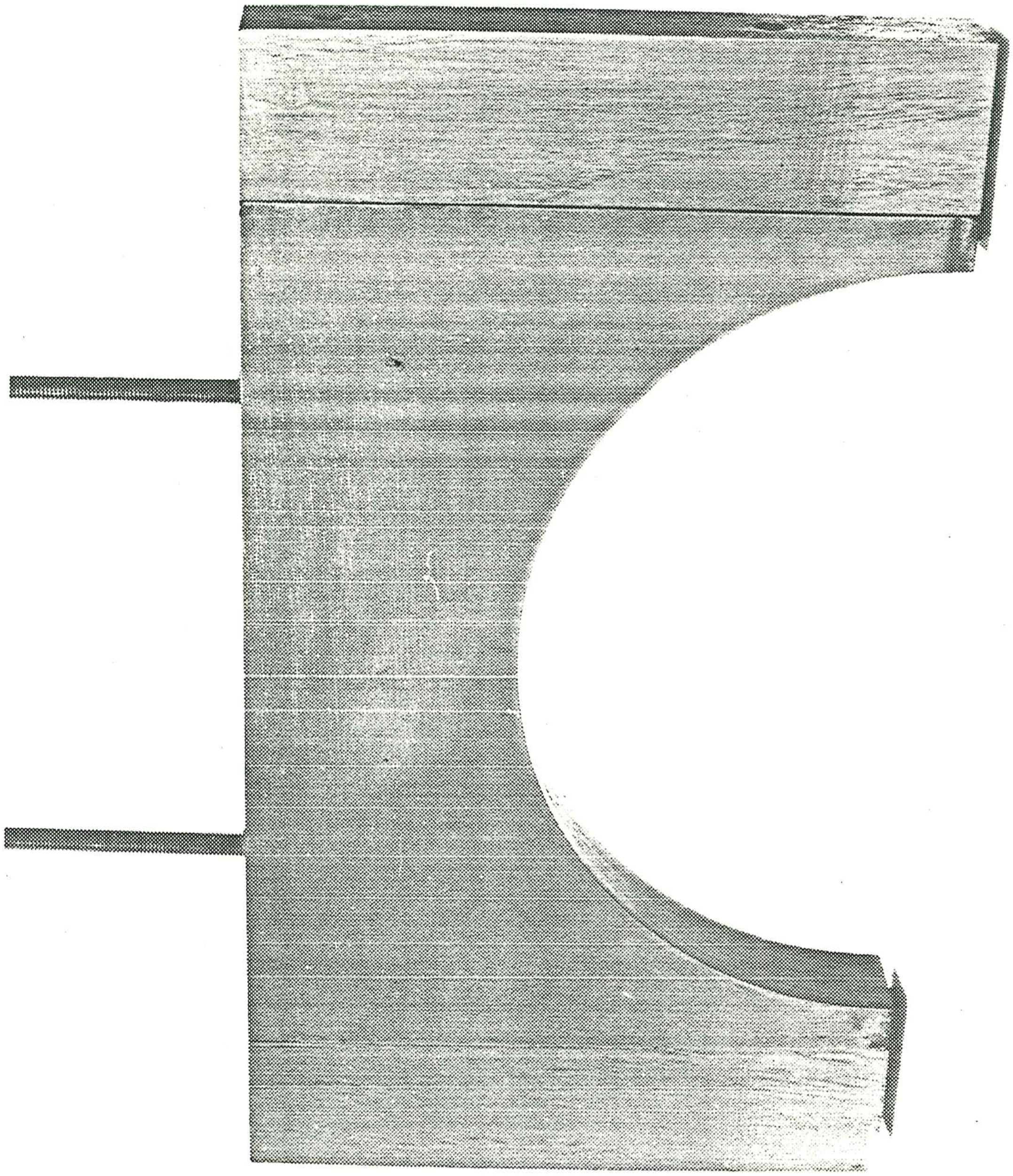

PLATE 5 Wider basic bridge

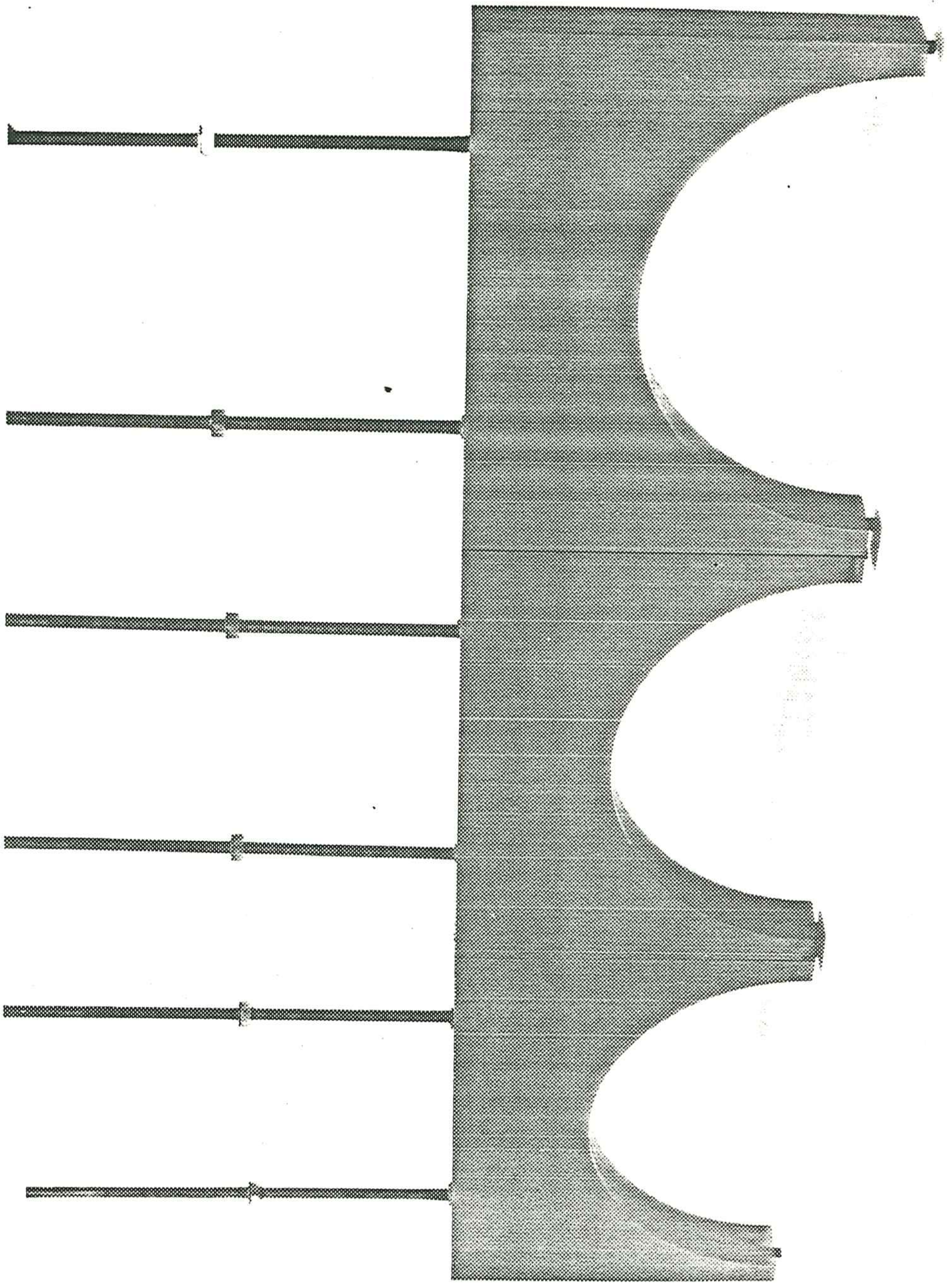

PLATE 6 Three arched bridge

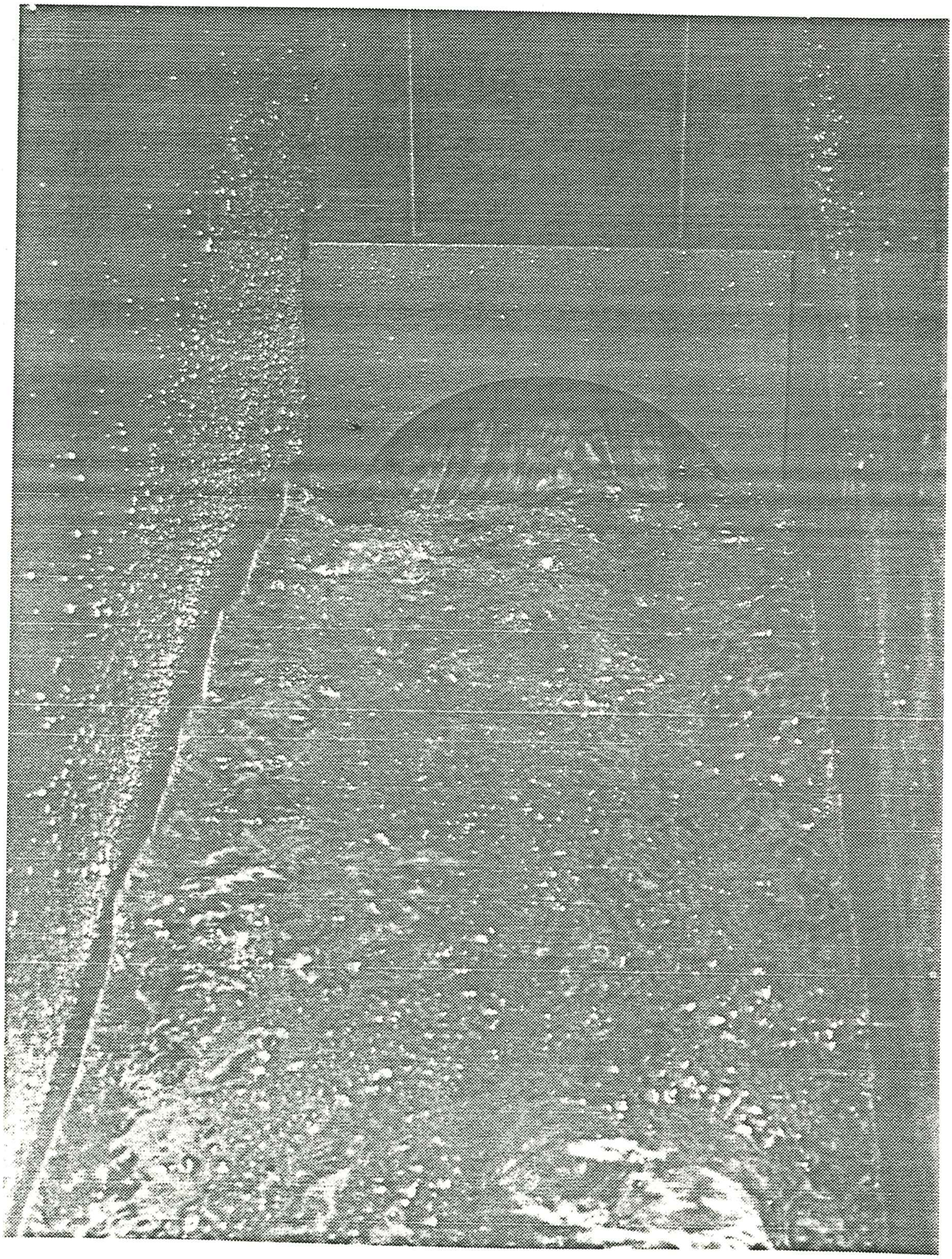

PLATE 7 Turbulent conditions downstream of basic bridge

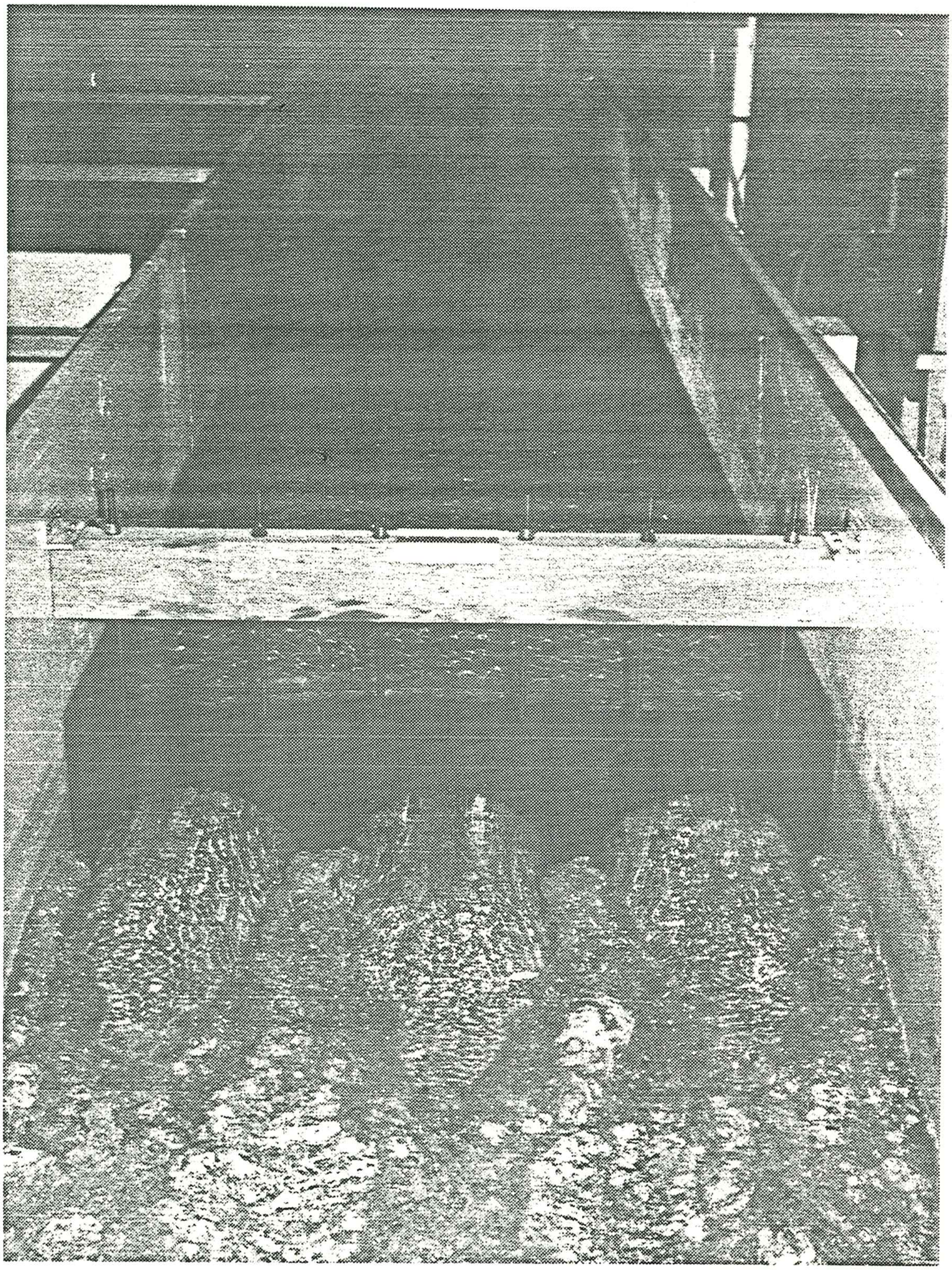

PLATE 8 Turbulent conditions downstream of three arch bridge

PLATE 9 Shallow vortices upstream of basic bridge

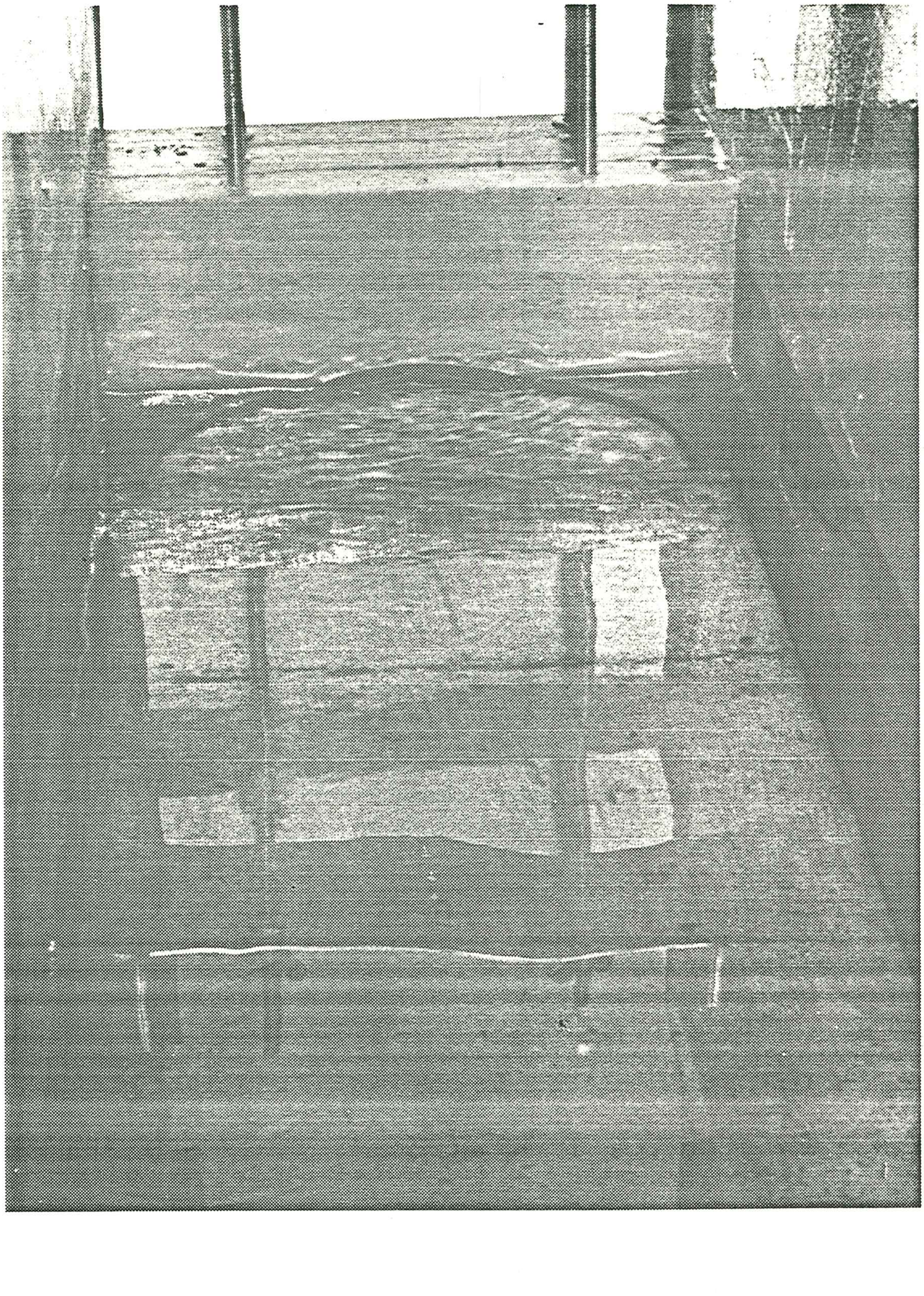

PLATE 10 Surface ripples upstream of basic bridge